Mechanisms and circuitry underlying direction selectivity in the mouse retina

by

Laura Hanson
BSc, University of Victoria, 2015

A Dissertation Submitted in Partial Fulfillment
of the Requirements for the Degree of

DOCTOR OF PHILOSOPHY

in the Division of Medical Sciences

Supervisory Committee

Mechanisms and circuitry underlying direction selectivity in the mouse retina

by

Laura Hanson

BSc, University of Victoria, 2015

Supervisory Committee

Dr. Gautam Awatramani, Division of Medical Sciences

Supervisor

Dr. Craig Brown, Division of Medical Sciences

Departmental Member

Dr. Kerry Delaney, Department of Biology

Outside Member

Abstract

Vision is a key sensory modality that is essential for survival. In the vertebrate visual system, light signals detected by photoreceptors are highly processed in the retina itself before being relayed to higher-order visual areas. The retina decomposes visual signals into specific features such as contrast, size, orientation, direction and/or velocity and relays this information via distinct output ganglion cells. For example, the direction-selective ganglion cells (DSGCs) are responsible for encoding the direction of objects moving across the retina. This may occur due to self-motion or as objects move through the environment. DSGCs respond robustly for motion of a particular "preferred" direction while exhibiting little to no response during motion in the opposite or "null" direction.

In this dissertation, I examined the synaptic mechanisms involved in generating direction selectivity, both at the level of the DSGC as well as in the dendrites of presynaptic GABAergic/cholinergic starburst amacrine cell, where direction selectivity is first observed. Using mouse genetics to selectively disrupt direction processing capabilities of starburst dendrites, I revealed a second mechanism for generating direction selectivity. This relies on the differential functional wiring of GABA and ACh to DSGCs, which provides a substrate for directional dependent changes in the timing of excitation and inhibition to DSGCs (Chapter 2).

In chapters 3 and 4, I turned my focus to the excitatory glutamatergic inputs to the DSGCs mediated by bipolar cells (that bridge the photoreceptor to output ganglion cells). Specifically, I examined the organization and AMPA and NMDA receptor composition (Chapter 3). By analyzing the spontaneous excitatory activity in the DSGC in combination with 2-photon

imaging of the NMDA mediated calcium responses and glutamate signaling, I show the ‘silent’ NMDA-rich synapses are able to encode information across a range of contrasts.

Finally, I also examined how the bipolar cell output to DSGCs is asymmetrically modified by another class of amacrine cell: the wide-field amacrine cells. In Chapter 4, I discovered that the subtype of nasal coding ON-OFF DSGCs are also orientation-selective (OS)-they respond best to vertically oriented bars. I show this selectivity originates at the level of bipolar cell axon terminals, which appear to be gap junction coupled to the vertically orientated processes of wide field amacrine cells. These finding led me to propose that orientation tuning in bipolar cells may act as a filter to simplify the task of encoding direction of motion for moving edges in the DSGC. This research highlights the mechanisms and circuitry required for the retina to accurately encode the direction of motion across the visual scene and provides us with a deeper understanding of the circuitry and mechanisms involved in direction selectivity in the mouse retina.

Table of Contents

List of Figures

List of Abbreviations

ACh	Acetylcholine
AMPA	α-amino-3-hydroxy-5-methyl-4-isoxazolepropionic acid
CART	Cocaine- and amphetamine-regulated transcript
ChAT	Choline aceytltransferase
CNQX	Cyanquixaline (6-cyano-7-nitroquinoxaline-2,3-dione)
CNS	Central nervous system
Cx36	Connexin 36
D-AP5	(2*R*)-2-Amino-5-phosphonopentanoic acid
DCG-IV	(1R,2R)-3-[(1S)-1-amino-2-hydroxy-2-oxoethyl]cyclopropane-1,2-dicarboxylic acid
DL-TBOA	DL-*threo*-β-Benzyloxyaspartic acid
DS	Direction-selective
DSGC	Direction-selective ganglion cell
EPSC	Excitatory postsynaptic current
GABA	γ-aminobutyric acid
GFP	Green fluorescent protein
HCS	High contrast sensitive
HEX	Hexamethonium
HWHM	Half-width half-max
IPSC	Inhibitory postsynaptic current

Kcng4	Potassium voltage-gated channel modifier subfamily G member 4
LCS	Low contrast sensitive
MPX-004	(5-(((3-chloro-4-fluoropheyl)sulfonamido)methyl)-N-((2-methylthiazol-5-yl)methyl)pyrazine-2-carboxamide).
NBQX	2,3-dioxo-6-nitro-7-sulfamoyl-benzo[f]quinoxaline
NMDA	N-methyl-D-aspartate
OS	Orientation-selective
OSGC	Orientation-selective ganglion cell
SAC	Starburst amacrine cell
TRHR	Thyrotropin releasing hormone receptor
TTX	Tetrodotoxin
UBP-310	(*S*)-1-(2-Amino-2-carboxyethyl)-3-(2-carboxy-thiophene-3-yl-methyl)-5-methylpyrimidine-2,4-dione
Vgat	Vesicular GABA transporter

Acknowledgments

Firstly, I would like to thank my supervisor, Dr. Gautam Awatramani, for his continuous support and mentorship throughout my PhD. Without him this work would not have been possible. I would also like to thank all of the past and present members of the Awatramani lab who have help a tremendous amount along the way. Particularly I would like to thank Dr. Santhosh Sethuramanujam, Dr. Benjamin Murphy-Baum and Dr. Varsha Jain for their support and guidance with techniques, experimental design and data analysis as well as Tracy Michaels for all the viral injections, confocal imaging and mouse colony work.

I would like to thank my supervisory committee, Dr. Kerry Delaney and Dr. Craig Brown for their support and input throughout this project.

Finally, I would also like to thank my family, particularly my parents, for their endless support and my friends who have been there for me from the start. A special thanks to the second-floor biology group for making this journey extra enjoyable.

Chapter 1: Introduction

1.1 The mouse as a model organism

Vision research has been conducted in an array of model organisms such as cat, rabbit, mouse, zebrafish, primate, and many others. Each different model provides unique benefits as well as unique caveats. In this study, mouse retina was used due to the large number of genetic tools available. The use of different combinations of genetic knockouts and knock-ins allowed me to examine complex circuitry in the retina and answer questions that non-specific pharmacology may not be able to address. It also allowed me to target specific cell populations; both visually using GFP expression to target cells as well as functionally using Cre-recombinase to control the expression of different molecular sensors used to study neuronal activity and synaptic transmission.

It has long been thought that rodents had poor visual perception and were therefore poor models for vision research. However, recent advancements in visual and behavioral work have started to question that hypothesis and shown that rodents rely heavily on visual cues for navigation and object recognition and are capable of more advanced visual processing than previously believed (Tafazoli *et al.*, 2017; Storchi *et al.*, 2019).

1.2 The retina

Peripheral sensory systems function mainly as relay circuits; however, the retina is much more complex. Many integrative and processing functions are performed at the level of retina prior to further processing in the cortex. The retina is the most accessible part of the visual system and allows a complex system to be studied while keeping the circuitry intact during ex

vivo retinal preparations. The natural sensory stimulus for the retina is light, therefore studying retinal activity during a variety of different stimulus conditions can be performed and controlled reliably by changing the pattern of light stimuli that is projected onto the intact ex vivo retina. While many of the key features of the retina have been studied extensively, a vast number of unanswered questions remain. With the development of new tools and the advancement in our genetic understanding of the retina we are able to address more complex questions regarding the circuitry and computations occurring across the many different cell types.

1.3 Retinal cell types and organization

The retina is a highly organized cellular structure at the back of the eye that contains five different cell types; they are identified by their distinct locations in the different layers of the retina as well as distinct cellular morphologies. Light travels through the retina to the outer nuclear layer which contains the photoreceptors, the inner nuclear layer contains the bipolar cells as well as the horizontal and amacrine cells, and the ganglion cell layer contains the ganglion cells whose axons travel through the optic nerve to different regions of the brain. Separating each of these three nuclear layers are the outer and inner plexiform layers which contain the synaptic connections between cell types but are devoid of cell bodies (Fig 1.1) (Dowling, 1987).

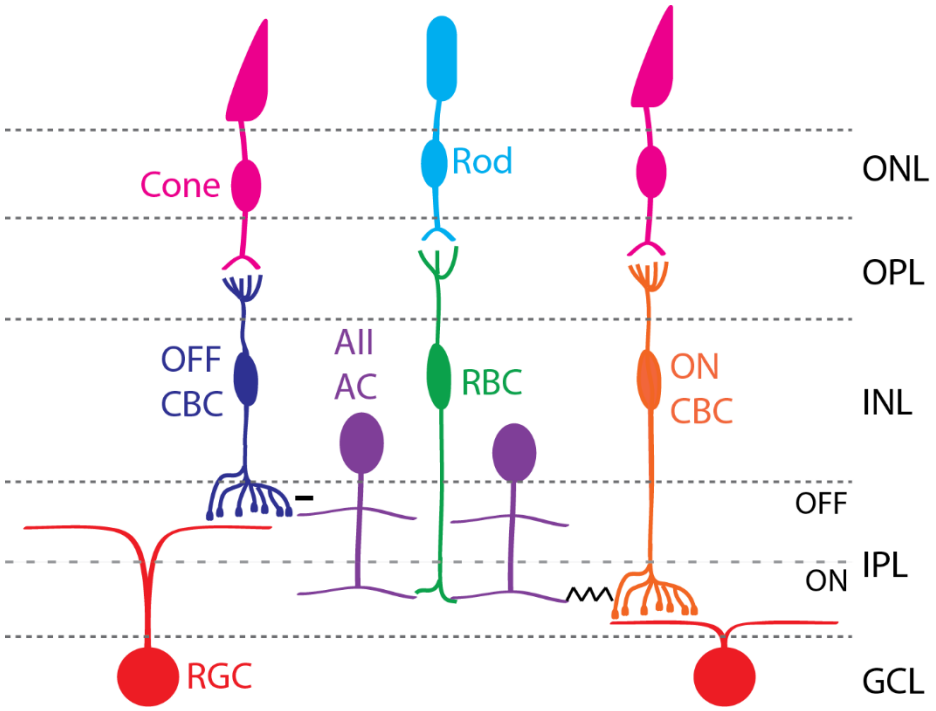

Figure 1.1 Schematic of the retinal circuitry

Photons pass through the retina and are detected by the rod and cone photoreceptors in the outer nuclear layer (ONL). They then transmit that signal to bipolar cells, with rod photoreceptors transmitting to the rod bipolar cells (RBC) and cone photoreceptors transmitting to the cone bipolar cells (CBC). The rod bipolar cells then cross over to the cone pathway via the AII amacrine cell (AC) which provide excitation to the ON cone bipolar cells through electrical gap-junction coupling and inhibition to the OFF cone bipolar cells through glycinergic transmission. The ON and OFF bipolar cells then activate the retinal ganglion cells (RGC). All synaptic transmission from bipolar cells is glutamatergic (OPL = outer plexiform layer, INL = inner nuclear layer, IPL = inner plexiform layer which can be separated into the ON and OFF layers, GCL = ganglion cell layer).

1.3.1 Photoreceptors

The first stage of visual processing begins at the back of the retina, in the outer nuclear layer, where the photoreceptors are located. These cells are known as the transducers of the retina as they convert absorbed photons into neural signals that can be transmitted throughout the retina. There are two types of photoreceptors; rods and cones, which exhibit different light

sensitivities, allowing the retina to process changes in light signals across a wide range of luminance(Farrow *et al.*, 2013). Rod photoreceptors contribute the most to visual processing during dim light conditions (scotopic) and cone photoreceptors during bright light conditions (photopic) (Baylor *et al.*, 1984). Both rod and cone photoreceptors have outer segments that project into the retinal pigment epithelium and express photosensitive opsin proteins which, when activated, cause a phototransduction event. The absorption of photons by photoreceptors causes hyperpolarization of the cell membrane, as opposed to the depolarization that is typically seen during cell activation. Photoreceptors also respond in a graded fashion to changes in light intensity by utilizing ribbon synapses as opposed to relying on all-or-none action potentials to send signals to downstream targets, allowing them to signal varying degrees of change in light intensity in an analogous fashion (Raviola and Gilula, 1973; Heidelberger, Thoreson and Witkovsky, 2005). The inner segment of photoreceptors contains the nucleus and synaptic terminals which make synaptic contacts with excitatory bipolar cells and inhibitory horizontal cells. Photoreceptors also exhibit a high degree of both homologous (cone-cone or rod-rod) and heterologous (cone-rod) electrical coupling through gap-junctions, which are heavily modulated by background light intensities (Bloomfield and Völgyi, 2009; Roy and Field, 2019).

1.3.2 Bipolar cells

At the level of the bipolar cells, the signal from the cone photoreceptors is split into two parallel pathways known as the ON and OFF pathways, which signal light increments or decrements, respectively. In the mouse retina, there are six types of OFF cone bipolar cells and eight types of ON cone bipolar cells (Shekhar *et al.*, 2016). Whether a cone bipolar cell is ON or OFF depends on the glutamate receptors that are expressed in the synaptic cleft, which in turn

determines whether they will be depolarized or hyperpolarized in response to increases in glutamate release from cone photoreceptors (Masland, 2001). ON bipolar cells express the metabotropic glutamate receptor type 6 (mGluR6), this results in a hyperpolarization of the cell in the dark (when the glutamate levels in the synaptic cleft are high) and a depolarization with light onset, when photoreceptors are no longer releasing glutamate. OFF bipolar cells differ in that they express ionotropic AMPA and kainate receptors, which result in a depolarization in the dark when there is increased glutamate release (Fig 1.2).

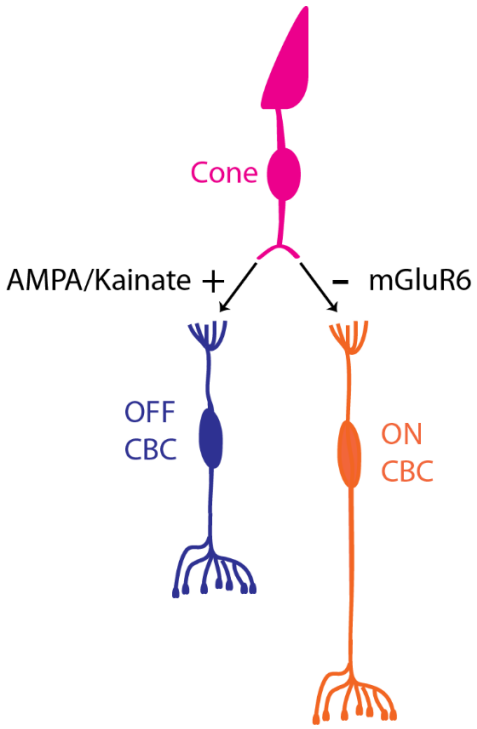

Figure 1.2 Schematic of the signaling from a cone photoreceptor to cone bipolar cells

Cone photoreceptors are glutamatergic, releasing glutamate in dark conditions and decreasing glutamate release upon photon absorption. OFF cone bipolar cells express ionotropic glutamate receptors (AMPA/kainate) which cause a depolarization during glutamate release (light offset). ON cone bipolar cells express metabotropic glutamate receptors (mGluR6) which cause a hyperpolarization during glutamate release (light offset) and a depolarization when there is a decrease in glutamate (light onset).

The signal from the rod photoreceptors is relayed to the rod bipolar cells (Euler and Masland, 2000). In comparison to the cone bipolar cells, the rod bipolar cells do not provide direct contact to most types of amacrine cells or to ganglion cells. Instead, they cross over to the

cone pathway through a specialized amacrine cell (AII) to modulate the ON and OFF cone bipolar cells through either electrical connections or glycinergic inhibitory synapses, respectively (Fig 1.1) (Demb and Singer, 2012). Due to this crossover, the signals to ganglion cells during both dim and bright light conditions (mediated by the rod or cone pathways, respectively) are occurring though the same cone bipolar cell to ganglion cell synapse (Fig 1.2). Similar to photoreceptors, bipolar cells also utilize ribbon synapses to release glutamate in a graded fashion as opposed to the action potential mediated all-or-none mechanism that is classically observed in other neurons (Heidelberger, Thoreson and Witkovsky, 2005).

1.3.3 Amacrine and ganglion cells

Amacrine cells are the most abundant cell type in the retina with between 45-60 different types and are predominantly inhibitory (with some exceptions), providing either GABAergic or glycinergic inhibition to bipolar cell terminals, other amacrine cells and ganglion cells (Yan *et al.*, 2020). The different types are divided into three main groups: wide-field amacrine cells (WAC), medium-field amacrine cells (MACs) and narrow-field amacrine cells (NACs). They can be classified as ON or OFF, depending on their dendritic stratification and can have cell bodies in either the INL or the GCL (displaced amacrine cells).

In the mouse retina, recent studies have estimated that there are up to 45 different types of retinal ganglion cells (Baden *et al.*, 2016; Tran *et al.*, 2019). Ganglion cells receive excitatory glutamatergic input from bipolar cells as well as inhibitory and/or excitatory input from amacrine cells. They can be classified based on their response properties to different visual stimuli as well as genetically and morphologically. Different combinations of inhibitory and excitatory inputs allow the different retinal ganglion cell types to encode different features of the visual scene (see

1.5). Ganglion cells are the projection neurons of the retina, sending their axons through the optic nerve to varying regions of the brain. Because they have to send signals over a long distance, they are also the only class of neurons in the retina in which all types rely on action potentials for signal transduction.

1.4 Neurotransmitters and Receptors in the Retina

In the light detection pathway, the first synapse in the retina is the one between the photoreceptors and the bipolar cells. Because glutamate release from photoreceptors is increased during decreasing light, the signal at this first synapse needs to be inverted before being relayed through the retina. To do this, the ON bipolar cells utilize a metabotropic glutamate receptor, mGluR6, while the OFF bipolar cells utilize ionotropic glutamate receptors (AMPA and/or kainate). Because of this difference in receptor expression between the ON and OFF bipolar cells, different pharmacology can be utilized to block either the ON or OFF pathway in the downstream cells by using an mGluR6 agonist or AMPA and kainate receptor antagonists, respectively.

Bipolar cells are purely glutamatergic, contacting predominantly AMPA receptors on amacrine cells and AMPA and/or NMDA receptors on ganglion cells. However, bipolar cells also have extensive bidirectional electrical coupling with other bipolar cells and amacrine cells. The degree of coupling differs between different bipolar cell types and is mediated via gap-junctions containing either connexin 36 or connexin 45.

Most of the amacrine cells in the retina are predominantly inhibitory, releasing GABA and/or glycine. However, there are also at least two known populations of glutamatergic

amacrine cells (VGlut) and the starburst amacrine cells (SAC) are cholinergic in addition to being GABAergic (Yan *et al.*, 2020). The retina can also be globally modulated via the dopaminergic amacrine cells and the nitric oxide amacrine cells. Dopamine levels in the retina typically follow circadian rhythms with the highest levels being detected during the day or during high light levels. D1 and D2 dopamine receptors are expressed throughout the retina and can modulate gap-junction coupling and regulate voltage-gated channels in a cell type specific way, therefore changing the response properties of the retina based on light levels or time of day (Baldridge, Vaney and Weiler, 1998).

1.5 Feature Selectivity

The retina does not simply relay visual information on a pixel-by-pixel basis but instead breaks up the signals into different visual streams, each relaying different features of the visual scene such as size, colour, contrast, motion, and orientation. Based on the most recent findings, there are approximately 45 different ganglion cell types in the mouse retina, each type relaying different information to the visual areas of the brain. To be able to encode these specific features, different ganglion cells rely on different combinations of synaptic inputs from approximately 60 different types of amacrine cells and 14 different types of cone bipolar cells.

1.5.1 Direction Selectivity

One of the most well studied features that is detected by the rodent retina is direction-selectivity. Direction-selective ganglion cells (DSGCs) respond robustly to motion in a specific (preferred) direction with little to no response to motion in the opposite (null) direction (Barlow, Hill and Levick, 1964; Barlow and Levick, 1965). This direction selectivity relies on precise

GABAergic wiring between the DSGC and SAC. While physiological recordings from SAC somas are non-directional, calcium imaging in starburst dendrites show that individual dendrites are tuned to centrifugal motion (moving from soma to dendritic tip)(Euler, Detwiler and Denk, 2002). Connectomic reconstruction has shown that the SAC dendrites make precise synaptic connections with DSGCs in an asymmetric manner, with the majority of SAC tight synaptic inputs occurring from SAC dendrites oriented along the DSGCs null direction (Briggman, Helmstaedter and Denk, 2011)(see Figure 2.1). Together, this dendritic direction-selectivity and asymmetric wiring results in more inhibition being provided to the DSGC during null direction stimulus, causing a suppression of spiking activity, while preferred direction stimulus results in little inhibition, allowing a large amount of spiking activity. The DSGCs also receive excitatory cholinergic inputs from SACs and glutamatergic excitation from multiple different types of bipolar cells which has been shown to be predominantly symmetric. DSGCs can be divided into three groups based on dendritic stratification: ON DSGCs, OFF DSGCs and ON-OFF DSGCs, which respond to light increments, decrements or both, respectively.

1.5.2 Orientation selectivity

A second prominent feature that is detected through each layer of visual processing is orientation-selectivity, where neurons respond preferentially to objects or edges of a specific orientation (Hubel and Wiesel, 1959). Compared to the DS circuitry, much less is known about the exact circuitry that gives rise to orientation-selectivity in the retina. Two main types of orientation-selective (OS) ganglion cells (OSGCs) have been identified in mouse retina, the horizontal preferring (hOS) and the vertical preferring (vOS) cells (Levick, 1967). While hOS ganglion cells exhibit an elongated dendritic field, which is thought to play a major role in

generating orientation-selectivity, vOS cells do not appear to exhibit this morphological elongation. Instead, vOS cells use a combination of tuned inhibitory and excitatory inputs. Where these inputs originate from is still largely unknown (Nath and Schwartz, 2016, 2017; Antinucci and Hindges, 2018). Orientation-selective amacrine cells have been identified in mouse, rabbit and zebrafish and have been proposed to provide the orientation tuned inhibitory inputs to some types of OSGCs (Bloomfield, 1991, 1994; Murphy-Baum and Taylor, 2015; Antinucci *et al.*, 2016; Nath and Schwartz, 2017). The source of the tuned excitation to vOS ganglion cells is still largely unknown, however, in zebrafish, orientation-tuned glutamate signals have been observed in bipolar cell terminals (Johnston *et al.*, 2019). Overall, it appears that multiple mechanisms are combined to generate a robust orientation tuning in the orientation-selective ganglion cells of the retina, but more research is needed to fully understand how this orientation-selectivity is generated presynaptically.

1.7 Research outline

The aim of this research was to utilize the ON-OFF direction-selective ganglion cell to study both pre- and post-synaptic processing of visual information in the mouse retina. In the first chapter, I investigate the direction selective circuitry at the level of both starburst amacrine and direction-selective ganglion cells and highlight the role of asymmetric connectivity in generating direction selectivity in the retina. Previous research has indicated that DS in DSGCs relies solely on the asymmetric release of GABA from SAC dendrites, however, because the mechanism driving the SAC DS remains unknown, it has been difficult to directly test. Here, I identify parallel mechanisms of SAC DS and develop a technique to render GABA release from

SACs non-DS. Using this technique, I unveil a secondary mechanism of DS in the DSGCs which does not rely on asymmetric GABAergic transmission from SAC dendrites.

In chapter 2 and 3 I investigate the role of excitatory bipolar cell input to the DSGC by looking at the different receptor contributions and the role they play in encoding across contrasts (chapter 2) as well as how presynaptic processing can alter the glutamatergic input to the DSGC (chapter 3). Based on previous findings in our lab, NMDA receptors are responding to glutamate release from bipolar cells independently from AMPA receptors, allowing us to hypothesize the presence of 'silent' NMDA synapses. In chapter 2, I propose three mechanisms that could be mediating the NMDA-only responses then use electrophysiology and 2-photon calcium imaging to confirm the presence of silent, NMDA-only synapses and investigate the abilities for these synapses to encode information across a range of contrasts.

Chapter 3 focuses on the role of bipolar cells in driving orientation-selectivity in a subtype of DSGCs. Previously, OS and DS were thought to be encoded by separate populations of ganglion cells in the retina and the mechanisms driving the ON OS responses remain unknown. Using a combination of pharmacology and genetic manipulation I show that the ON OS detected in a subtype of DSGCs relies on gap-junction coupling at the level of bipolars cells.

Chapter 2: Retinal direction selectivity in the absence of asymmetric starburst amacrine cell responses

Published:

Hanson, Laura*, Sethuramanujam, Santhosh*, deRosenroll, Geoff, Jain, Varsha, Awatramani, Gautam B. 2019. **Retinal direction selectivity in the absence of asymmetric starburst amacrine cell responses'**, *eLife*. DOI: 10.7554/eLife.42392

This work was done in collaboration with Dr. Santhosh Sethuramanujam who performed data collection and analysis for figures 4E-F, 5,6B-C & 7A-F as well as Geoff deRosenroll who performed the computational modeling included in figures 6 and 7. Laura Hanson, Santhosh Sethuramanujam and Gautam Awatramani wrote the manuscript. Preface added for clarity.

2.1 Preface

Previously, it has been shown that direction-selectivity in the mammalian retina requires directionally tuned GABAergic inhibition from starburst amacrine cells (SAC) to direction-selective ganglion cells (DSGC). The mechanisms driving this direction-selectivity at the level of starburst amacrine cell dendrites remains unknown but multiple different mechanisms have been proposed. One of the main mechanisms relies on the reciprocal, SAC-SAC GABAergic inhibition. This model would result in a SAC dendrite receiving both inhibition and excitation close in time and space during motion from dendritic tip to soma (centripetal) resulting in a

shunting of the response while motion from the soma towards the dendritic tip (centrifugal) would result in excitation occurring earlier than the inhibition and evoking a large response. To test this model, I utilized the conditional $GABA_A$ α2 receptor knockout crossed to a ChATcre line to selectively disrupt the inhibition to starburst dendrites while leaving the GABA release from these dendrites intact. Another proposed model relies on the kinetic differences and distribution of the excitatory bipolar cell inputs to the SAC dendrites. In this model, SACs receive more sustained inputs near the soma in the proximal dendritic region and more transient inputs further from the soma in the distal region. This synaptic organization results in a stronger summation of excitatory inputs during centrifugal motion than during centripetal motion. To test this model, I crossed ChR2 with ChATcre to selectivity express ChR2 in SACs which allowed me to remove the bipolar cell inputs and stimulate the SAC directly using optogenetics. Additionally, using these techniques, I can render the SAC output non-DS and investigate the effect on the downstream DSGCs.

2.2 Abstract

In the mammalian retina, direction-selectivity is thought to originate in the dendrites of GABAergic/cholinergic starburst amacrine cells, where it is first observed. However, here we demonstrate that direction selectivity in downstream ganglion cells remains remarkably unaffected when starburst dendrites are rendered non-directional, using a novel strategy combining a conditional $GABA_A$ α2 receptor knockout mouse with optogenetics. We show that temporal asymmetries between excitation/inhibition, arising from the differential connectivity patterns of starburst cholinergic and GABAergic synapses to ganglion cells, form the basis for a parallel mechanism generating direction selectivity. We further demonstrate that these distinct

mechanisms work in a coordinated way to refine direction selectivity as the stimulus crosses the ganglion cell's receptive field. Thus, precise spatiotemporal patterns of inhibition and excitation that determine directional responses in ganglion cells are shaped by two 'core' mechanisms, both arising from distinct specializations of the starburst network.

2.3 Introduction

The direction-selective (DS) circuit in the retina is arguably one of the most well-defined circuits in the mammalian brain (Vaney, Sivyer and Rowland Taylor, 2012; Mauss *et al.*, 2017). In this circuit, direction is encoded by output DS ganglion cells (DSGCs), whose response properties are shaped by DS inputs arising from GABAergic/cholinergic starburst amacrine cells (starbursts) and non-DS inputs from glutamatergic bipolar cells (Figure 2.1 A). However, despite comprehensive connectomic analysis of the circuit (Briggman, Helmstaedter and Denk, 2011; Ding *et al.*, 2016) and many decades of physiological investigations, the fundamental mechanisms underlying direction selectivity, both at the level of starbursts and DSGCs remain to be fully elucidated.

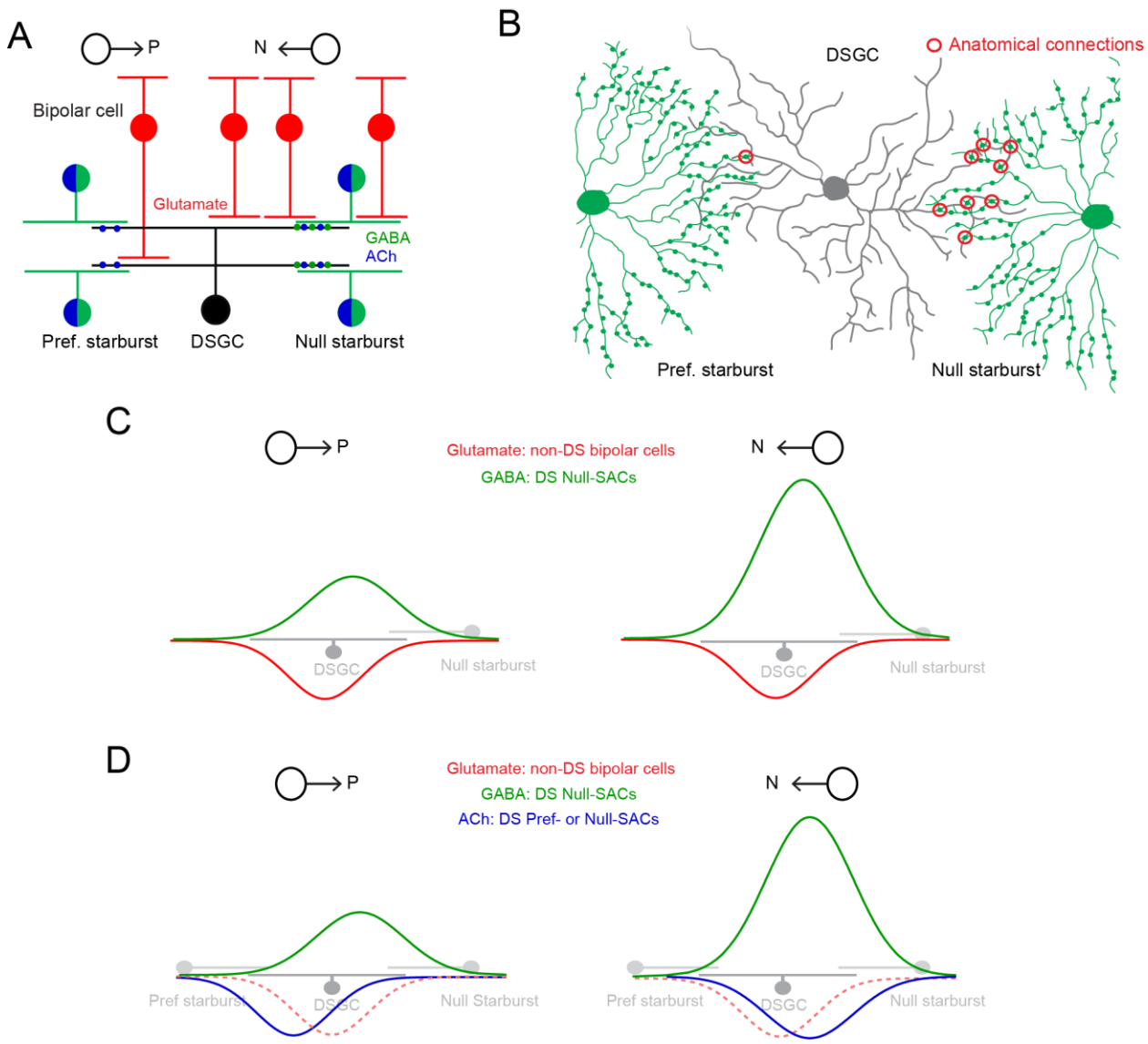

Figure 2.1 Parallel 'core' mechanisms generating direction selectivity in DSGCs

(**A**) A cross section of the functional circuitry underlying direction selectivity in ON-OFF DSGCs. DSGCs receive glutamatergic inputs from ON and OFF bipolar cells, and inputs from mirror symmetric populations of ON and OFF GABAergic/cholinergic starburst amacrine cells. In this study, the stimuli used emphasized the ON responses. Preferred-side starbursts (p-starburst) provide mainly cholinergic excitation, while null-side starbursts (n-starburst) provide cholinergic excitation and a dominant GABAergic inhibition (Lee, Kim and Zhou, 2010; Yonehara *et al.*, 2011). Thus, GABAergic/cholinergic signals mediated by starbursts are differentially transmitted to the DSGC. (**B**) Schematic depicting the asymmetric anatomical connectivity between starbursts and DSGCs (top view). *Bona fide* 'wrap-around' synaptic connections (circled in red) are made largely by null-side starbursts, enabling DS dendrites of starbursts to mediate a 'null' inhibition (Briggman, Helmstaedter and Denk, 2011). This contrasts with the symmetrical functional cholinergic connectivity depicted in (**A**). Paracrine or 'volume' transmission could make cholinergic signals agnostic to the specific synaptic

connectivity (Briggman, Helmstaedter and Denk, 2011; Brombas, Croft and Williams, 2017). (**C**) In conventional models, direction selectivity in DSGCs is largely shaped by asymmetric postsynaptic GABAergic inhibition. Asymmetric inhibition is contingent on the DS release of GABA from dendrites of starbursts; and on the asymmetric wiring (**B**). By contrast, excitation is non-directional, mainly mediated by glutamate released from bipolar cells (Yonehara *et al.*, 2013; Park *et al.*, 2014). In this model, the cholinergic receptive field is co-extensive with the glutamatergic receptive field. ACh is usually thought to play a non-directional role (Ariel and Daw, 1982; Amthor, Grzywacz and Merwine, 1996; Chiao and Masland, 2002; Park *et al.*, 2014), although some studies note amplitude differences between preferred and null-evoked cholinergic currents (as shown here) suggesting that ACh may directly contribute to direction selectivity (Lee, Kim and Zhou, 2010; Pei *et al.*, 2015). (**D**) In the revised model proposed here, cholinergic excitation is directional by virtue of its timing with GABAergic inhibition rather than by its response amplitude (**C**). The differences in the functional connectivity of GABA and ACh (**A**) predict that for preferred-direction motion, excitation would lead inhibition; and for null-direction motion, E/I would be activated together. In this study, the central hypothesis is that E/I offsets contribute to a parallel DS mechanism, which does not necessarily rely on the modulation of the peak amplitude of GABA or ACh inputs (in contrast to the model shown in **C**)

The first points in the visual system where direction selectivity is observed are the radiating dendrites of starbursts (Euler, Detwiler and Denk, 2002), which release GABA and acetylcholine (ACh) (O'Malley and Masland, 1989). To explain direction selectivity, initial studies emphasized mechanisms that were based on intrinsic properties of starburst dendrites (Tukker, Taylor and Smith, 2004; Gavrikov *et al.*, 2006; Hausselt *et al.*, 2007). In contrast, more recent studies have proposed two distinct network mechanisms. The first relies on inhibition within the dense array of starburst cells, where dendrites of neighboring starbursts with opposite directional preferences mutually inhibit each other. This ensures that dendrites pointing in a particular direction are maximally activated as the moving stimulus sequentially activates the starbursts (Lee and Zhou, 2006; Münch and Werblin, 2006; Ding *et al.*, 2016). The second network mechanism relies on the specific wiring of temporally distinct bipolar cells along the proximal-distal axis of the starburst dendrite. This arrangement results in an optimal summation of inputs when the stimulus moves centrifugally (from soma-to dendrite) along the starbursts

dendrites (Kim *et al.*, 2014; Fransen and Borghuis, 2017). When tested experimentally, however, neither of these mechanisms appears to be critically required for generating DS, at least in the context of simple spot/grating stimuli (Chen *et al.*, 2016; Sethuramanujam *et al.*, 2016).

Starbursts play an obligatory role in generating direction selectivity in downstream DSGCs (Yoshida *et al.*, 2001; Vlasits *et al.*, 2014). They provide the neural substrate for a powerful GABAergic 'null' inhibition that is required for the generation of DS responses in ganglion cells (Figure 2.1 C). Null inhibition relies on both the DS properties of starburst dendrites and also a specific 'anti-parallel' wiring scheme (Figure 2.1 B). Only starbursts with somas displaced to the null-side of the DSGC's receptive field (i.e. the side from which null-stimuli enter the receptive field) make synaptic connections with DSGCs (Fried, Munch and Werblin, 2002; Lee, Kim and Zhou, 2010; Briggman, Helmstaedter and Denk, 2011; Yonehara *et al.*, 2011; Chen *et al.*, 2016; Brombas, Croft and Williams, 2017). By contrast, excitatory inputs to DSGCs arising from bipolar cells are non-DS (Yonehara *et al.*, 2013; Park *et al.*, 2014). Together, these findings have given rise to a well-accepted model in which direction selectivity in DSGCs is largely inherited from starburst dendrites, contingent on the DS release of GABA (Figure 2.1 C) (reviewed by Vaney, Sivyer and Rowland Taylor, 2012; Mauss *et al.*, 2017).

However, in addition to GABA, starbursts also co-release ACh (O'Malley and Masland, 1989), which mediates fast excitatory postsynaptic currents (EPSCs) in DSGCs via the activation of nicotinic ACh (nACh) receptors (Lee, Kim and Zhou, 2010; Taylor and Smith, 2012; Pei *et al.*, 2015; Sethuramanujam *et al.*, 2016; Brombas, Croft and Williams, 2017). Unlike GABA, however, cholinergic signals appear to be more symmetrical at the level of DSGCs, giving rise to the notion it modulates the amplitude of DSGC responses (Ariel and Daw, 1982; Amthor,

Grzywacz and Merwine, 1996; Chiao and Masland, 2002; Park *et al.*, 2014). Recent voltage-clamp recordings on the other hand, reveal amplitude differences between preferred and null-evoked cholinergic currents (Figure 2.1 C), suggesting that ACh may directly contribute to direction selectivity (Lee, Kim and Zhou, 2010; Pei *et al.*, 2015). However, the mechanisms underlying DS cholinergic excitation remain unknown.

Elegant starburst/DSGC paired recordings demonstrate that cholinergic inputs arise from starbursts surrounding DSGCs from all directions, in sharp contrast to GABA inputs (Figure 2.1 A) (Lee, Kim and Zhou, 2010; Yonehara *et al.*, 2011; Chen *et al.*, 2016; Brombas, Croft and Williams, 2017). Given the asymmetric anatomical wiring of the starbursts and DSGCs (Figure 2.1 B), it is presumed that cholinergic excitation is mediated by paracrine mechanisms that are agnostic to the specific connectivity (Briggman, Helmstaedter and Denk, 2011; Brombas, Croft and Williams, 2017). Building on these findings, in this study we hypothesized that the differential functional connectivity of spatially offset GABA and ACh signals produces excitation-inhibition (E/I) timing differences that generate direction selectivity, as originally envisioned (Torre and Poggio, 1978; Koch, Poggio and Torre, 1982; Taylor *et al.*, 2000). This could serve as a parallel 'hard-wired' DS mechanisms that does not necessarily require DS starburst output (Figure 2.1 D).

It is important to note that temporal E/I asymmetries have often been noted in the literature, but their impact has been difficult to assess, as they are always associated with changes in E/I amplitude ratio (Figure 2.1 D) (Taylor and Vaney, 2002; Fried, Mu and Werblin, 2005; Kostadinov and Sanes, 2015; Pei *et al.*, 2015; Sethuramanujam *et al.*, 2016). Further, blocking cholinergic inputs, which is expected to decrease E/I timing differences arising from the

above-mentioned specific wiring of starburst ACh/GABA synapses (Figure 2.1 D), does not appear to affect the ability of DSGCs to encode direction (Ariel and Daw, 1982; Kittila and Massey, 1997). It has also been shown that robust direction selectivity is observed in instances where E/I temporal offsets are not apparent (Taylor and Vaney, 2002). Additionally, modeling studies suggest that E/I temporal offsets play a negligible role in this computation in the context of the E/I amplitude modulation (Schachter *et al.*, 2010). Thus, the contribution of E/I temporal offsets to direction coding by DSGCs are generally neglected.

Here, we describe two major advancements that better our understanding of the DS circuitry in the mouse retina. First, using a novel combination of optogenetics/mouse KO technology/pharmacology, we render starburst output non-DS for the first time. This provides valuable insights into the biophysical mechanisms underlying direction selectivity in starburst dendrites. Second, we found that blocking starburst DS had a surprisingly weak effect on direction selectivity in ganglion cells. This demonstrates the existence of a second 'core' DS mechanism, which we demonstrate relies on E/I temporal offsets. Interestingly, while changes in E/I ratios or timing differences are each sufficient to drive robust DS responses in ganglion cells, these mechanisms contribute to distinct phases of the DSGC response, ensuring that direction is computed rapidly and with high fidelity.

2.4 Methods

2.4.1 Animals

Experiments were performed using adult (either sex) Trhr-EGFP (RRID: MMRRC_030036-UCD) or ChAT-IRES-Cre (RRID: MGI_5475195) crossed with Ai32 (RRID: MGI_5013789) with or without Gabra2$^{tm2.2Uru}$ (RRID: MGI_5140553). All procedures were performed in accordance with the Canadian Council on Animal Care and approved by the University of Victoria's Animal Care Committee.

2.4.2 Physiological Recordings

Mice were dark-adapted for approximately 30–60 min before being briefly anesthetized and decapitated. The retina was extracted and dissected in Ringer's solution under infrared light. The isolated retina was then mounted on a 0.22 mm membrane filter (Millipore) with a pre-cut window to allow light to reach the retina, enabling the preparation to be viewed with infrared light using a Spot RT3 CCD camera (Diagnostic Instruments) attached to an upright Olympus BX51 WI fluorescent microscope outfitted with a 40× water-immersion lens (Olympus Canada). The isolated retina was then perfused with warmed Ringer's solution (35–37 °C) containing 110 mM NaCl, 2.5 mM KCl, 1 mM $CaCl_2$, 1. 6 mM $MgCl_2$, 10 mM dextrose and 22 mM $NaHCO_3$ that was bubbled with carbogen (95% O_2:5% CO_2).

DSGCs were identified by their genetic labeling or by their characteristic DS responses. Light stimuli, produced using a digital light projector (Hitachi Cpx1, refresh rate 75 Hz), were focused onto the outer segments of the photoreceptors using the sub-stage condenser. The background luminance, measured with a calibrated spectrophotometer (Ocean Optics), was set to ~10

photoisomerisations/s (R*/sec). Visual stimuli created in the Matlab environment (Psychtoolbox) were of positive contrasts, ranging between 15% and 1,000% (Weber contrast). Stimulus intensity was increased by 5 log units using neutral density filters to stimulate starburst-ChR2. Light-evoked activity was measured for 200 µm spot moving in eight directions at 1-1.6 mm/s.

Spike recordings were made with the loose cell-attached patch-clamp technique using 5–10-MΩ electrodes filled with Ringer's solution. Voltage-clamp whole-cell recordings were made using 4–7-MΩ electrodes containing 112. 5 mM CH3CsO3S, 7. 75mM CsCl, 1 mM MgSO4, 10 mM EGTA, 10 mM HEPES, 5 mM QX-314 (Tocris) and 100 µM spermine (Abcam Biochemicals). The pH was adjusted to 7.4 with CsOH. The reversal potential for chloride was calculated to be –56 mV. The recordings were not corrected for junction potential. Recordings were made with a MultiClamp 700B amplifier (Molecular Devices). Signals were digitized at 10 kHz (PCI-6036E acquisition board, National 9 Instruments) and acquired using custom software written in LabVIEW developed by Dr. David Balya (Friedrich Miescher Institute, Switzerland; https://github.com/GBAlab/Presentinator). Unless otherwise noted, all reagents were purchased from Sigma-Aldrich Canada. D-AP5, and UBP310 were purchased from ABCAM Biochemicals. DL-AP4, SR-95531 and CNQX were purchased from Tocris.

2.4.3 Computational Modeling

Here we modified a detailed multi-compartmental model that was built previously by Poleg-Polsky and Diamond (2016) in the NEURON simulation environment (https://github.com/geoffder/Spatial-Offset-DSGC-NEURON-Model). This model was based on a morphological reconstruction of a real DSGC (Poleg-Polsky and Diamond, 2016), with

membrane capacitance and axial resistance set to 1 μF/cm2 and 100 Ωcm respectively. Membrane channels and noise were modelled using a stochastic Hogkin and Huxley distributed mechanism (NEURON MOD file) as previously descried. Non-voltage-gated leak conductances were set to reverse at -60mV. Active membrane conductances were placed at the soma, primary dendrites and dendrites with the following densities (mS/cm^2) for soma, primary and terminal dendrites respectively: sodium (150/150/30), potassium rectifier (70/70/35), delayed rectifier (3/0.8/0.4). Sodium and potassium conductances were blocked for voltage-clamp recordings. This enabled the model DSGC to process inputs actively i.e. via dendritic spikes (Sivyer et al., 2013).

In our model DSGC, synapses were placed on terminal dendrites throughout the dendritic arbor. Synapses housed glutamatergic (AMPA receptor), cholinergic (nicotinic receptor) and GABAergic ($GABA_A$ receptor) synaptic inputs, whose kinetic properties were based on experimentally measured miniature events. Synaptic inputs were activated by a simulated bar moving over the model DSGC in 8 directions at 1mm/s. Cholinergic inputs were symmetrical across the simulated directions, with their probabilities of release (Pr) set at 0.5. Cholinergic inputs were also spatially offset by ~50 μm (corresponding to an E/I temporal offset of 50ms for preferred stimuli moving at 1mm/s), and for simplicity modeled based on fast modes of transmission, (similar to AMPA) rather paracrine transmission (see Discussion). AMPA receptor-mediated inputs were modelled to occur without any offset relative to their position on the DSGC's dendritic arbour. Thus they were simply activated on average (Pr ~ 0.5) when the simulated light stimulus passed over their synapse location. By contrast, GABAergic inhibitory inputs were made highly asymmetric, their Pr scaling down from ~0.5 in the null to ~.012 in the preferred direction to simulate control conditions; or Pr was set constant at 0.5 to simulate

conditions in which the starburst dendrites were non-DS. Their spatial offset ranged from ~50 µm in the null to ~0 µm in the preferred direction. The precise values across direction were estimated using sigmoidal fits to the tuning curves of the IPSCs (Sethuramanujam et al., 2016) and E/I temporal offsets measured experimentally (Figure 2.4):

$Pr = pPr + (nPr - pPr) * (1.0 - 0.98/(1.0 + e^{(angle - 91.0)/25.0}))$

$spatial\ offset = pOff - (pOff - nOff) * (1.0 - 0.98/(1.0 + e^{(angle - 74.69)/24.36}))$

Where, pPr, nPr refer to the probabilities of release in preferred and null directions, respectively. pOFF, nOFF refer to the spatial offsets in preferred and null directions, respectively; and angle refers to the direction of stimulated bar stimulus motion (0° is preferred, and 180° is null). Spatial offsets were then divided by the stimulus velocity to arrive at the final temporal offset. Importantly, the sequential activation of synapses by a moving bar stimulus, produced macroscopic inhibitory and excitatory currents are well-matched to those measured experimentally using whole-cell patch-clamp techniques (Figure. 2.7; supplementary figure 1).

2.4.4 Quantification and statistical analysis

DSI was calculated as (Taylor and Vaney 2002):

$$DSI = \frac{\sum v_i}{\sum r_i}$$

where v_i are vectors pointing in the direction of the stimulus and having length r_i, equal to the number of spikes recorded during that stimulus. DSI ranged from 0 to 1, with 0 indicating a perfectly symmetrical response, and 1 indicating a response in only one of eight directions. The angle was calculated from the direction of the resultant of Σv_i.

The E/I temporal offset window was calculated with the following protocol. First, the 20-80% rise time of the synaptic currents (EPSCs or IPSCs) was fit by a straight line (Figure 2.4). The response onset latency was measured as the point at which the extrapolated linear fit crossed the x axis (time axis). The E/I temporal offsets were calculated as difference in the excitatory and inhibitory onsets. Positive offsets indicate that excitation leads inhibition and vice versa. For the purposes of estimating DSI, negative offsets were set to 0.

In order to determine the early and peak spike responses (Figure 2.7), the spike trains in control conditions were aligned to the edge of the glutamate receptive field, measured either by the spike activity or EPSCs in glutamate isolation i.e. in cholinergic and GABA receptor antagonists (Figure 2.7A). After alignment, the number of spikes occurring before the stimulus entered the glutamate receptive field (~50ms in the preferred direction) was considered as the early phase responses. These spikes were completely blocked by cholinergic receptor antagonists (Figure 2.7A, Figure 2.7 – Figure Supplement 1). The peak phase was estimated as a ~50 ms region close to the peak firing rate in the preferred direction (Figure 2.7A).

Population data have been expressed as mean ± SEM and are indicate in the figure legend along with the number of samples. Student's t test was used to compare values under different conditions and the differences were considered significant when $p \leq 0.05$, unless otherwise noted in the figure legend.

2.5 Results

2.5.1 Rendering starburst dendrites non-directional

We first sought to develop ways to abolish direction selectivity in starburst dendrites to test its contribution to direction selectivity in the postsynaptic DSGCs. Previous attempts to perturb DS in starburst dendrites have been met with little success. For example, selectively eliminating mutual inhibition between anti-parallel starburst dendrites using the $GABA_A$ α2 receptor KO mouse line (*Gabra2* KO) leaves starburst DS largely intact (Chen *et al.*, 2016). Consistent with these findings, we found the DS output of the starbursts measured as inhibitory postsynaptic currents (IPSCs) in DSGCs, was similar in *Gabra2* KO mice and wild type mice. This was quantified using a direction selectivity index (DSI; calculated as the normalized vector sum of responses measured across eight directions; Wt = 0.33 ± 0.019, n = 6; KO = 0.28 ± 0.022; n = 6; data are presented as mean ± SEM; Figure 2.2 A,B,E,F).

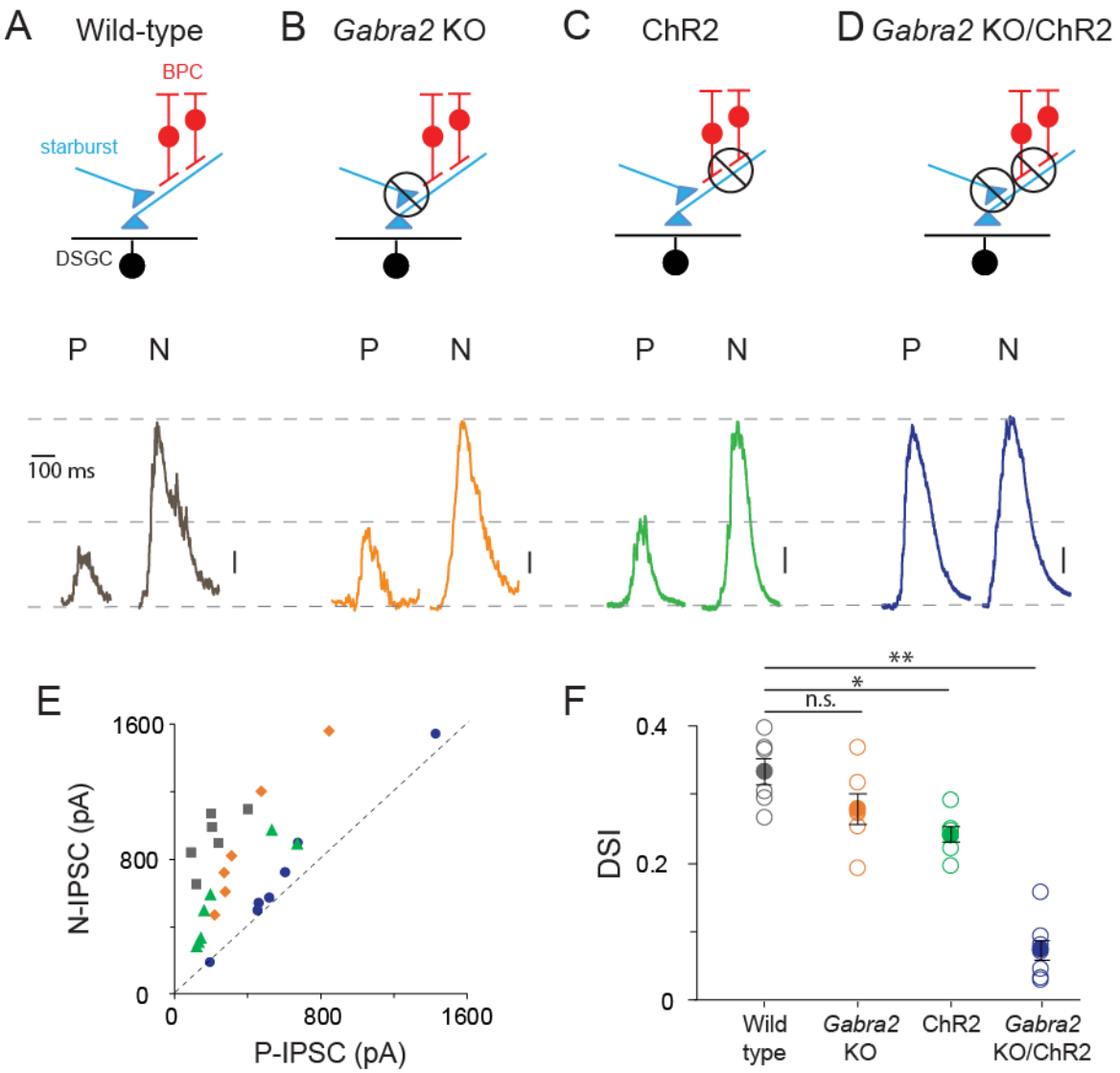

Figure 2.2 Direction selectivity in starburst dendrites relies on both excitatory and inhibitory network mechanisms

(**A**–**D**) Starburst output monitored as IPSCs in voltage-clamped DSGCs (V_{HOLD} ~0 mV) in a variety of mouse lines (as indicated). For simplicity, only ON IPSCs are shown for stimulus motion in the DSGC's preferred (P) or null-direction (N) under conditions in which (**A**) all synaptic inputs are intact; (**B**) mutual inhibition between starbursts is selectively disrupted using the conditional *Gabra2* KO; (**C**) bipolar cell inputs are blocked and ChR2-expressing starbursts are directly stimulated; (**D**), both mutual inhibition and bipolar cell inputs are blocked. Vertical scale bar = 100 pA (**A**–**C**) or 200 pA (**D**). Responses are averaged over three trials. (**E**) The peak amplitudes of the IPSCs evoked during preferred- and null-direction motion are plotted against each other for the conditions noted in (**A**–**D**). A reference line with slope = 1 (dashed line) is shown to facilitate comparisons. n = 6 for wild type, *Gabra2* KO and ChR2; n = 7 for *Gabra2* KO/ChR2. (**F**) The average direction-selectivity index (DSI) computed from the normalized vector sum of the peak amplitude of IPSCs evoked by stimuli moving in eight

directions, for the conditions in (**A**–**D**) (See Materials and methods for DSI calculation; DSI = 0 indicates non-directional responses; DSI = 1 indicates strongly tuned responses). Pooled data are represented as mean ± SEM (Solid circles), while single cell responses are denoted by open circles. Statistical significance was estimated by unpaired t-tests, where *, ** or n.s. indicate p=0.0026, 0.0001 and 0.1068, respectively

Arguing against excitatory network mechanisms (Kim *et al.*, 2014; Fransen and Borghuis, 2017), robust DS output was observed in the absence of bipolar cell input, when the starbursts were directly stimulated using optogenetics (Figure 2.2 C, E & F) (Sethuramanujam *et al.*, 2016). In these experiments, photoreceptor/bipolar cell driven responses were blocked using conventional pharmacology (50 µM DL-AP4, 10 µM UBP310 and 20 µM CNQX) and the stimulus intensity was increased 1000-fold (R*/s) to directly activate starburst-expressing channelrhodopsin2 (ChR2) in relative isolation. While there was considerable variability in the amplitude of IPSCs, which may have arisen from variable expression of ChR2 and/or run down of optogenetic responses over the course of the recording session (which could last up to 8 hr), within a given cell the responses and their direction selectivity remained reliable between trials. We thus included weaker responding cells in this analysis.

Remarkably, combining these two approaches to block both inhibitory and excitatory network DS mechanisms, led to the near-complete block of the asymmetry in responses mediated by starburst cells, i.e. the amplitudes of inhibitory inputs evoked by optogenetic stimulation of starbursts in the *Gabra2* KO background were nearly equal for preferred and null-direction motion (DSI = 0.07 ± 0.02, n = 7; Figure 2.2 D–F). The ability to block direction selectivity in starbursts, while leaving its output relatively intact, provides for the first time direct evidence for the mechanisms generating it. The requirement to block both the excitatory (Kim *et al.*, 2014; Fransen and Borghuis, 2017) and inhibitory network mechanisms (Lee and Zhou, 2006; Münch

and Werblin, 2006; Ding *et al.*, 2016) suggest that they work in parallel to shape DS responses in starburst dendrites.

2.5.2 Retinal direction selectivity in the absence of asymmetric starburst amacrine cell responses

Abolishing the directional properties of starbursts is expected to suppress the output of DSGCs, as under these conditions DSGCs would receive strong inhibition in all directions. Contrary to this notion, we found that DSGCs in *Gabra2* KO mice continued to exhibit robust spiking responses when starburst output was rendered non-DS (Figure 2.3 A). Strikingly, these spiking responses were robustly tuned for direction similar to control conditions (Figure 2.3 B–D). While the direction encoded was the same under conditions in which starburst output was DS or non-DS (Figure 2.3 A), we did observe a significant reduction in the duration of the DSGC's spiking response (Figure 2.3 A). Since starbursts are critically required for DS computation (Yoshida *et al.*, 2001; Vlasits *et al.*, 2014), it follows that they must utilize an alternate mechanism to confer direction selectivity upon DSGCs, in the absence of amplitude modulation of inhibitory inputs. In addition, the finding that the direction tuning properties of the DSGC remains unchanged when starburst output is rendered non-DS (Figure 2.3 B,D), indicates that this second DS mechanism is well-aligned to the classical mechanism relying on the direction selectivity of starburst dendrites.

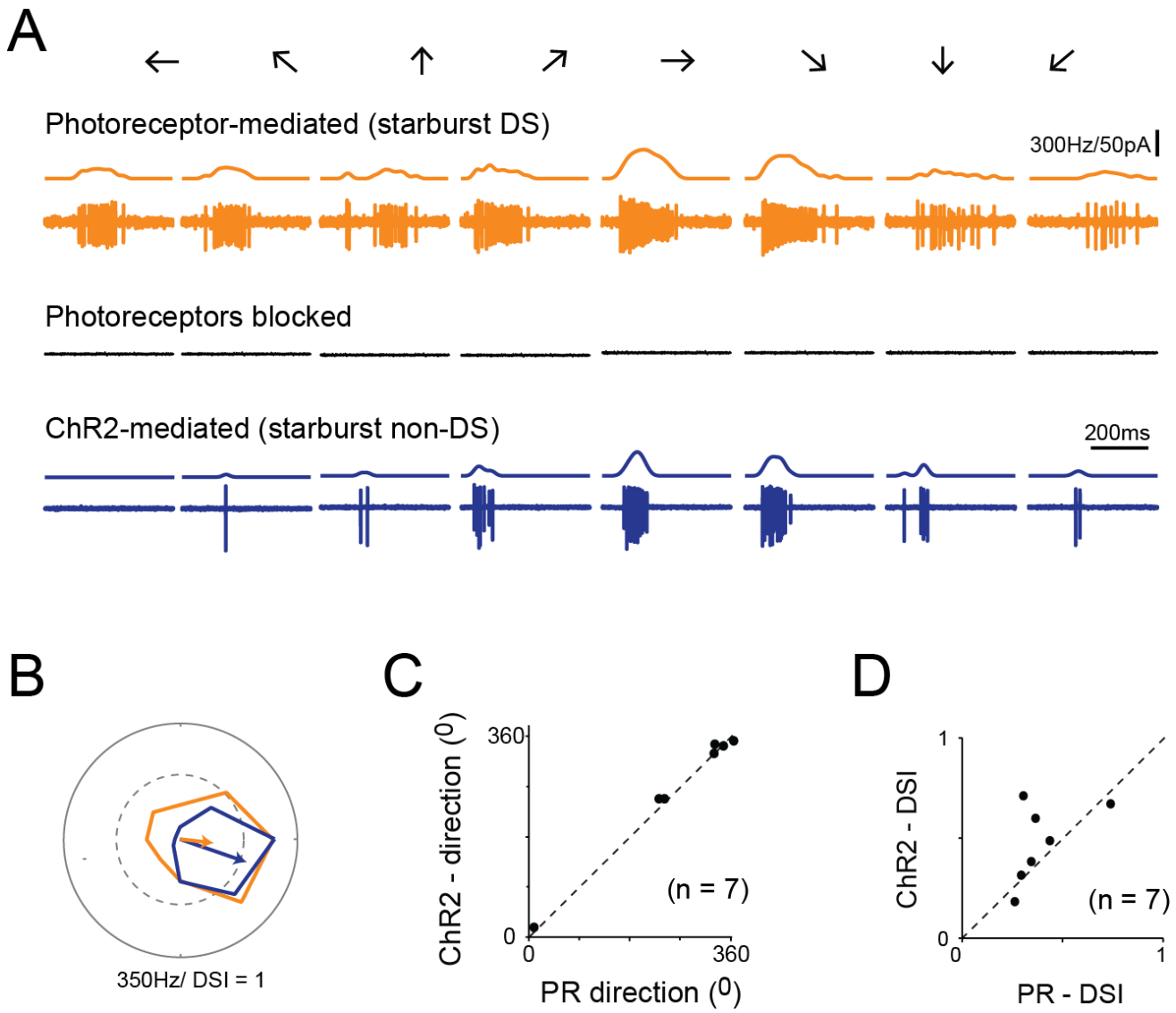

Figure 2.3 Retinal direction selectivity in the absence of asymmetric starburst amacrine cell responses

(**A**) Spiking responses from a DSGC in the *Gabra2* KO/ChR2 mouse line measured under conditions when photoreceptor (PR) output is intact (*top*), when photoreceptor synapses are blocked pharmacologically (50 µM DL-AP4, 10 µM UBP310 and 20 µM CNQX (*middle*)), and subsequently, when stimulus intensity is increased to directly activate starbursts using ChR2 (*bottom*). This enables a direct comparison of direction selectivity in a DSGC under conditions in which starburst output is DS (*top*) or non-DS (*bottom*). Stimuli were moved in eight directions indicated by the arrows at a velocity of 1200 µm/s. The smooth traces on top of each spike train indicates the average spike rate estimated by low-pass filtering the spike train via convolution with a Gaussian kernel (σ = 25 ms). (**B**) Polar plots of the peak spike rates for the responses in the two conditions shown in (**A**). The arrow indicates the DSGC's preferred direction, scaled to the DSI. (**C**–**D**) A comparison of the preferred direction (**C**) and DSI (**D**) of the responses

evoked during ChR2 stimulation, and during intact photoreceptor stimulation in the *Gabra2* KO/ChR2 mouse line (n = 7)

We hypothesized that asymmetries in the timing of excitation and inhibition arising from the differential functional starburst-DSGC connectivity gives rise to a parallel DS mechanism (Figure 2.1 D). When we examined the onset latencies for GABA and ACh in the *Gabra2* KO, we found E/I temporal offsets were exquisitely tuned for direction (Figure 2.4 A–D). The magnitude of the offsets provided a good indication of the DSGC's preferred-direction when compared to its spiking responses measured prior to the voltage-clamp experiments (Figure 2.4 B–D). These results provided strong evidence that temporal asymmetries in E/I onsets alone can drive direction selectivity in ganglion cells. Moreover, since temporal asymmetries are observed under conditions in which photoreceptor/glutamate receptors are blocked, it indicates that they arise from the starburst network itself, through a differential functional connectivity of cholinergic/GABAergic synapses to DSGCs (Figure 2.1 B,D).

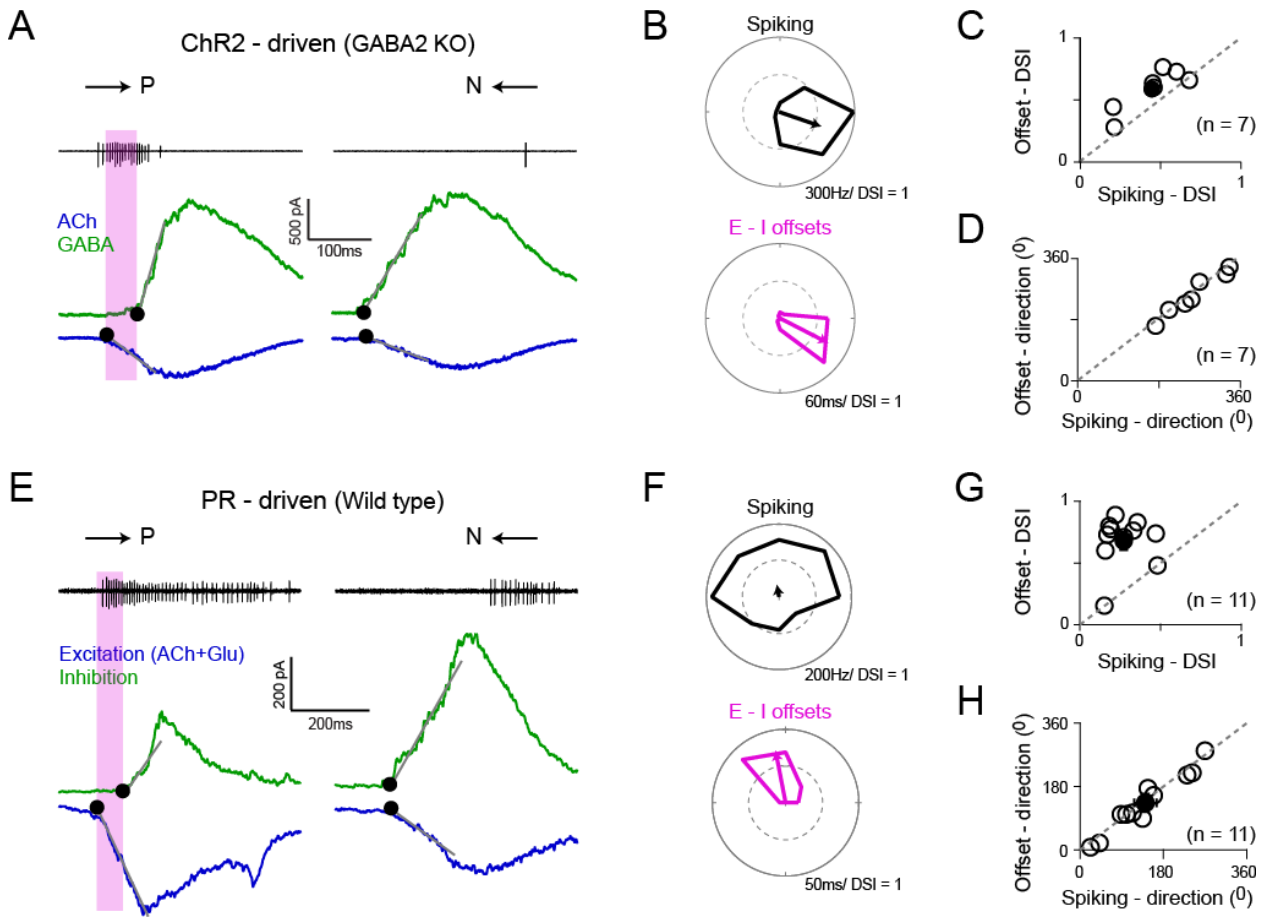

Figure 2.4 Directionally tuned E/I temporal offsets maintain direction selectivity in DSGCs in the absence of asymmetric starburst responses

(**A**) Optogenetically evoked spikes, EPSCs and IPSCs recorded in succession from the same DSGC in the *Gabra2* KO/ChR2 mouse line (in the absence of photoreceptor input). The onset of excitation and inhibition (indicated by ●), was estimated by back extrapolating the lines of best fit of the initial response (grey lines; see Materials and methods). The shaded box indicates the E/I temporal offset window during which a large fraction of the spikes appear to be generated. (**B**) Polar plots of the peak firing rates (*top*) and E/I temporal offsets (*bottom*) for optogenetic responses (depicted in **A**) to eight stimulus directions. **C–D**, A comparison of the DSI (**C**) and direction coded (**D**) estimated from the peak firing rates or E/I temporal offsets (as shown in **B**) across 7 cells (open circles). Pooled data (closed circles) are represented as mean ± SEM. (**E–H**) Similar to **A–D** but for responses measured under physiological conditions i.e. responses driven by photoreceptors in the wild-type retina (n = 11). The DSI of the E/I temporal offsets was higher than the DSI of spiking ($p<0.001$). Pooled data are represented as mean ± SEM.

2.5.3 Differential transmission of Ach/GABA under physiological conditions

Temporal asymmetries were also observed under natural conditions, i.e. when responses were driven by photoreceptors (Figure 2.4 E–H), consistent with previous studies (Fried, Munch and Werblin, 2002; Taylor and Vaney, 2002; Kostadinov and Sanes, 2015; Pei *et al.*, 2015; Sethuramanujam *et al.*, 2016). Similar to the optogenetic experiments, the magnitude of the E/I temporal offsets measured under physiological conditions (i.e. photoreceptor mediated) was greatest for preferred-direction motion and progressively decreased as the stimulus direction approached the DSGC's null-direction (Figure 2.4 F). In these experiments, superior coding DSGCs were excluded from the analysis, since in these ganglion cells gap junctions are known to drive early excitatory inputs (Trenholm *et al.*, 2013). The E/I temporal offset tuning was significantly sharper when compared to the tuning of the spiking responses, as indicated by the DSI (Figure 2.4 G). In a later section, we use modeling to show that this difference arises because the DS spiking responses are shaped by two distinct mechanisms with different tuning properties (Figure 2.7). By contrast, the predicted direction based on offsets were almost perfectly aligned with the direction encoded based on the spiking responses (Figure 2.4 H).

Consistent with the notion that E/I temporal offsets arise from a differential transmission of ACh/GABA (Figure 2.1 D), blocking nicotinic ACh (nACh) receptors using a specific antagonist (100 μM hexamethonium) increased the onset latency for excitation evoked by motion in the preferred-direction, and largely abolished the E/I temporal offsets in this direction (Figure 2.5 A). For null-direction motion, blocking these receptors resulted in a negative offset, as the GABAergic inhibition arising from null-side starbursts was no longer balanced by cholinergic inputs but continued to arrive before glutamate inputs (Figure 2.5 A). Further

blocking GABAergic inhibition did not alter the delay induced by blocking nACh receptors, indicating that the E/I temporal offset estimates were not confounded by voltage-clamp errors associated with large inhibitory conductances (Figure 2.5—figure supplement 1) (Poleg-Polsky and Diamond, 2011). Plotting the E/I temporal offsets for all stimulus directions reveals that hexamethonium uniformly reduces the E/I temporal offsets by ~25 ms (average delay = 26 ± 2 ms; n = 8) regardless of direction (Figure 2.5 B,C), consistent with the idea that starbursts make cholinergic connections from all around the DSGC (Figure 2.1 D). Given the stimulus moved at 1000 μm/s, this corresponds to a spatial offset of ~25 μm (see Discussion). It is also worth noting that, both ACh and GABA signals arising from starburst dendrites are spatially offset relative to glutamate inputs (Figure 2.1 B,D), unlike the co-extensive glutamatergic/cholinergic receptive fields observed in rabbit retina (Fried, Mu and Werblin, 2005; Lee, Kim and Zhou, 2010; Brombas, Croft and Williams, 2017). Therefore, we conclude that the differential transmission of ACh/GABA produces E/I that are temporally synchronized in the null- but not preferred-direction (Figure 2.1 D and Figure 2.5 A), providing the substrate for a timing based mechanism for generating direction selectivity in ganglion cells.

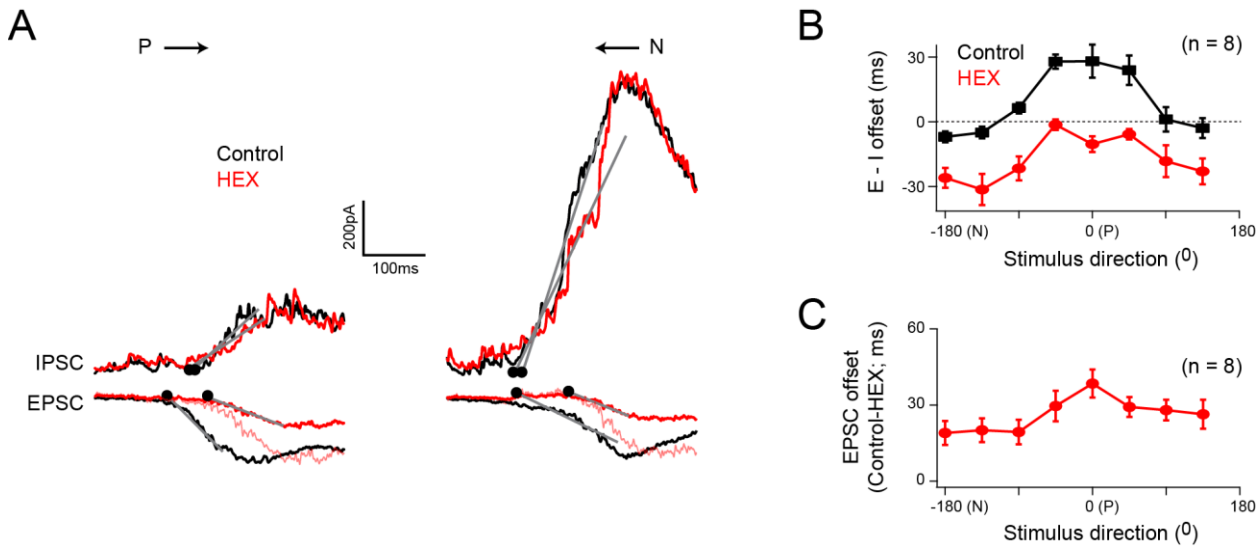

Figure 2.5 Cholinergic excitation shapes temporal E/I offsets under physiological conditions

(**A**) The EPSCs and IPSCs elicited in a DSGC for preferred and null stimuli, in control (black), and in the presence of a nicotinic acetylcholine receptor antagonist (hexamethonium, HEX; red traces). A normalized version of the EPSC measured in HEX (light red trace) is illustrated to emphasize the delay in excitation that occurs when cholinergic receptors are blocked. (**B**) The directional tuning of the E/I temporal offsets in control and HEX averaged across 8 cells. The offsets were aligned to the preferred direction (P) of the spike responses, which were measured in the same DSGC before performing the whole cell recording. HEX significantly reduced the E/I temporal offsets across all directions ($p<0.01$). Data are represented as mean ± SEM. (**C**) The directional tuning of the timing delay of the EPSC in HEX relative to control (n = 8). Data are represented as mean ± SEM. The increased onset latency observed in HEX continued to be observed when inhibition was blocked, indicating that they cannot be accounted for by large voltage–clamp errors associated with inhibitory conductances

2.5.4 E/I temporal offset mechanisms contribute to direction selectivity over a range of velocities

Next, we examined how E/I temporal offsets could contribute to direction selectivity across a range of stimulus velocities. In the *Gabra2* KO-ChR2, where DS in DSGCs relies solely on temporal E/I offsets, the number of optogenetically evoked spikes were found to decrease as a function of velocity, as expected (Figure 2.6 A). However, despite the drop in the spike

responses at higher stimulus velocities, the direction selectivity was not altered (Figure 2.6 A). As it is not possible to isolate the effects of temporal offsets under physiological conditions, instead, we measured the velocity dependence of the E/I temporal offsets under physiological conditions (Figure 2.6 B), and used these values to drive DS responses in a model DSGC, generated in the NEURON environment (Figure 2.6 D; see Materials and methods for details).

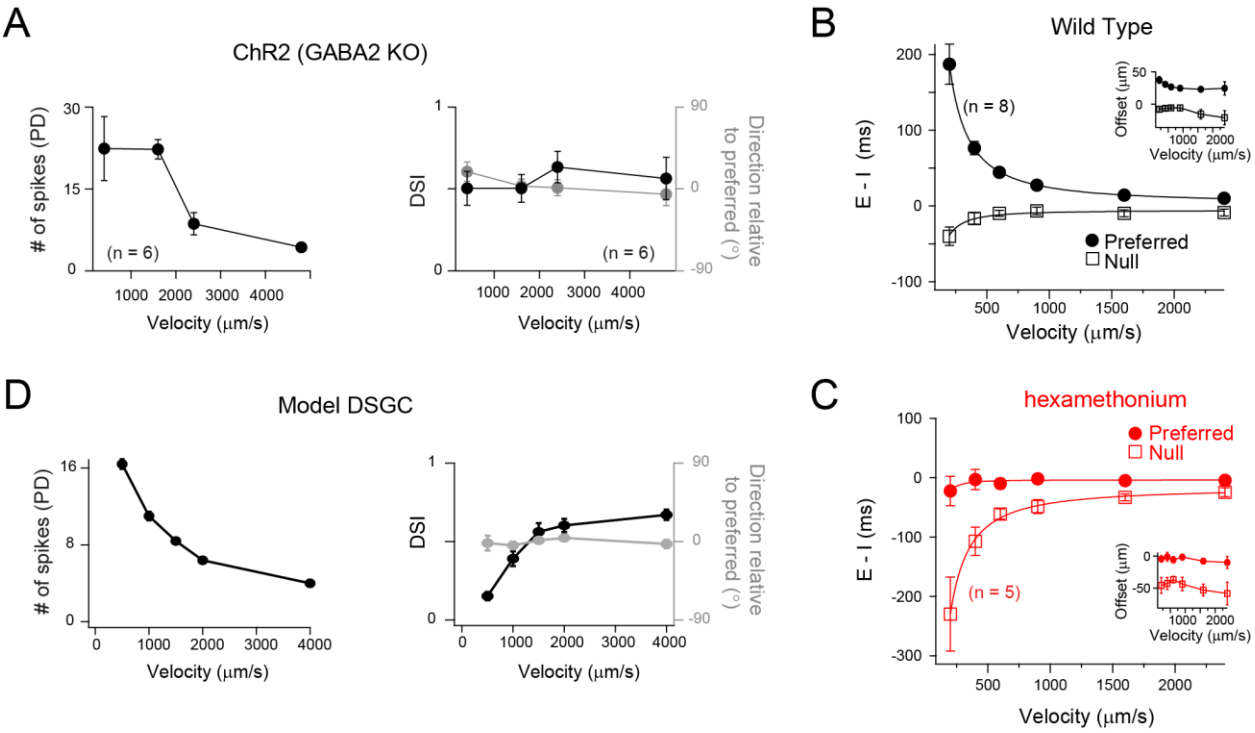

Figure 2.6 Velocity tuning of E/I temporal offsets in DSGCs

(**A**) A plot of the average number of ChR2-evoked spikes for preferred direction motion as a function of stimulus velocity (*left panel;* n = 6), measured from DSGCs in the *Gabra2* KO/ChR2 mouse line. The average DSI and preferred direction remains stable across velocity (*right panel*; n = 6). Data are represented as mean ± SEM. (**B–C**) The E/I temporal offsets measured from DSGCs in the wild-type retina, for both preferred and null directions as a function of velocity (**B**); n = 8). The offsets during preferred direction motion were significantly larger than those for null direction motion for all velocities ($p<0.001$). The temporal offsets correspond to a relatively fixed spatial offset (calculated by velocity x E/I temporal offsets) across a range of velocities tested (*inset*). The effects of blocking cholinergic transmission (hexamethonium) on E/I temporal offsets is shown in **C**). Data are represented as mean ± SEM. (**D**) Spike output of a computer simulated model DSGC in which the E/I ratio was fixed (1/2) but the E/I temporal offsets were varied according to measurements in **B**). E/I temporal offsets alone could generate robust DS across a range of velocities, except of the lowest velocity tested (see text for details)

The amplitude of E/I temporal offsets measured in the DSGC's preferred direction reduced with velocity, but were still measurable at the highest velocities tested (2400 μm/s; Figure 2.6 B). The values of the E/I temporal offsets measured at different speeds corresponded to a ~ 30 μm spatial offset between excitatory and inhibitory receptive fields (Figure 2.6 B, inset). Addition of nACh receptor antagonists (hexamethonium) abolished the E/I temporal offsets, confirming that the spatial offsets are mediated by starburst inputs at all velocities (Figure 2.6 C). Conversely, for null-direction motion, E/I were co-activated through most of the velocity range, except for the lower velocities where inhibition tended to lead excitation (Figure 2.6 B). For null-direction motion, the nACh receptor antagonists revealed negative offsets, as previously noted (Figure 2.6 C).

Next, to examine the impact of E/I temporal offsets at different velocities we generated a model DSGC with excitatory and inhibitory inputs having timing offsets that varied with direction as measured experimentally, but with their amplitude ratio constant (E:I set at 1:2 for all directions; Figure 2.4 F). As with our optogenetic study, for preferred motion, the number of spikes decreased as a function of velocity (Figure 2.6 D) but remained robustly directional through most of velocity range. Only at the lowest speed, where the edges moving in the null direction spent considerable time on the excitatory receptive field after inhibition ceased, the model generated a few null-direction spikes, resulting in a decreased DSI (Figure 2.6 D). In real DSGC this does not appear to be an issue, indicating that GABAergic inhibition must be slower and more powerful than that implemented in our model. On the other hand, the direction encoded remained largely unaltered with velocity. Thus, the simplified model captures many aspects of the DSGC response properties, and supports the idea that the E/I temporal offset mechanism contributes to direction selectivity in ganglion cells over a wide range of velocities.

2.5.5 Complementary roles for E/I temporal offset and amplitude based DS mechanisms

Finally, we explored the possible computational benefits offered by the distinct DS mechanisms relying on temporal and amplitude E/I asymmetries. When the spiking responses were averaged over the entire trial, the direction selectivity generated with or without DS inhibition was similar, and thus the DS mechanisms appear redundant (Figure 2.3). However, when the DS tuning was examined on a finer time-scale (Figure 2.7), it showed distinct characteristics in the early and peak phases of the response, raising the possibility that the two mechanisms operate on distinct time-scales. While the direction encoded remained constant throughout the response, the tuning curve broadened as the response approached its peak, resulting in a marked decrease in the DSI (Figure 2.7 A–D). Moreover, the initial estimate of direction was more variable compared to that made during the peak of the response (standard deviation of early and peak responses were 16 ± 2^0; and 8 ± 2^0, respectively; Figure 2.7 B,E,F). This difference in variability may reflect the ability of distal vs. proximal dendritic sites to effectively transmit directional information to the soma via dendritic spikes (Sivyer and Williams, 2013). It is also important to note that the broadening of the tuning curve did not arise simply from a thresholding effect (i.e. an iceberg effect), as the last spikes at the tail end of the response were not sharply tuned (data not shown).

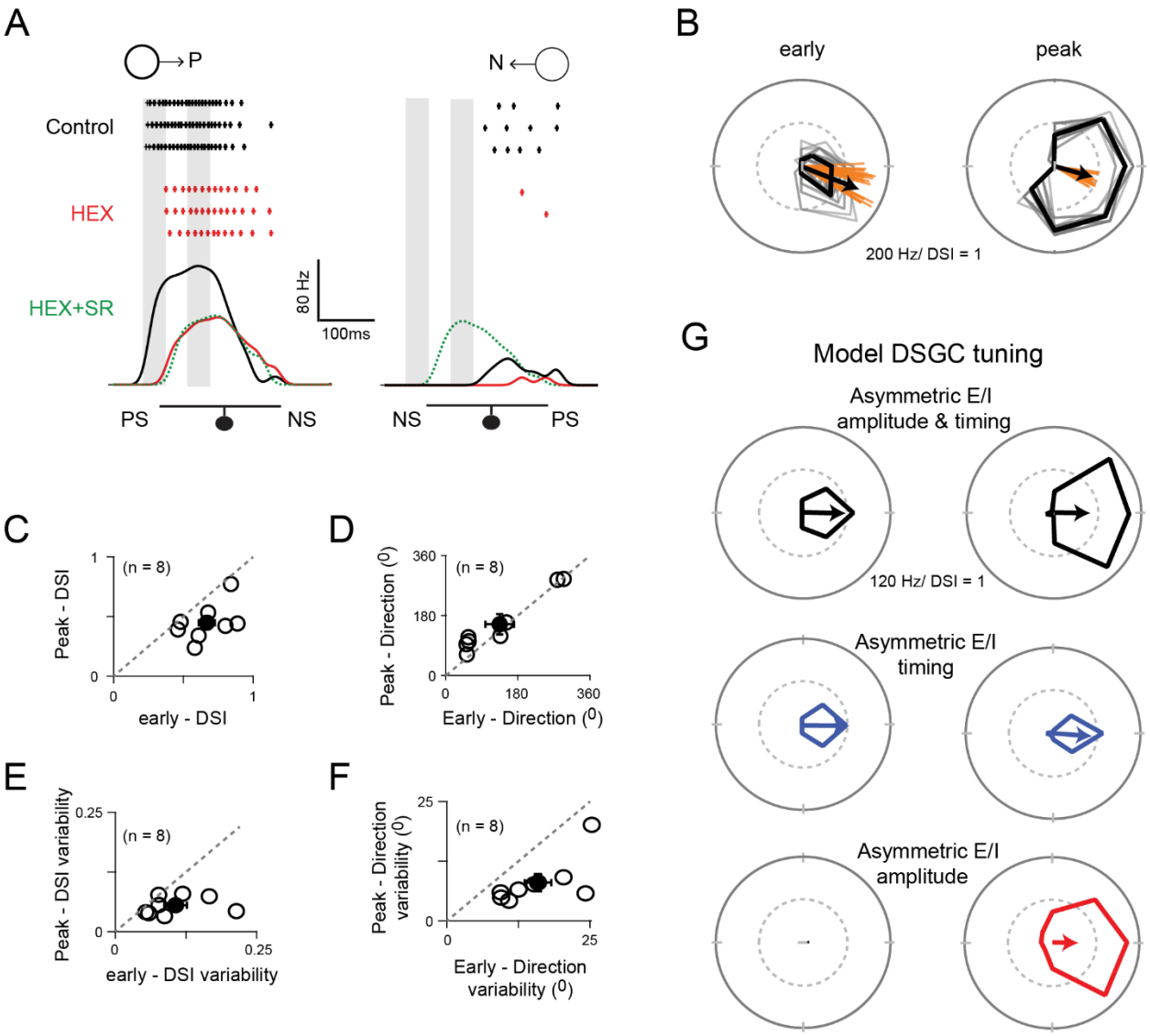

Figure 2.7 Two 'core' DS mechanisms are engaged during different phases of the DSGC response

(**A**) Spike rates during stimulus motion in the preferred or null directions in control conditions (black), after cholinergic excitation is blocked by HEX (red), and in the added presence of a GABA receptor blocker (5 μM SR-95531; green) to isolate the glutamate receptive field. Preferred and null responses could be accurately aligned, temporally, based on the glutamatergic receptive field measurement, which was important in estimating the temporal evolution of the DS tuning shown in (**B–G**). The effects of HEX on the response latency were reversible, and not observed when responses were weakened by blocking NMDA receptors (see Figure 7—figure supplement 1). PS and NS indicates the preferred- and null-sides of the DSGC. (**B**) Polar plots of a DSGC's early (*left*) and peak (*right*) spike responses (the 50 ms shaded regions in **A**) over 29 trials. The mean response is shown in black, while the individual trials are shown in grey. Note early responses are more sharply tuned but provide a less reliable indication of the direction (i.e. the direction encoded is more variable; orange lines) compared to

the peak response. (**C–D**) A comparison of the average DSI (**C**) and preferred direction (**D**) calculated from the early and peak spike responses for individual cell (n = 8). The DSI of the early responses was significantly higher than the peak responses ($p<0.01$), while the direction encoded in both phases were near identical. Pooled data are represented as mean ± SEM. (**E–F**) A comparison of the trial-to-trial variability of the DSI (**E**) and preferred direction (**F**) of the early and peak responses (n = 8). Trial-to-trial variability was estimated by the standard deviation of DSI/preferred direction across trials within each cell (minimum 10 trials). The variability was higher for early responses for both DSI ($p<0.05$) and preferred direction ($p<0.005$). Pooled data are represented as mean ± SEM. (**G**) Tuning properties of a computer simulated model DSGC in which both E/I temporal offsets and amplitude asymmetries (*top*), only E/I temporal offsets (*middle*) or only E/I amplitude asymmetry (*bottom*) were implemented. E/I temporal offsets alone resulted in a sharper tuning similar to the early responses in **B**), but the tuning became broader when E/I ratios were intact, similar to the peak responses in **B**) (see Figure 7—figure supplement 2 for synaptic currents and spiking responses measured in the model). Responses were averaged over 20 trials

Given that early spikes appear to be driven largely by cholinergic excitation (Figure 2.7 A), but not by glutamate inputs (Figure 2.7—figure supplement 1), we envisioned that E/I temporal offsets are likely to be more important in determining direction selectivity during the initial phase of the response, while the later phase would likely be dominated by E/I amplitude differences. It is important to note that both DS mechanisms rely on transmitter release from starbursts and thus operate on roughly the same spatial scales. Next, we tested these ideas in our model DS circuit, where we could easily control the timing and amplitude of E/I, independently (see Materials and methods for details).

Indeed, the characteristic properties of the DSGC's direction tuning were reproduced in a model DSGC driven with both temporal and amplitude asymmetries in E/I that arise from the specific arrangement of GABA, ACh and glutamate inputs (Figure 2.7 G; Figure 2.7—figure supplement 2A illustrates the synaptic inputs/spiking response of the model DSGC). When starbursts were rendered non-DS in the model DSGC (Figure 2.7 G; Figure 2.7—figure

supplement 2B), temporal asymmetries alone were sufficient to generate DS responses with sharp tuning (Figure 2.7 G), as observed in the ChR2-*Gabra2* KO mouse. When E/I temporal offsets were removed, modulating the peak amplitude of inhibition generated robust DS responses, but with wider tuning (Figure 2.7 G; Figure 2.7—figure supplement 2C). However, in this model lacking offsets, the early responses were lost (Figure 2.7 G). Thus, the DS mechanisms based on temporal and amplitude asymmetries appear to be complementary, each conferring distinct advantages: the former enables DSGCs to respond in a direction-selective manner sooner than they would have done otherwise, while the latter enables DSGCs to encode direction with higher fidelity albeit on a slower time scale.

2.6 Discussion

2.6.1 Parallel 'core' mechanisms generating direction selectivity in the retina

In the mammalian retina, direction selectivity is observed at the level of starburst dendrites as well as in downstream DSGCs. Our experiments using various pharmacological, optogenetic and cell-specific KO strategies to analyse synaptic inputs to DSGCs, suggest that multiple circuit mechanisms serve to generate direction-selectivity at both these points in the DS circuit.

At the level of starburst dendrites, three distinct mechanisms have been proposed to underlie direction selectivity. These include excitatory and inhibitory network mechanisms (Lee and Zhou, 2006; Münch and Werblin, 2006; Kim *et al.*, 2014; Ding *et al.*, 2016; Fransen and Borghuis, 2017), and cell intrinsic mechanisms (Euler, Detwiler and Denk, 2002; Tukker, Taylor

and Smith, 2004; Hausselt *et al.*, 2007). However, pinpointing the 'core' mechanism has been complicated because blocking these mechanisms individually, leaves starburst DS output relatively intact. Our result, using ChR2 to stimulate starburst output in a mouse line where inhibitory network mechanisms have been inactivated (Chen *et al.*, 2016), demonstrate for the first time a condition where starburst release of GABA is non-directional. These results highlight the apparently redundant roles for excitatory and inhibitory network mechanisms and help amalgamate divergent views (Lee and Zhou, 2006; Münch and Werblin, 2006; Kim *et al.*, 2014; Ding *et al.*, 2016; Fransen and Borghuis, 2017).

While intrinsic DS mechanisms in starburst dendrites may be important for DS computations, the current results do not appear to reveal them in an obvious manner. This could be for several reasons. First, it is possible that the artificial activation of starbursts using optogenetics does not recruit dendritic voltage-gated channels that may underlie direction selectivity (reviewed in Taylor and Smith, 2012). Second, the removal of GABAergic inhibition between starbursts may hinder or occlude intrinsic DS mechanisms. Third, it is also possible that the limited set of stimuli (moving spots) which we utilized were not optimally designed to recruit cell intrinsic mechanisms. Thus, although DS is suppressed under conditions in which inhibitory and excitatory network mechanisms are blocked, we do not exclude the possibility that intrinsic mechanisms could serve as a third 'core' DS mechanism. A challenge for future experiments is to determine if and how each of these mechanisms work to maintain starburst DS output under different stimulus conditions.

At the level of DSGCs too, multiple DS mechanisms appear to be in play. Here, two fundamental mechanisms appear to originate from unique specializations of the starburst

network. The first mechanism, which relies on amplitude asymmetries arising from the DS starburst dendrites (Figure 2.1 C) and asymmetric starburst-DSGC wiring (Figure 2.1 B), is well established (reviewed by Vaney, Sivyer and Rowland Taylor, 2012; Mauss *et al.*, 2017). The second mechanism relies on temporal asymmetries in excitation and inhibition (Figure 2.1 D). While E/I temporal offsets have often been noted in the literature (Taylor and Vaney, 2002; Fried, Mu and Werblin, 2005; Sivyer *et al.*, 2010; Kostadinov and Sanes, 2015; Pei *et al.*, 2015; Sethuramanujam *et al.*, 2016), our results demonstrate for the first time that they are tuned precisely to the DSGC's preferred direction, and are alone sufficient to generate direction selective responses in ganglion cells.

Recent studies using voltage-clamp techniques have also shown the amplitude of the cholinergic signal to vary according to direction (Lee, Kim and Zhou, 2010; Park *et al.*, 2014; Pei *et al.*, 2015; Sethuramanujam *et al.*, 2016). However, these results need to be interpreted with caution. Dynamic changes in the inhibitory conductance could lead to serious voltage-clamp errors and estimates of the relative peak amplitude of cholinergic input in the preferred and null direction (Poleg-Polsky and Diamond, 2011) (Figure 2.5—figure supplement 1). Thus, the development of alternate methods, such as functional imaging, is required to fully resolve this issue. Importantly, the E/I offset mechanisms generating DS described here do not require amplitude changes in cholinergic inputs.

It is also worth noting that cholinergic, GABAergic and glutamatergic synapses are made relatively uniformly throughout the DSGC receptive field and are thought to constitute repeating dendritic DS subunits (Barlow and Levick, 1965; Taylor *et al.*, 2000). Thus, although the temporal asymmetries are most apparent at response onset in our recordings made from the

DSGC soma, they are likely present throughout the dendritic tree. Local E/I amplitude and timing differences are expected to shape dendritic responses, which may be further refined by dendritic non-linearities (Oesch, Euler and Taylor, 2005; Sivyer and Williams, 2013; Trenholm *et al.*, 2014). This is one reason why the spikes generated by E/I temporal offset mechanisms alone often outlast the E/I temporal offsets measured macroscopically (Figure 2.7 G). The precise degree to which timing and amplitude differences in local inputs influence the DSGC's response directly depends on the extent to which dendrites operate independently (Schachter *et al.*, 2010).

2.6.2 The network of starburst amacrine cells produces temporal E/I asymmetries in DSGCs

Before the discovery of DS in starburst dendrites, classic models suggested that DS responses in ganglion cells were based on E/I timing differences (Torre and Poggio, 1978; Koch, Poggio and Torre, 1982; Taylor *et al.*, 2000). Previous studies have speculated that an intermediary cell in the inner and/or outer retina may control E/I timing differences at DSGCs (Taylor and Vaney, 2002; Rivlin-Etzion, Wei and Feller, 2012; Vlasits *et al.*, 2014). In contrast, another study found that perturbing starburst cell morphology led to parallel changes in E/I amplitude ratio and E/I temporal offsets suggesting that these processes may be inextricably linked (Kostadinov and Sanes, 2015).

Our combined results from optogenetic, pharmacological and modelling experiments indicate that the temporal asymmetries in E/I are a natural consequence of the asymmetric/symmetric GABAergic/cholinergic connectivity of starburst cells to DSGCs (Figure 2.1) (Lee, Kim and Zhou, 2010; Yonehara *et al.*, 2011; Chen *et al.*, 2016). In this scheme, null-side starbursts extend the inhibitory receptive fields of DSGCs during null motion, producing a

more powerful inhibition (Fried, Munch and Werblin, 2002). Conversely, cholinergic excitation provided by preferred-side starbursts enable DSGCs to respond sooner to the moving edge than they would otherwise. We found that the degree to which cholinergic inputs advance the response is proportional to stimulus velocity, corresponding to a fixed spatial offset ~30 μm. In mouse retina, starbursts receive excitatory and inhibitory inputs on proximal dendrites but release transmitter from varicosities located on their distal dendrites (Kim *et al.*, 2014; Ding *et al.*, 2016; Vlasits *et al.*, 2016). Mapping the receptive fields of individual starburst varicosities using Ca^{2+} imaging shows them to be displaced by ~25 μm towards the soma (Poleg-Polsky, Ding and Diamond, 2018). Thus, the extent to which cholinergic inputs expand the receptive field of the DSGC is well predicted by the input/output properties of starburst dendrites. The dimensions of the cholinergic receptive fields also indicate that despite being generated by paracrine mechanisms (which loosens the constraints set by the asymmetrical starburst-DSGC 'hard-wiring'; Figure 2.1 B) (Briggman, Helmstaedter and Denk, 2011; Brombas, Croft and Williams, 2017), the distance over which ACh spreads appears relatively limited.

In contrast to our findings, in rabbit retina, cholinergic excitation is co-extensive with the glutamatergic receptive field and does not appear to extend the DSGC's receptive field beyond the dendritic field (Yang and Masland, 1992; Fried, Mu and Werblin, 2005; Lee, Kim and Zhou, 2010; Brombas, Croft and Williams, 2017). One reason for this could be that static stimuli employed in previous studies to measure the receptive field properties of DSGCs do not optimally stimulate starbursts, and therefore fail to reveal cholinergic excitation (Yang and Masland, 1992; Fried, Mu and Werblin, 2005). Alternatively, in rabbit retina, the release of ACh may require a stronger stimulation of the starbursts (Lee, Kim and Zhou, 2010). This causes a delay in the release of ACh, making it co-extensive with glutamate input (Lee, Kim and Zhou,

2010). Indeed, under conditions where inhibition is blocked and starburst dendrites are more strongly stimulated, cholinergic inputs do provide lateral excitation (Fried, Mu and Werblin, 2005; Lee, Kim and Zhou, 2010; Vaney, Sivyer and Rowland Taylor, 2012). Together, these findings have given rise to the notion that the role of ACh is modulatory (Ariel and Daw, 1982; Amthor, Grzywacz and Merwine, 1996; Chiao and Masland, 2002; Lee, Kim and Zhou, 2010; but see Pei *et al.*, 2015), in contrast to what we observed in mouse retina.

The demonstration that the parallel circuit mechanisms driving direction selectivity in ganglion cells are individually dispensable necessitates a re-evaluation of the conclusions drawn from a multitude of studies carried out over the last several decades that considered a single 'core' DS mechanism. For example, numerous studies over the last forty years have found that blocking cholinergic receptors does not affect direction selectivity in DSGCs and have taken this to mean that ACh does not play an integral role in DS (reviewed by Vaney, Sivyer and Rowland Taylor, 2012; Mauss *et al.*, 2017), but rather provides an additional source of non-directional excitation to boost DSGC responses (Lee, Kim and Zhou, 2010; Chen *et al.*, 2016; Brombas, Croft and Williams, 2017), that is especially important under limiting conditions (Sethuramanujam *et al.*, 2016, 2017). In sharp contrast, our results here indicate that in fact ACh signals (unlike glutamate signals) are highly directional, not so much in their amplitudes as previously envisioned (Grzywacz, Tootle and Amthor, 1997; Grzywacz, Merwine and Amthor, 1998; Lee, Kim and Zhou, 2010; Pei *et al.*, 2015; Chen *et al.*, 2016), but rather by virtue of their relative timing with inhibition. Cholinergic excitation and GABAergic inhibition are relatively imbalanced (or out of phase) during preferred-direction motion, but extremely well-balanced (or in phase) during null-direction motion, which is important for the computation (Figure 2.1 D).

2.6.3 Spatiotemporal dynamics of Ach, GABA and glutamate inputs

Traditional models of DS raised questions regarding the role of cholinergic excitation in driving direction selectivity. In the revised model (Figure 2.1 D), the role of canonical bipolar cell glutamate pathways becomes questionable. Previously, we have shown that under low contrast conditions, glutamate appears to be mediated by NMDA receptors (Sethuramanujam *et al.*, 2016, 2017) and play an important role modulating cholinergic excitation. Under high contrast conditions, as we have used here, glutamate signaling is mediated by both AMPA and NMDA receptors. Glutamate input is relatively delayed and therefore makes the DSGC's preferred response more sustained. This contributes to changes of the DS tuning over time.

Moreover, since AMPA inputs are non-directional they are expected to broaden the DS tuning curve, by changing the E/I ratio across direction (Poleg-Polsky and Diamond, 2016). Indeed, a measurable broadening of the real DSGC tuning curves is noted at higher contrasts, although these effects are relatively small (Sethuramanujam *et al.*, 2017). Additionally, given the difference in receptive fields between bipolar and starburst inputs to DSGCs, the E/I ratio is predicted to change over the duration of directional light responses (Figure 2.1 D). Our model indicates that this effect is most pronounced during slow stimulus velocities, as temporal offsets caused by spatial differences are exacerbated as more time is spent between activations of each input to the DSGC, leading to a deterioration of DS (Figure 2.6 F). However, in real DSGCs, DS is stable across velocities (Brombas, Croft and Williams, 2017), indicating that there must be additional mechanisms that compensate for these effects (e.g. inhibition from non-DS sources).

2.7 Conclusions

Here we have shown how E/I amplitude and timing differences are orchestrated by parallel circuit mechanisms. In the case of pinpointing the mechanisms generating direction selectivity in starbursts (Lee and Zhou, 2006; Münch and Werblin, 2006; Kim *et al.*, 2014; Ding *et al.*, 2016; Fransen and Borghuis, 2017), or understanding whether timing (Torre and Poggio, 1978; Koch, Poggio and Torre, 1982; Taylor *et al.*, 2000) or amplitude ratios generate DS in ganglion cells, the realization of multiple DS mechanisms helps settle divergent views. In contrast, the suggestion of a central role for starburst ACh in driving E/I temporal offsets, necessitates re-enquiry into previous results which indicated a modulatory role.

Given the multiple DS mechanisms in the retina, it is interesting to speculate that DS neurons in higher visual areas are also created using a variety of circuit mechanisms. This may help explain conflicting results from recent studies regarding the origin of DS in cortex. For example, thalamocortical inputs to the visual cortex exhibit strong DS properties (Sun *et al.*, 2016), apparently with retinal origin (Cruz-Martín *et al.*, 2014). Yet, abolishing retinal direction selectivity has modest effects on cortical DS (Hillier *et al.*, 2017), indicating that direction selectivity must also arise de novo through alternate parallel mechanisms (Saul, Carras and Humphrey, 2005; Lien and Scanziani, 2018; Wilson, Scholl and Fitzpatrick, 2018). Strikingly, in primate visual cortex, distinct mechanisms appear to shape early and late response (Pack and Born, 2001; Thiele *et al.*, 2004) similar to what we have observed here for DSGCs, suggestive of a common organizational principle. It is also interesting to note that direction selectivity in other sensory areas including the auditory and somatosensory systems (Wilent and Contreras, 2005; Kuo and Wu, 2012) may also rely on temporal and amplitude E/I asymmetries (Zhang *et al.*,

2003; Ye *et al.*, 2010; Li *et al.*, 2015). While large-scale ultrastructural circuit mapping is bound to reveal circuit elements involved in the computation, it is only through the marriage of anatomical and physiological approaches can the circuit mechanisms be fully realized, as we have demonstrated here for the generation of direction selectivity at multiple levels in the mouse retina.

Chapter 3: NMDA-rich synapses in the mature mouse retina can encode information across visual contrasts

3.1 Abstract

Synapses lacking the functional expression of AMPARs are often considered 'silent' (Kerchner and Nicoll, 2008), as glutamate binding to NMDARs alone does not substantially activate them (due to the voltage-dependent block of NMDARs by external Mg^{2+} ions). Previous studies have identified silent synapses in the direction-selective ganglion cells of the retina and silent synapses have also been studied extensively throughout the central nervous system, however, whether they arise presynaptically or post-synaptically still remains unclear. Additionally, the visual system is tasked with the challenge of responding to varying degrees of stimulus intensity rather than signaling in the classical all-or-none fashion. In order to achieve this signaling pattern, they rely on ribbon synapses which allow for rapid and tunable multivesicular release, resulting in graded glutamate release into the synaptic cleft. However, how the postsynaptic receptors interpret this graded release remains unknown. Previous evidence has indicated that NMDA receptors in the ganglion cells of the mature mouse retina are located extrasynaptically and therefore are not saturated during univesicular release. Here, we examined miniature-like EPSCs in the direction-selective ganglion cell to show that both NMDA and AMPA receptors are located synaptically but are isolated to different synapses, therefore confirming the presence of 'silent' synapses in the mature retina. We also utilized 2-photon imaging of calcium influx through NMDA receptors to show that the synaptically localized NMDA receptors exhibit graded responses to increasing contrasts and are therefore not saturated by univesicular glutamate release.

3.2 Introduction

'Silent' glutamatergic synapses—those that only express N-methyl-D-aspartate (NMDA) receptors—are observed in both mature and developing brain. They are silent owing to a voltage-dependent blockade of the NMDA channel by external Mg^{2+} ions (Mayer, Westbrook and Guthrie, 1984). However, when presynaptic glutamate release is coupled with coincident postsynaptic depolarization, NMDA receptors can strongly amplify neural activity. In the developing CNS, such coincident activity can drive plasticity. In the mature CNS silent NMDA receptor-dominated pathways have been implicated in the processing of motor (Shima and Tanji, 1998), auditory (Mooney and Konishi, 1991), visual (Rivadulla, Sharma and Sur, 2001), attention (Self *et al.*, 2012; Herrero *et al.*, 2013) and memory formation (Wang, 2001). Despite their central importance the mechanistic basis for silent synapses remains poorly understood.

In the developing CNS, where silent synapses were first discovered and have since been heavily investigated, it has been particularly difficult to distinguish whether pre-or postsynaptic mechanisms underlie silent synapse expression (Reviewed by Hanse, Seth and Riebe, 2013). Early experiments using minimal stimulation revealed synaptic responses that could only be measured at depolarized potentials, which were mediated by NMDA receptors (Isaac, Nicoll and Malenka, 1995; Durand, Kovalchuk and Konnerth, 1996). This indicated that these synapses were devoid of AMPA receptors, an idea which was supported by anatomical studies (Petralia *et al.*, 1999). In some areas of the brain such as visual cortex, NMDA miniature EPSCs (mEPSCs) were found to occur at a relatively higher frequency compared to AMPA mEPSCs, indicating that distinct synapses might harbour different complements of postsynaptic AMPA and NMDA receptors. However, the time course of NMDA receptor mediated activity observed at immature synapses is often extremely slow. Spontaneous and evoked NMDA EPSCs rise over a few

milliseconds and decay over ten to hundreds of millesconds (Silver, Traynelis and Cull-Candy, 1992; Haas, Cline and Malinow, 1998). This makes it difficult to ascertain whether activity originates from rapid release of high-concentrations of glutamate from a single vesicle; or from low-concentration of glutamate 'spilling-over' from distal sites. Low glutamate concentrations would favour the activation of high-affinity, non-desensitizing NMDARs rather than low affinity, quickly desensitising AMPA receptors (Renger, Egles and Liu, 2001; Andreae and Burrone, 2015). Thus, whether presynaptic or post-synaptic mechanisms generate silent synapses, remains an open question.

In the mature mouse retina, direction selective ganglion cells (DSGCs) receive glutamate input from retinal bipolar cells that are mediated by both AMPA and NMDA receptors. However, recently we discovered that AMPA and NMDA receptor-mediated responses exhibit different sensitivities to stimulus contrast (Figure 3.1A) (Sethuramanujam *et al.*, 2017). During low-contrast stimulus, only NMDA mediated responses are detected; while in high contrast scenarios, both AMPA and NMDA receptors mediate the excitatory responses in DSGCs. Based on the prior literature in the developing CNS, we considered 3 models which could explain the appearance of silent synapses during low contrast stimulation. The first model relies on the ability of mature ribbon synapses in bipolar cell terminals to modulate glutamate concentration in the cleft, by controlling the number of glutamate vesicles released near simultaneously (i.e. uni-vesicular vs. multi-vesicular release) (Singer, 2007; Rudolph *et al.*, 2015). It also relies on the different sensitivities of AMPA and NMDA receptors (Figure 3.1B) (Renger, Egles and Liu, 2001; Andreae and Burrone, 2015). Second, we considered whether the evoked NMDA only response in DSGCs was mediated by glutamate 'spilling-over' from bipolar to starburst amacrine cells synapses (Figure 3.1C) (Zhang and Diamond, 2009). Third, we considered a model in

which separate bipolar inputs with different sensitivities to contrast mediated NMDA and AMPA receptor-mediated responses (Figure 3.1D). To distinguish between these models, we analyzed spontaneous miniature-like EPSCs mediated by AMPA and NMDA receptors as well as examined the properties of NMDA-receptor mediated Ca2+ in the dendritic tree of DSGCs. Our experiments reveal the 'quantal' nature of silent synapses and show them to be mediated by unusually fast NMDA receptors.

Based on the millimolar concentration of glutamate released into the synaptic cleft during single vesicle release compared to the micromolar affinity of NMDA receptors it has largely been accepted that NMDA receptors in close proximity to the release site will become fully saturated to release of a single vesicle of glutamate (Clements *et al.*, 1992; Zhang and Diamond, 2009; Manookin *et al.*, 2010; Singh *et al.*, 2011). However, as more research is conducted, it is becoming apparent that this is not the case for all NMDA synapses (Frerking and Wilson, 1996). In the hippocampus, single synapse analysis has identified synaptic NMDA receptors which are not saturated to single events, as increasing presynaptic glutamate release causes increases in the amplitude of postsynaptic NMDA mediated currents (McAllister and Stevens, 2000). Paired-pulse stimuli have also been used to show that secondary pulses within 10 ms can result in an increase in the NMDA mediated calcium influx (Svoboda, Mainen and Malinow, 1999). However, in this example it appears that the secondary pulse results in a near saturation effect, leading to the questions of what happens when the number of released vesicles exceeds two.

In the retina, similar to other sensory systems, photoreceptors and bipolar cells do not transmit information in the classical all-or-none fashion that is predominately observed in other regions of the central nervous system. Instead, both the photoreceptors and retinal bipolar cells rely on specialized release machinery known as ribbon synapses to relay graded information

regarding stimulus intensity in the form of multivesicular release where up to eight or more vesicles can be released near simultaneously (Jarsky *et al.*, 2011; Oesch and Diamond, 2011; James *et al.*, 2019). The NMDA receptors expressed in retinal ganglion cells have been shown to be important for coding this contrast dependent information in the retina (Manookin *et al.*, 2010; Sethuramanujam *et al.*, 2017), however, how the postsynaptic receptors are able to encode this graded transmitter release across cell types is not fully understood.

Previous studies measuring the contribution of NMDA receptors to contrast coding have predominately been performed using somatic recordings which cannot distinguish between a global summation of inputs (increase in synapse number) or a local increase in individual synaptic strength during increasing contrast. Previous studies in rat, mouse and guinea pig retina have shown that a large population of retinal ganglion cells express NMDA receptors which are localized extrasynaptically, especially in the ON pathway, as can be shown through anatomical and pharmacological studies (Chen and Diamond, 2002; Sagdullaev, McCall and Lukasiewicz, 2006; Singer, 2007; Zhang and Diamond, 2009; Manookin *et al.*, 2010). It is believed that this localization prevents the high affinity NMDA receptors from becoming saturated to single vesicle release of glutamate and allows them to respond to increasing concentrations of glutamate spilling over from the synaptic cleft during increases in stimulus contrast. Alternatively, NMDA receptors located close to the release site may avoid saturation by expressing the lower affinity NR2A subunit (Hansen, Brauner-Osborne and Egebjerg, 2008). These different models of contrast encoding are also not mutually exclusive, as the retinal ganglion cells may rely on both an increase in synaptic number and an increase in synaptic strength through either synaptic or non-synaptic NMDA receptors or both.

Here, we utilize patch clamp and 2-photon imaging techniques to identify “silent”, NMDA-only synapses in the direction-selective ganglion cells of the mouse retina and show that, although these receptors are located synaptically, they are still able to exhibit graded responses to increasing stimulus contrasts. These findings show that synaptic NMDA receptors in a subtype of ganglion cells in the retina do not saturate to single vesical release as previously believed.

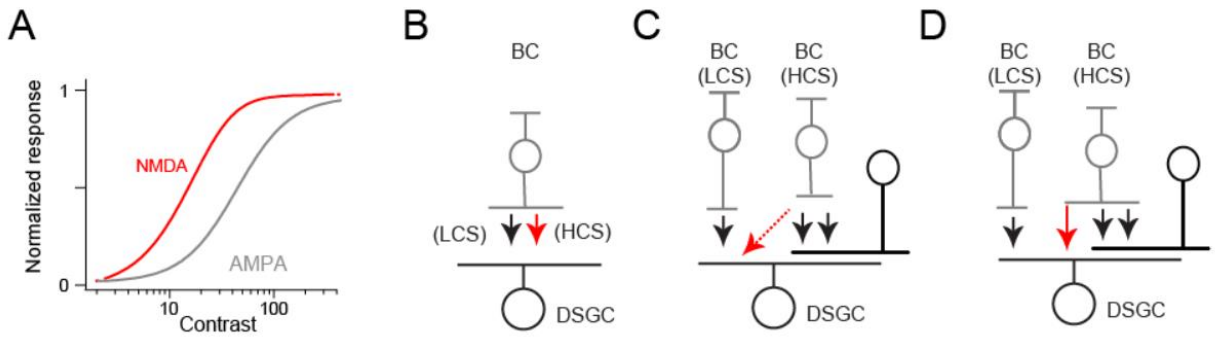

Figure 3.1 Synaptic organization of glutamate input onto DSGCs

(**A**) The difference in contrast sensitivities between AMPA and NMDA receptor-mediated responses can be explained by three main models: (**B**) AMPA and NMDA receptors share the same glutamate source but the concentration of glutamate in the cleft can be modulated by ribbon synapses to preferentially active the high-affinity, non-desensitizing NMDARs rather than the low affinity, quickly desensitizing AMPARs at low glutamate concentrations. (**C**) NMDA responses are mediated by glutamate ‘spilling-over’ from bipolar to starburst amacrine cell synapses. (**D**) Separate bipolar inputs with different sensitives to contrast mediate AMPA and NMDA receptor-mediated responses.

3.3 Methods

3.3.1 Animals

All procedures were performed in accordance with the Canadian Council on Animal Care and approved by the University of Victoria’s Animal Care Committee. Experiments were performed

using mice of both sexes aged between P21-P140. Animals were group housed in a 12 hour dark/light cycle.

Experiments were performed using either C57BL/6J (RRID: IMSR_JAX:000664), Trhr-EGFP (kindly provided by Dr. Marla Feller, UC Berkeley; RRID: MMRRC_030036-UCD) or CART-cre (B6; 129S-*Cartpt*$^{TM1.1(cre)Hze/J}$ JAX 028533).

3.3.2 Retinal Preparation

Prior to retina extraction, mice were dark adapted for 30-60 minutes to optimize light evoked responses and limit photoreceptor bleaching. Mice were anesthetized with isoflurane and euthanized by cervical dislocation then the retina was extracted and dissected in Ringer's solution (110 mM NaCl, 2.5 mM KCl, 1 mM $CaCl_2$, 1.6 mM $MgCl_2$, 10 mM glucose and 22 mM $NaHCO_3$) under dim red light. The whole retina was mounted ganglion cell layer up on a 0.22 mm membrane filter (Millipore) with a pre-cut square window approximately 2 mm^2 in size to allow light to reach the retina. For imaging experiments, the retina was instead mounted on a poly lysine coated 12 mm circular cover slip. The tissue was viewed with infrared light using a Spot RT3 CCD camera (Diagnostic Instruments) on an upright Olympus BX51 WI fluorescent microscope equipped with a 60x water immersion lens (Olympus Canada). Throughout the experiment, the retina was continuously perfused with warmed (~37 ^oC) Ringer's solution bubbled with carbogen (5% CO_2:95% O_2).

3.3.3 Visual Stimulation

Light stimuli, produced using a digital light projector (Hitachi Cpx1, refresh rate 75 Hz), were focused onto the outer segments of the photoreceptors using the sub-stage condenser. The

background luminance, measured with a calibrated spectrophotometer (Ocean Optics), was set to ~10 photoisomerisations/s (R*/sec). Visual stimuli were created in the Matlab environment (Psychtoolbox) and were 100 μm spots ranging from 3% to 100% Weber contrast.

3.3.4 Viral injections

All viral injections were performed by Tracy Michaels. The single-stranded AAV vector pAAV.hSynap-FLEX.SF-Venus-iGluSnFR.A184S (AAV1) was acquired from Addgene (Addgene #106183-AAV1). The AAV vectors were intravitreally injected in CART-Cre mice to selectively target DSGCs. To begin, mice were anesthetized with isoflurane (2-3% at 1-1.5 L/min), along with a single dose of subcutaneously injected buprenorphine (0.05-0.1 mg/kg body weight). In addition, a drop of 1% proparacaine was applied topically to the eye. Next, using a 30-gauge needle, a small hole was made at the margin of the cornea and sclera. The AAV preparation (~1.5 μL of 2.2×10^{12} vg/mL) was injected through this hole using a Hamilton injection system (syringe: 7633-01, needle: 7803-05, point style 3, length 10 mm). After injection, mice were returned to their home cage on a heating pad and monitored, until fully recovered.

3.3.5 Electrophysiology

Direction-selective ganglion cells were identified by their characteristic DS responses during loose cell patch clamp recordings while providing stimuli moving in eight directions or through genetic labelling and 2-photon targeting.

For spontaneous miniature EPSC acquisition, voltage-clamp recordings were performed in 0 Mg^{2+} Ringer's solution (110 mM NaCl, 2.5 mM KCl, 1 mM $CaCl_2$, 10 mM glucose and 22 mM

$NaHCO_3$) using 3-5 MΩ electrodes containing (containing 112. 5 mM CH3CsO3S, 7. 75mM CsCl, 1 mM MgSO4, 10 mM EGTA, 10 mM HEPES, 5 mM QX-314 (Tocris), the pH was adjusted to 7.4 with CsOH) and cells were held at -60 mV. 20 μM L-AP4 (Abcam Biochemicals) and 10 μM UBP-310 (Abcam Biochemicals) were applied through bath perfusion to block the ON and OFF photoreceptor responses, respectively. To isolate AMPA and NMDA mediated events, either 50 μM D-AP5 (Alomone Labs) or 10 μM NBQX disodium salt (Alomone Labs) were washed on and circulated through perfusion. To modulate the degree of glutamate spill-over, the glutamate esterase inhibitor TBOA (10 μm, tocris) was added to the bath. To test the NMDA receptor subunit contribution, the NR2A antagonist MPX-004 (10 μm, Alomone Labs) was used.

Recordings were made with a Multiclamp 700B amplifier (Molecular Devices, Inc.) and signals digitized at 10 kHz (National Instruments A/D board) were acquired using custom software written in the LabVIEW (National Instruments) environment. Analysis was performed offline using custom written software in MATLAB and Igor.

3.3.6 2-photon imaging acquisition

For NMDA mediated calcium imaging, voltage-clamp recordings were performed in regulator Ringer's solution using 3-5 MΩ electrodes containing the calcium indicator X-Rhod-5F (500 μM, Life Technologies) in high chloride internal solution (110 mM CsCl, 1 mM MgSO4, 10 mM EGTA, 10 mM HEPES, 5 mM QX-314) and cells were held at 0 mV. Cells were left for approximately 20 minutes after patching and prior to imaging to allow the calcium indicator to fill the dendrites.

2-photon excitation was delivered using a Mai Tai Ti:Sapphire laser (Spectra Physics) tuned to 910 nm, guided by X/Y galvanometer mirrors (Cambridge Technology). Image scans were acquired using custom software developed by Dr. Jamie Boyd (University of British Columbia) in the Igor Pro environment. To prevent the light stimulus from contaminating the fluorescent response, the LED projector was modified to match the light stimulation with the mirror flyback signal. The projector then sends an inverse signal to the gated photomultiplier tubes (PMTs) so that they are only open when the projector is off and the laser is scanning. This also protects the PMTs from harmful photo damage from the bright LED projector. The PMT signals were digitized at 1 MHz (PCI-6110, National Instruments) for image formation.

3.3.7 Miniature EPSC analysis

Traces were first analyzed in Clampfit (Molecular Devices) to detect miniature spontaneous EPSCs. Once events were detected, the traces were imported into IGOR pro and analyzed further using custom written procedures to first cut the traces into individual events based on the event start time determined in clampfit. All events were then baselined and filtered using a low band pass filter at 1000 Hz. Each event was then manually examined while calculating the rise time (20-80%), decay tau (exponential fit), and amplitude. This was done on individual events to try to ensure that each signal was a real event and not noise. Only events which had an amplitude above 10 pA were included in this analysis.

3.3.8 2-photon imaging analysis

The 2-photon imaging data was analyzed in the IGOR pro environment using programs written by Dr. Santhosh Sethuramanujam and Dr. Benjamin Murphy-Baum. Spatial profiles were

calculated as the peak ΔF/F across distance by manually tracing individual dendrites and converting the pixel number to length based on the pixel size. Signals were smoothed using a 2nd order Savitzky-Golay filter. NMDA "hotspots" were measured using a Gaussian fit on the obtained spatial profiles and measuring the width at the half-max of each fit. The same sites were used to analyze both the control and TBOA conditions.

To determine the percent of sites active in iGluSnFR vs. X-Rhod-5F calcium, small ROIs (approximately 2 μm) were placed along the entire dendrite without overlapping. To be considered as a signal, a peak response above 0.1 ΔF/F was required to ensure the signal was not due to noise and signals were averaged across multiple trials.

To determine the peak calcium response across contrasts, responses were measured from small regions of interest (ROIs) that were approximately 3 μm in size and the peak ΔF/F was plotted across contrast for each ROI. ROIs from the same cells were then averaged and shown in figure 4G (gray lines). Cells were normalized to the semi-saturation constant (C50) before being averaged across the population (black line) to account for any day-to-day differences in contrast sensitivity.

3.4 Results

To understand the synaptic organization of glutamate input onto DSGCs in the mature retina, we first recorded spontaneous AMPA and NMDA receptor-mediated miniature-like EPSCs (mEPSCs) at -70mV, in a nominally Mg^{2+} -free Ringer's solution. 100 μM hexamethonium (HEX) was included in the bath to block cholinergic activity and isolate AMPA and NMDA mediated events. Analysis of the spontaneous activity allows us to identify whether the glutamate to the AMPA and NMDA receptors is coming from the same or different sources. If AMPA and NMDA receptors are located at the same synapse and receive the same glutamatergic inputs, there will be a single population of spontaneous events, exhibiting a combination of the AMPA and NMDA kinetics, however, if the receptors are at different synapses and receive different glutamatergic inputs, there will be two distinct populations of events, each exhibiting the distinct kinetics of AMPA or NMDA receptors. Surprisingly, under these conditions, we did not observe the long-lasting NMDA mEPSCs, that are typically observed at other synapses.

Nevertheless, analysis of the rise time (20-80% of peak) and decay tau (single exponential fit) revealed two separate populations of events under control conditions. The first exhibited fast rise times (<1ms) and fast decay tau (<4ms), while the second population displayed slower rise times (1ms<5ms). To reveal the source of the two populations of spontaneous activity, we used different combinations of pharmacology to selectively isolate the different glutamatergic receptors located on the DSGCs. When D-AP5 (50 μM) was washed on to inhibit NMDA receptors, all slower events were blocked, leaving only those events residing in the lower quadrant with fast rise and fast decay indicating an AMPA only population (Figure 3.2 C). In comparison, in the presence of NBQX (10 μM) to inhibit the AMPA receptors, a

substantial portion of the fast events were blocked, leaving mainly those events which exhibit slower rise and decay indicative of the NMDA only events (Figure 3.2 B). The kinetics of the events remaining in D-AP5 match those fast events found in control (95% confidence integral <1ms) while the mEPSCs remaining in NBQX have a large overlay with the slower population of mEPSCs in control (Figure 3.2 D). Additionally, blocking either the AMPA or the NMDA receptors did not change the distribution of the measured mEPSC amplitude in comparison to control, indicating that AMPA and NMDA mediated quantal events are separate, since blocking either AMPA or NMDA receptors would result in a reduction in the peak amplitude if the observed events were mediated by both receptors simultaneously (Figure 2 E). The presence of separate AMPA only and NMDA only spontaneous activity in control conditions provides the first piece of evidence that these receptors are spatially separated into different synapses on the ON-OFF DSGC and the presence of NMDA mEPSCs indicates that these receptors are located in close proximity to the synaptic release site as peri-synaptic NMDA receptors are not believed to exhibit miniature EPSCs due to the low concentration of glutamate released during spontaneous activity and the distance it would have to travel to reach the peri-synaptic receptors.

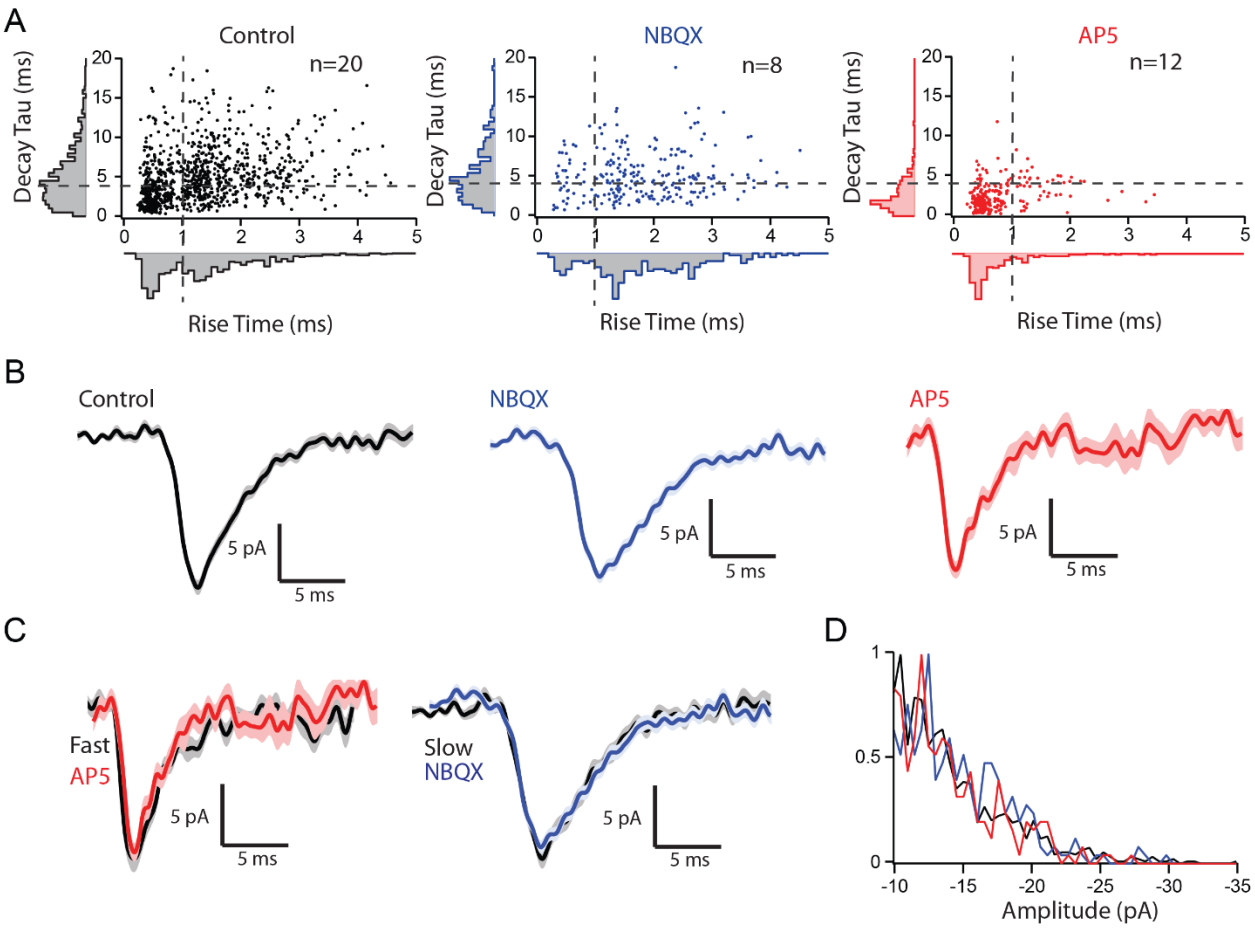

Figure 3.2 Spontaneous miniature-like EPSCs mediated by AMPA and NMDA receptors

(**A**) Spontaneous miniature-like EPSCs recorded from ON-OFF DSGCs in 0 Mg2+ ringers and 100 µM HEX allowed for the detection of AMPA and NMDA ESPCs in unison. Left is control conditions showing the distribution with both AMPA and NMDA mediated events, middle is NMDA only conditions and right is AMPA only conditions. Dotted line indicates the 95% confidence interval for AMPA mediated events. (**B**) Average wave forms for each of the three recording conditions in A. (**C**) Control wave forms (grey) can be separated into fast and slow populations based on the 95% confidence interval which overlay with the pharmacologically isolated AMPA and NMDA mediated events. (**D**) The amplitude of sEPSCs does not change with the application of NBQX or AP5

Our results are in sharp contrast to the retinal literature, where NMDA is thought to be mostly peri-synaptic, especially in the ON pathway, and requires spillover of glutamate for activation (Chen and Diamond, 2002; Sagdullaev, McCall and Lukasiewicz, 2006; Zhang and Diamond, 2009). To ensure that the NMDA mediated mEPSCs we observe are in fact indicative

of synaptic NMDA receptors and not due to spillover to peri-synaptic receptors, we blocked glutamate uptake using an EAAT inhibitor (10 μm TBOA) to increase the amount of spillover. If NMDA receptors were located peri-synaptically, an increase in the concentration of glutamate outside of the cleft would result in an alteration of mEPSC dynamics while synaptic receptor responses would remain unaffected (Chen and Diamond, 2002). We find that the addition of TBOA does not increase either the decay or amplitude of the NMDA-mediated spontaneous EPSCs ($p = 0.6$ for decay, $p = 0.5$ for amplitude). Previously, it has been shown in the retina that NMDA receptors that are localized in the synaptic cleft express the NR2A subunit while receptors that are extrasynaptic express the NR2B subunit (Zhang and Diamond, 2009; Manookin *et al.*, 2010). To further test the localization of the NMDA receptors in the DSGC, MPX-004 which blocks the synaptic NR2A subunits was used after application of NBQX. Under these conditions, MPX-004 abolished all NMDA-mediated spontaneous activity (Figure 3.3 C&D). These results further suggest that NMDA receptors are located within the synapse but are isolated to separate synapses from AMPA receptors and can therefore be identified as "silent" synapses.

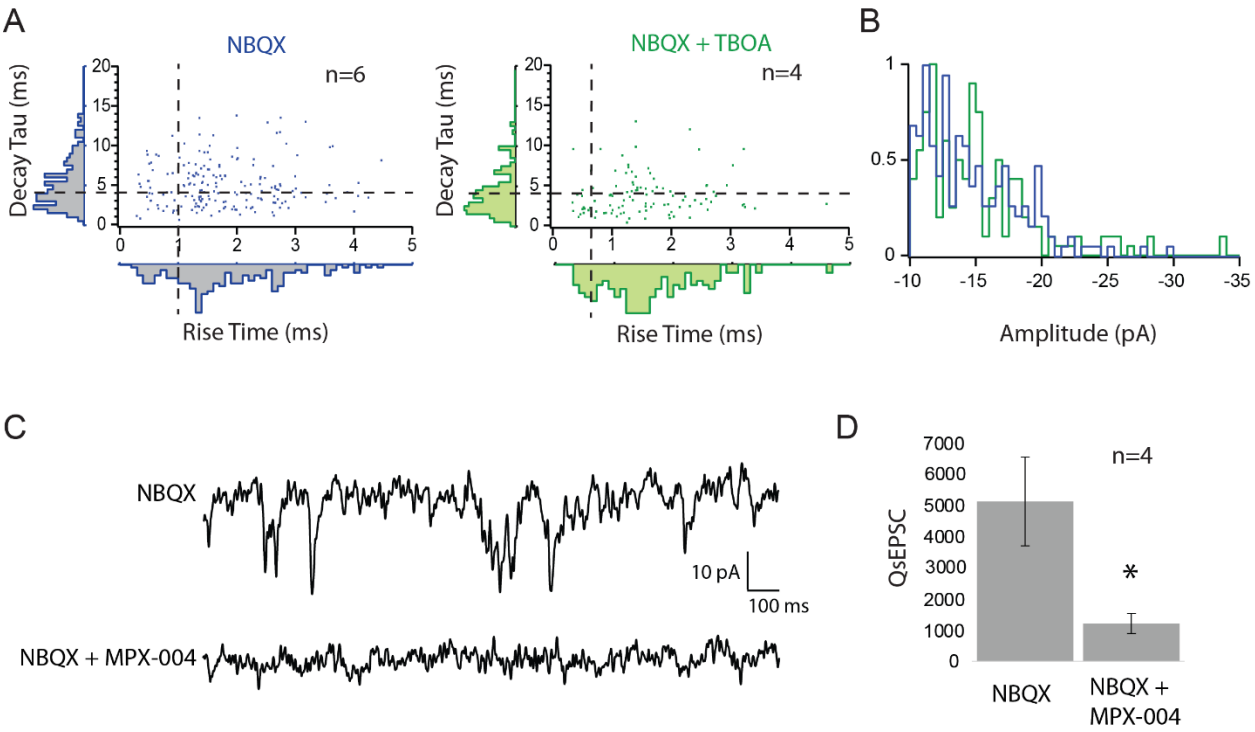

Figure 3.3 NMDA sEPSCs are mediated by synaptic NR2A receptors

(**A**) Increasing the amount of glutamate spillover with the application of TBOA did not change the rise time or decay tau of NMDA-mediated sEPSCs (**B**) Amplitdue of sEPSCs in NBQX and NBQX + TBOA (**C**) Baseline activity from an ON-OFF DSGC recorded at -60 mV in NBQX then NBQX + MPX-004 (**D**) The NR2A subunit specific antagonist MPX-004 blocks spontaneous NMDA-mediated activity (n = 4, $p < 0.005$)

In the retina, it is believed that NMDA receptors in the ON layer are located peri-synaptic while NMDA receptors in the OFF layer are both peri-synaptic as well as synaptic (Chen and Diamond, 2002; Zhang and Diamond, 2009). Because we utilized patch clamp techniques for the detection of synaptic NMDA receptors in the ON-OFF DSGC, we are unable to distinguish whether the NMDA-mediated mEPSCs observed here are originating from the ON or the OFF arbors. To further test the localization of glutamate receptors in DSGCs we relied on the high calcium permeability of NMDA receptors versus the non-permeable AMPA receptors expressed in the cells to allow for 2-photon calcium imaging of NMDA receptor mediated calcium influx in

the ON arbor of the DSGC. Hotspots of NMDA mediated calcium activity spread across approximately 2 μm in length (HWHM = 0.78 ± 0.07) and were not impacted by the addition of TBOA to increase glutamate spillover (HWHM = 0.67 ± 0.075, n.s.), indicating that NMDA mediated responses from the ON arbor are not driven by glutamate spillover which would result in a more global calcium response.

We also combined this technique with simultaneous iGluSnFR imaging, allowing us to compare the presynaptic and postsynaptic glutamate responses to light evoked stimuli at individual sites along the dendrite. Two populations of iGluSnFR hotspots were identified. One group was highly colocalized with the NMDA mediated calcium responses, indicating that those glutamate synapses contained NMDA receptors. The second group exhibited similar iGluSnFR signals while lacking any NMDA mediated calcium responses, indicating that these sites may be the AMPA only synapses or that there is glutamate spillover occurring which is not activating NMDA receptors (Figure 3.4 F,G). Although we cannot decisively conclude that the iGluSnFR signals which are not colocalized with NMDA calcium responses are truly AMPA only synapses nor that the sites which exhibit both calcium and iGluSnFR responses only contain NMDA receptors and not AMPA receptors, these results complement the spontaneous EPSC findings and strengthening the argument for separate AMPA and NMDA synapses on the ON arbor of DSGCs.

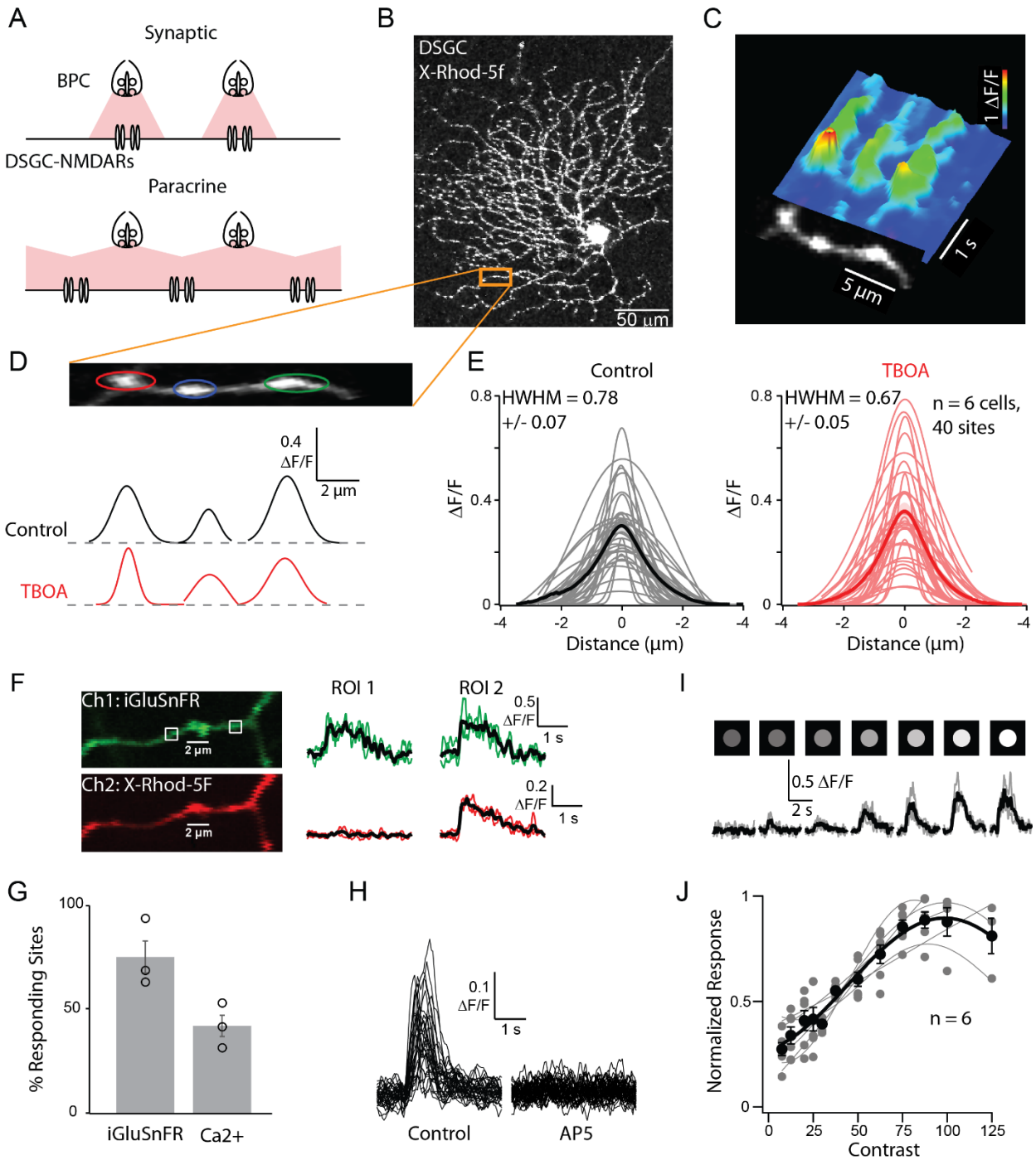

Figure 3.4 2P imaging of NMDA receptor mediated response localization and properties

(**A**) Two models of glutamate transmission via NMDARs in DSGCs. (**B**) 2-photon image stack of DSGC filled with X-Rhod-5f (**C**) Spatio-temporal Ca2+ profile along a dendrite during stimulus. (**D**) Top: Spatial profile of Ca2+ response of the same dendrite (black) fitted to a gaussian function (color coded as synaptic sites). Bottom: Gaussian fits in control (black) and TBOA (red) of the spatially isolated synaptic sites along the dendrite. (**E**) Gaussian fits in control (black) and TBOA (red) across the population (n= 6 cells, 40 synaptic sites) shows that

increasing glutamate spillover does not increase the spatial extent of the calcium response (p = 0.98). (**F**) Simultaneous iGluSnFR (green channel) and calcium (red channel) imaging shows two populations of sites along the dendrite: ones with iGluSnFR only (ROI 1) and ones with both iGluSnFR and calcium responses (ROI 2). (**G**) 75% of the sites analyzed had a iGluSnFR signal while only 42% had a calcium signal (n=3). (**H**) Calcium responses in control and AP5 indicate that the responses measured here are mediated by NMDA receptors. (**I**) Ca2+ responses (grey, individual trials; black, average) to a flash of increasing contrast. (**J**) Contrast response function across the population (grey lines are the average from all ROIs of a single cell, black line is the average across the population).

Previously, it was believed that NMDA receptors in the retina are required to be located extrasynaptically to allow for a graded postsynaptic response during multivesicular release from bipolar cells because synaptic NMDA receptors are thought to become saturated by single quantal events. This raised the question of how DSGCs are able to exhibit graded responses to increasing contrasts when both AMPA and NMDA receptors are located synaptically. To address this question, we performed contrast response function recordings of calcium influx through NMDA receptors to identify whether graded responses are encoded locally where each synaptic site exhibits an increase in response or whether it is a global effect where an increase in contrast results in more synapses being activated to saturation. As seen in Figure 3.4, increasing stimulus contrast results in an increase in calcium response at each individual NMDA-rich synapse. This proves that although the NMDA receptors in ON-OFF DSGCs are located in the synapse, they are still able to encode graded responses and do not saturate to single vesicles of glutamate. Together, these results build on previous findings from our lab that DSGCs in the mouse retina express “silent” synapses (Sethuramanujam *et al.*, 2017) and additionally shows that these synapses are able to locally encode graded responses.

3.5 Discussion

The NMDA mediated responses reported here exhibit kinetics that are much more rapid than those typically reported in the literature (Dzubay and Jahr, 1996; Umemiya, Senda and Murphy, 1999). One explanation for this difference could result from a difference in receptor subunit composition. It has been shown that NMDA receptors expressing the NR2a subunits exhibit faster kinetics than those expressing NR2b (Tovar, Sprouffske and Westbrook, 2000; Hansen *et al.*, 2014), consistent with our findings of fast NR2a mediated responses which are blocked by MPX-004 (Figure 3.3). A second explanation could come from a difference in cell properties between DSGCs and other cell types that have been examined, leading to a difference in the filtering properties between cell types which would alter the kinetic properties recorded from the cell soma (D'Angelo, Rossi and Garthwaite, 1990). It is also important to note that these experiments were performed in a solution that is free of Mg2+ to allow both AMPA and NMDA mediated EPSCs to be recorded simultaneously at -60 mV which may alter the observed NMDA kinetics compared to those seen at +40 mV.

Typically, silent synapses have been identified as synapses which exhibit responses at holding potentials of +40mV but lack responses at 0 or -60mV due to the voltage dependence of NMDA receptors (Kerchner and Nicoll, 2008). This standard is useful for identifying silent synapses but does not provide insight into the mechanisms responsible for the silencing effect (pre- or post-synaptic). The use of mEPSCs analysis allowed us to study the responses at individual synapses and determine the spatial separation of glutamatergic inputs onto the DSGC to distinguish between the three proposed models of silent synapses (Figure 3.1). The presence of NMDA only mEPSCs along with the calcium imaging showing quantal NMDA "hotspots"

allows us to conclude that silent synapses in mature DSGCs represent synapses lacking the postsynaptic expression of AMPA receptors.

Multivesicular release from retinal bipolar cell terminals has been widely accepted in the literature. However, how the postsynaptic receptors can encode these graded responses has been difficult to address using electrophysiology alone. Previously, glutamate imaging in zebrafish has shown that bipolar cells can release up to 11 vesicles of glutamate near simultaneously but how the postsynaptic receptors respond to these varying concentrations of glutamate in the cleft remains unknown (James *et al.*, 2019). Here, combining GluSnFR imaging with NMDA mediated calcium imaging has allowed us to simultaneously compare the presynaptic and postsynaptic actions of graded glutamate release and conclude that the increase in amplitude seen at the soma during increased contrast is due to a local increase in receptor activation at individual synapses. In other cell types of the retina, it is believed that synaptic NMDA receptors containing the NR2A subunit are responsible for low contrast encoding while extrasynaptic NMDA receptors containing the NR2B subunit respond to high contrast stimuli (Zhang and Diamond, 2009; Manookin *et al.*, 2010; Singh *et al.*, 2011). In contrast, our data suggests that the synaptic, NR2A containing, NMDA receptors in the ON-OFF DSGC are able to respond over a range of contrasts (Figure 3.4). The non-saturation of NMDA receptors from single vesicles of glutamate could be due to the subunits expressed but could also be due to synaptic properties such as the rate of glutamate uptake or diffusion, similar to the mechanism used by hair cells to prevent AMPA saturation (Graydon *et al.*, 2014; Li, Cho and von Gersdorff, 2014).

Additionally, the contrast range used here is lower than that typically used during somatic recordings because high stimulus intensities cause contamination in the fluorescent signal during imaging. Because of this it is highly possible that NMDA receptors may still saturate at lower

levels than AMPA receptors and therefore may not be able to encode the full range of multivesicular release from the bipolar cells.

3.6 Conclusions

In this research the spontaneous miniature EPSCs from ON-OFF DSGCs were analyzed to confirm the presence of 'silent' NMDA-only synapses by identifying two separate populations of mEPSCs. Simultaneous NMDA-mediated calcium imaging and iGluSnFR glutamate imaging provides further evidence that NMDA and AMPA receptors are spatially separate. Analysis of the spatial extent of the calcium signals in control vs. TBOA indicated that these receptors are located within the synapse as opposed to being extrasynaptic and responding to glutamate spillover. The NMDA-mediated calcium responses during stimuli of increasing contrast determined that these NMDA-only synapses respond to glutamate release in a graded fashion, responding to multivesicular release without saturation.

Chapter 4: Orientation selectivity in the direction-selective ganglion cell

4.1 Abstract

Retinal ganglion cells split the visual information into many parallel channels, each conveying different features of the visual scene to higher order visual areas for further processing. Two prominent features detected in the retina are direction selectivity and orientation selectivity which are predominantly thought to be encoded by separate populations of ganglion cells, the direction-selective ganglion cells (DSGCs) and the orientation-selective ganglion cells (OSGCs), respectively. This contrasts with what has been observed in the visual cortex where all direction-selective cells are also orientation-selective. Using a combination of electrophysiology and 2-photon imaging we show that a population of ON-OFF direction-selective ganglion cells are also strongly orientation-selective, matching that seen in the visual cortex. We further show that this orientation selectivity arises from gap-junction mediated asymmetric spatial integration in the type 5a bipolar cells. These findings show that ON-OFF DSGCs utilize separate mechanisms to generate different feature selectivity, with starburst amacrine cells mediating DS and bipolar cells mediating OS and uncover a new role for electrical coupling in the retina.

4.2 Introduction

Throughout the visual system, visual signals are not simply relayed as single pixel values but are instead broken up into the many different features of the visual scene. Two prominent features of a natural visual scene that are detected at all levels of the visual system are direction of motion and stimulus orientation.

The ability to detect the direction of motion across the visual field during both self-motion as well as when objects are moving through the environment is a key visual feature that is critical to survival. In the retina, direction-selective ganglion cells (DSGCs) were first characterized in the 1960's when Barlow and Levick identified a population of ganglion cells which respond strongly to an object moving in a particular preferred direction but exhibited little to no response if the object was moving in the opposite (null) direction (Barlow and Levick, 1965). In the mammalian retina, there are four distinct types of ON-OFF DSGCs, each encoding one of the four cardinal directions (north, east, south, west), and have been thought of as acting like a compass for the visual system, potentially playing a critical role in navigation during self-motion (Oyster and Barlow, 1967). Typically, ON-OFF DSGCs have been studied using simple stimuli moving across a uniform background, however, the natural scene is much more complex, and the edges observed are much less salient than that of a simple stimulus typically used experimentally, making the task of encoding the direction of motion more difficult for the DSGCs under natural conditions. One way to overcome this obstacle is for the visual system to first perform an edge enhancement of the visual signal prior to performing motion encoding. In nature, most contrast changes occur along either the vertical or horizontal axes (Coppola *et al.*, 1998). Because of this orientational bias, one way that the visual system can perform edge enhancement is to use either vertical or horizontal spatial orientation filters (Girshick, Landy and

Simoncelli, 2011). In the retina, orientation-selectivity has been observed at the level of bipolar cells and amacrine cells (Bloomfield, 1991, 1994; Murphy-Baum and Taylor, 2015; Antinucci *et al.*, 2016; Johnston *et al.*, 2019), however, whether the direction-selective circuit utilizes an orientational spatial filter to simplify the task of encoding the direction of motion of moving edges has not been shown.

In the retina, direction selectivity and orientation selectivity are predominantly shown to be detected separately by two distinct populations of retinal ganglion cells, with directional information being encoded by the direction-selective ganglion cells (DSGCs) and orientation information encoded by the orientation-selective ganglion cells (OSGCs). This is in contrast to what is observed in the visual cortex, where the direction-selective cells also exhibit orientation selectivity (Hubel and Wiesel, 1959). The basic direction-selective circuit of the retina is well defined, where asymmetric inhibitory connectivity between directionally tuned starburst amacrine cell dendrites and DSGCs drives direction-selectivity in the ganglion cells (Euler, Detwiler and Denk, 2002; Taylor and Vaney, 2002; Briggman, Helmstaedter and Denk, 2011; Mauss *et al.*, 2017). The ON-OFF DSGCs also receive symmetric glutamatergic inputs from bipolar cells which are predominantly thought to be untuned. In contrast, the orientation-selective circuit and mechanisms in the retina are less well defined, where different types of OSGCs across different species have been shown to rely on multiple different mechanisms to generate orientation selectivity. These include elongated dendritic morphology, gap junction coupling, and orientation tuned inhibitory and/or excitatory inputs (Venkataramani and Taylor, 2010, 2016; Nath and Schwartz, 2016, 2017; reviewed by Antinucci and Hindges, 2018). Additionally, the source of the orientation tuned inhibition and excitation remain predominantly unknown but orientation selective amacrine cells have been detected in mouse, rabbit and

zebrafish retina and, orientation-selective glutamate release has also been observed from bipolar cell terminals in zebrafish (Bloomfield, 1991, 1994; Murphy-Baum and Taylor, 2015; Nath and Schwartz, 2017; Johnston *et al.*, 2019).

In rabbit retina, a population of cells have been observed which encode both directional and orientational preferences, however, there was no apparent relation between preferred direction and preferred orientation and the mechanisms involved in this dual feature detection have yet to be investigated (He, Levick and Vaney, 1998). Here, we identify a population of posterior tuned DSGCs in the mouse retina which exhibit both direction and orientation selectivity and show that this dual feature selectivity arises from independent circuitry, with orientation selectivity arising from tuned glutamatergic inputs from the presynaptic bipolar cells and not relying on the starburst circuitry that drives DS. We propose that this allows the DSGCs to perform hierarchical processing to simplify the task of detecting motion during complex stimulus by first performing orientational spatial filtering at the level of bipolar cells to enhance the vertically tuned edges, before using directional filtering at the level of the starburst amacrine cells to encode the direction of motion of those edges.

4.3 Methods

4.3.1 Animals

All animal procedures were performed in accordance with the Canadian Council on Animal Care (CCAC) and approved by the University of Victoria's Animal Care Committee. Mice of both sexes, aged between P21-P140 were used for experiments. Animals were group house in a 12-hour dark/light cycle.

Experiments were performed using TRHR-eGFP (provided by Dr. Marla Feller, UC Berkeley; RRID: MMRRC_030036-UCD) for posterior DSGC recordings. For calcium imaging, the Kcng4-cre (B6.129(SJL)-Kcng4$^{tm1.1(cre)Jrs/J}$, JAX stock #029414) was crossed to GCaMP6f (B6J.Cg-Gt(ROSA)26Sor$^{tm95.1(CAG-GCaMP6f)Hze/MwarJ}$, JAX stock #028865). To investigate the role of electrical coupling, the Kcng4cre;GCaMP6f line was crossed to the Cx36-floxed line (provided by Dr. David Paul, Harvard). To disrupt SAC GABA release the ChATcre-mouse line (RRID: MGI_5475195) was crossed with a floxed allele of Slc32a1 (*Slc32a1*^{tm1Lowl} , JAX stock # 012897), which also is commonly referred to as *Vgat*$^{flox/fox}$.

4.3.2 Experimental conditions

Retinal preparations, visual stimulation and electrophysiology were all performed as described in section 2.5.

CNQX and DCG-IV were purchased from Tocris, TTX was purchased from Alomone, UBP-310 was purchased from Abcam and 18bGA was purchased from Sigma-Aldrich.

4.3.3 Sharp-electrode electroporation

To visualize single bipolar or ganglion cells, sharp electrodes (80-120 mΩ) were back filled with 15 mM of sulforhodamine-101 (SR-101, Sigma Aldrich) then brought into contact with the cell of interest. Iontophoresis was achieved by applying the pulse function in the MultiClamp 700B software (Molecular Devices) set at 50 ms (Ding et al., 2016).

4.3.4 2-photon image acquisition

NMDA-mediated calcium imaging was performed as described in Chapter 3.

For bipolar cell calcium imaging, the Kcng4cre;GCaMP6f mouse line was used with or without Cx36-floxed. To ensure imaging was performed in the proper retinal layer, DSGCs were filled with a sulforhodamine-101 via sharp electrode electroporation (see above) to visualize the dendritic arbor while calcium responses were recorded from labelled bipolar cell terminals.

Two-photon excitation was delivered using a Mai Tai Ti:Sapphire laser (Spectra Physics) tuned to 910 nm, guided by X/Y galvanometer mirrors (Cambridge Technology). Image scans were acquired using custom software developed by Dr. Jamie Boyd (University of British Columbia) in the Igor Pro environment. To prevent the light stimulus from contaminating the fluorescent response, the LED projector was modified to match the light stimulation with the mirror flyback signal. The projector then sends an inverse signal to the gated photomultiplier tubes (PMTs) so that they are only open when the projector is off, and the laser is scanning. This also protects the PMTs from harmful photo damage from the bright LED projector. The PMT signals were digitized at 1 MHz (PCI-6110, National Instruments) for image formation.

4.3.5 Quantification

DSI and OSI were calculated as:

$$DSI = \frac{\sum R(\theta)e^{i\theta}}{\sum R(\theta)} \qquad OSI = \frac{\sum R(\theta)e^{2i\theta}}{\sum R(\theta)}$$

where R(θ) is the response for θ direction or orientation calculated from the spike rate or peak EPSC/IPSC amplitude during that stimulus. The preferred angle was calculated from the resultant (DSI) or half phase of the resultant (OSI). DSI or OSI ranged from 0 to 1, with 0

indicating a perfectly symmetrical response, and 1 indicating a response in only one of eight directions or orientations presented.

Population data have been expressed as mean ± SEM and are indicated in the figure legend along with the sample size. Student's t test (paired or unpaired depending on the samples) was used to compare values under different conditions and the differences were considered significant when $p \leq 0.05$, unless otherwise noted in the figure legend.

4.3.6 Calcium imaging analysis

All imaging analysis was performed using custom written software by Dr. Benjamin Murphy-Baum in IGOR pro. ROIs of approximately 3 μm were drawn around individual terminals or regions of dendrites and the signals were smoothed using a 2^{nd} order Savitzky-Golay filter. Peak $\Delta F/F$ values were calculated for each ROI. During application of pharmacology, the same ROIs were used across conditions.

4.4 Results

4.4.1 Direction-selective ganglion cells are also orientation-selective

In the mouse retina, direction-selective ganglion cells (DSGCs) and orientation-selective ganglion cells (OSGCs) are thought to be two separate populations with little overlap between the two. However, to test for orientation-selectivity in DSGCs, previous studies have predominantly used drifting grating stimuli or moving bar stimuli where any orientation selectivity may be masked by the strong direction selectivity exhibited by these cells during motion. To probe for these two different features, we used both moving bar stimuli as well as stationary bar stimuli to show that in addition to being direction-selective (Figure 4.1 A,B), the majority of DSGCs also exhibit some degree of orientation selectivity (Figure 4.1 C,D). To study this effect, we utilized the TRHR;eGFP mouse line which labels a population of posterior tuned ON-OFF DSGCs. Consistently, these cells respond optimally to static bars which are oriented 90 degrees off from their preferred direction of motion (along the orthogonal axis) (Figure 4.1 E). Interestingly, this relation between preferred orientation angle and preferred direction angle matches that seen in the direction-selective simple and complex cells of the visual cortex (Hubel and Wiesel, 1959, 1962). Importantly, the strength of the orientation selectivity observed in these ON-OFF DSGCs is comparable to that observed in the ON OS RGCs of the mouse retina (Nath and Schwartz, 2016) (Figure 4.1 F).

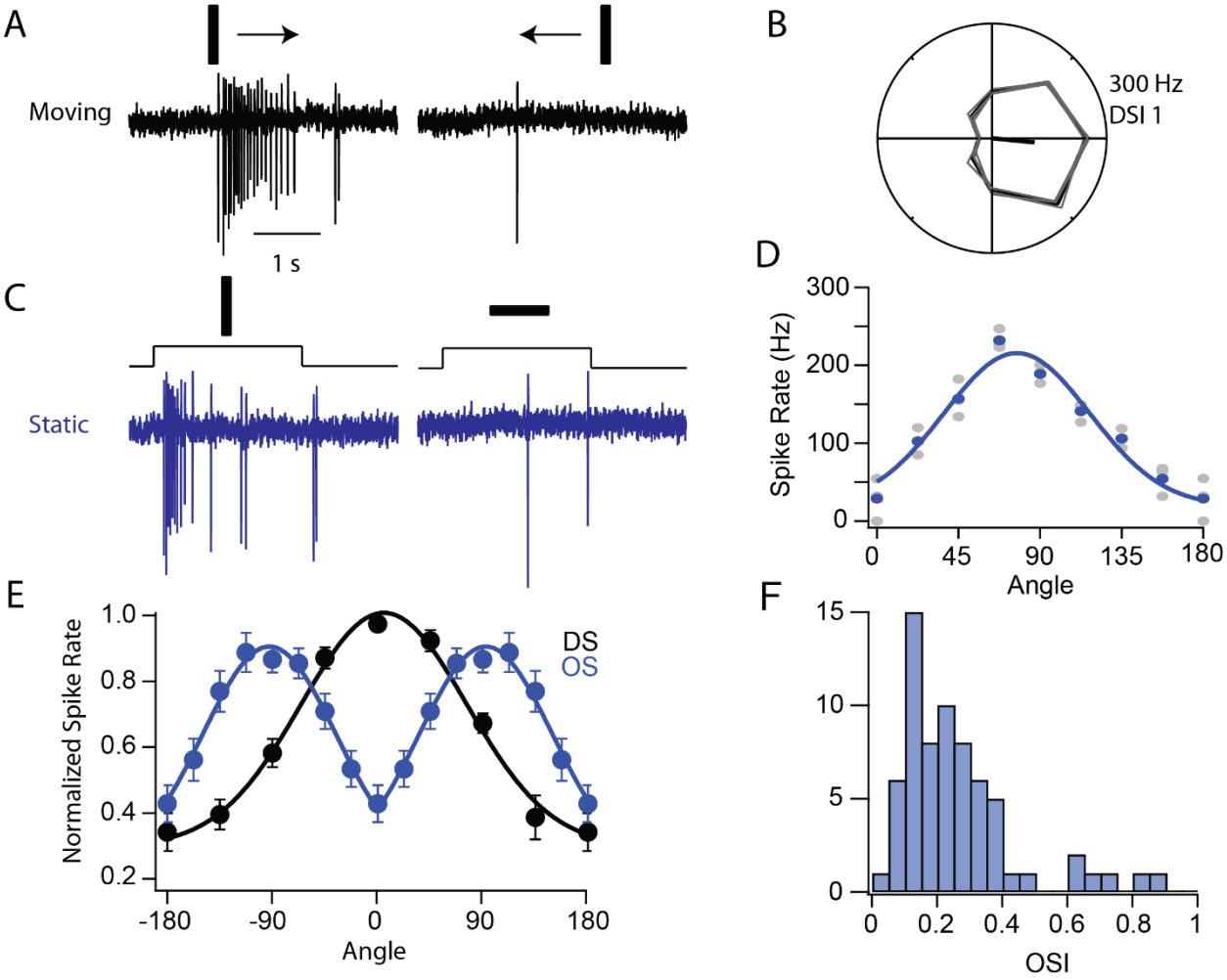

Figure 4.1 Orientation selectivity in direction selective ganglion cells

(**A**) Spike responses from an example TRHR GFP^{+} DSGC to moving stimulus in the preferred (left) and null (right) directions. (**B**) Polar plot calculated from the peak spike rate during 8 direction stimulation (grey = individual trials, black = average). (**C**) Spike responses to static bar stimulus in preferred (left) and null (right) orientations from the same cell as A and B. (**D**) Peak spike rate during 8 orientation stimulation (grey = individual trials, blue = average). (**E**) Relationship between preferred direction (black) and preferred orientation (blue) across the population (n=52) shows that TRHR DSGCs preferred nasal coding motion and bars orientated orthogonal to the preferred direction of motion, OS and DS responses are normalized together to the peak spike rate. Data shown as mean ±SEM. (**F**) Histogram of OSI across the population calculated as the vector sum from static bars in 8 orientations.

4.4.2 Orientation-selectivity does not rely on DS circuitry

Based on anatomical reconstructions, starburst amacrine cells have been shown to provide synapses onto DSGCs in an asymmetric manner, where the starburst dendrites are always synapsing onto the DSGC from the null side (Figure 4.2 A) (Briggman, Helmstaedter and Denk, 2011). This connectivity, in addition to the direction-selectivity of the starburst dendrites (Euler, Detwiler and Denk, 2002), results in asymmetric GABAergic inhibition to the DSGC which drives the direction-selectivity. In theory, this inhibitory asymmetry which is responsible for generating the DS responses in the DSGC may also generate OS in a similar fashion where bars orientated in line with the starburst dendrites (along the null axis) will drive the largest amount of inhibition to the DSGC. To examine the role of the DS circuitry in generating OS in the DSGC, we utilized two distinct techniques to either pharmacologically block the GABAergic and cholinergic transmission or by genetically disrupting only the GABAergic transmission from starburst amacrine cells while keeping the other circuitry intact. First, we utilized the mGluR2 agonist DCG IV (5 μM) which selectively blocks the starburst amacrine cell from releasing neurotransmitter (Sethuramanujam, Awatramani and Slaughter, 2018). Additionally, a genetic mouse model (ChATcre;VGat) was used to specifically knockout the vesicular GABA transporter (VGat) from starburst amacrine cells. Under both pharmacological and genetic knockout conditions, direction-selectivity was fully disrupted, as expected (Figure 4.2 B,C). However, under these same conditions, the orientation-selectivity in these cells remained intact, indicating that direction-selectivity and orientation-selectivity are generated through distinct circuitry (Figure 4.2 D,E). It is important to note that the VGat knockout mouse line appears to have inconsistent effects across cells so for this analysis, only those cells which were

TRHR;GFP + and which had weak or no DS tuning (DSI < 0.2) were analyzed for OS to ensure proper disruption of GABA transmission from the starburst amacrine cells.

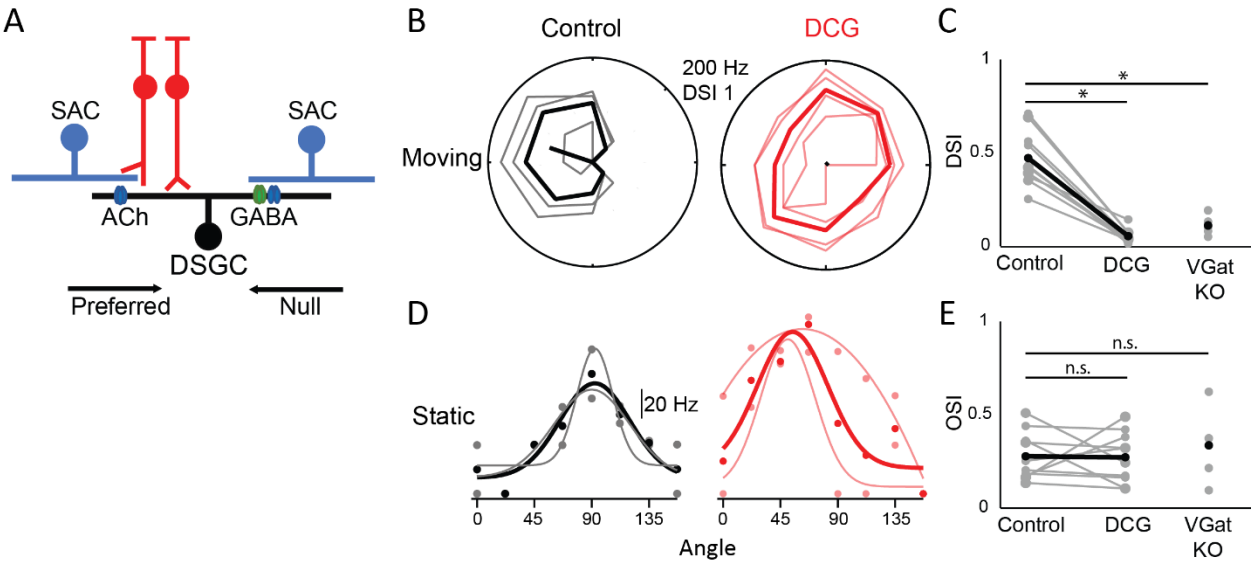

Figure 4.2 DSGC orientation selectivity does not rely on DS circuitry

(**A**) Diagram of the DS circuitry showing the asymmetric inhibitory connectivity between SACs and DSGCs. (**B**) Polar plots calculated from the peak spike rate during moving stimuli in 8 directions in control (black) and red (DCG) from an example cell. (**C**) Population data showing the DSI is significantly disrupted by application of DCG ($p<0.005$) and in the VGat KO mouse ($p<0.005$) showing that DS relies on SAC mediated inhibition. (**D**) Spike rate plotted against stimulus angle during static bar stimulus in 8 orientations in control (black) or DCG (red) from the same cell as B. (**E**) Population data showing the OSI is not affected by application of DCG ($p=0.9$) or in the VGat KO ($p=0.5$, grey = single cells, black = average) shows that the OS does not rely on SAC release ($n=10$ for control vs. DCG, $n=5$ for VGat KO).

4.4.3 Excitatory and inhibitory inputs are independently tuned for orientation

To examine the origin of the orientation-selectivity in DSGCs, we measured EPSCs and IPSCs under both control and DCG IV conditions. In control, both the excitatory and inhibitory

inputs were tuned to orientation, however, the tuning preference for the two were opposite where the excitatory inputs had a maximal response to the preferred orientation and the inhibitory inputs had a maximal response to the null orientation (Figure 4.3 A,C), similar to that seen in other types of orientation-selective ganglion cells in the retina (Venkataramani and Taylor, 2010, 2016; Nath and Schwartz, 2016). When starburst release was blocked, the inhibition was largely abolished and the small inhibitory conductance that remains is not OS (Figure 4.3 E, F). In comparison, the amplitude of the EPSC was only weakly affected and the remaining excitatory current remained orientation-selective (Figure 4.3 E, F). Together with the spiking data, these results further suggest that the starburst amacrine cell network may provide some orientation selectivity but is not required to generate OS in DSGCs. It is important to note that in some cells, the EPSCs did not appear to be strongly OS under both control and DCG conditions, this may be due to differences in tissue health or the adaptation state of the retina which may alter the contribution of excitation from the different bipolar cells providing glutamatergic inputs to the DSGC (see discussion).

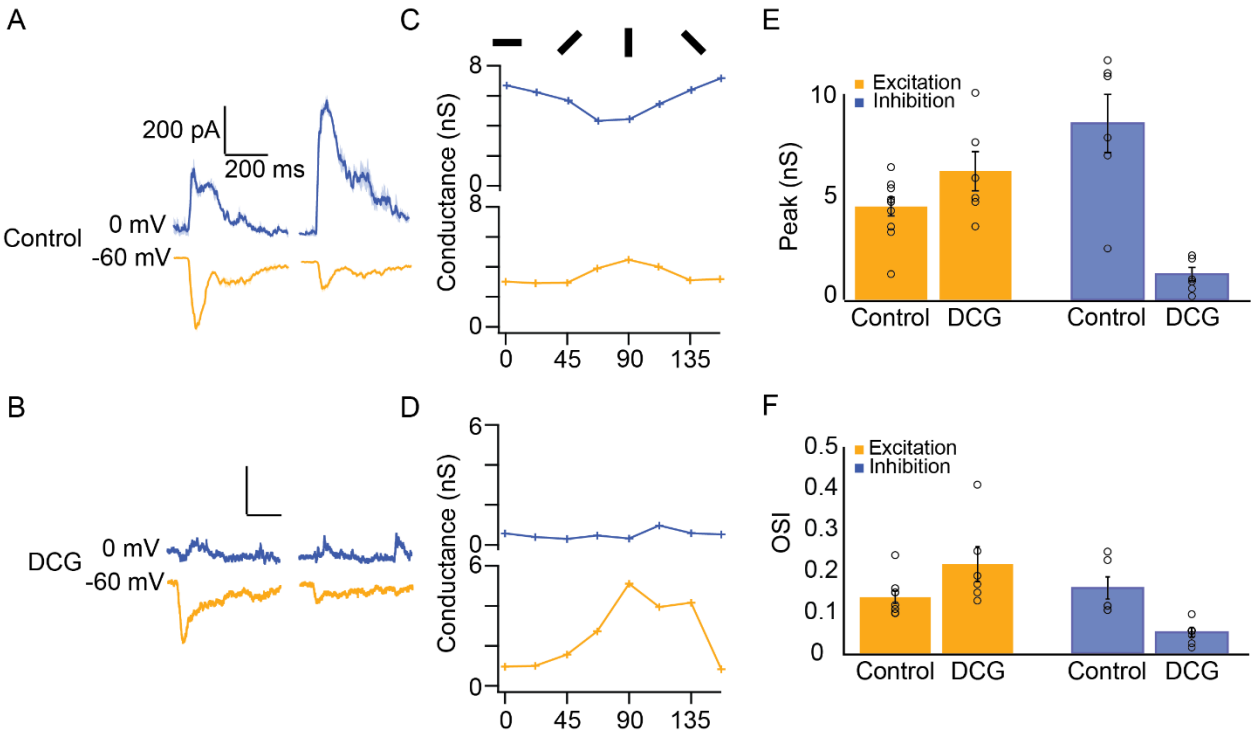

Figure 4.3 Excitation and inhibition are independently tuned for OS

(**A**) EPSCs (orange) and IPSCs (blue) recording from a TRHR-GFP^{+} DSGC during static bar stimuli in the preferred (left) and null (right) orientations indicating that both excitation and inhibition are OS, with excitation being largest for the preferred orientation bar and inhibition being largest for the null orientation bar. (**B**) Same as in A but after bath application of DCG. (**C**) Peak conductance across 8 orientations for IPSCs (top) and EPSCs (bottom). (**D**) Same as in C but after bath application of DCG. (**E**) Peak conductance of the excitation and inhibition across the population shows that DCG does not have a significant effect on the excitation ($p=0.09$) but significantly reduces the inhibition ($p<0.005$). (**F**) Excitatory OS does not rely on SAC release ($p=0.06$) but inhibitory OS does ($p<0.005$, $n=9$ for control excitation, $n=6$ for inhibition and DCG excitation, bars show mean ±SEM, circles are each cell).

4.4.4 Orientation-selective bipolar cells

In the mouse retina, the vertically tuned ON orientation-selective ganglion cells have also been shown to exhibit orientation-selective excitatory inputs which are insensitive to inhibitory blockers. The source of this excitatory OS remains unknown but has been proposed to arise either postsynaptically from untuned inputs synapsing onto the OSGC in an elongated manner

along the OS axis or presynaptically from excitatory inputs which are independently tuned for OS (Nath and Schwartz, 2016). Since previous experiments relied on recordings obtained from the soma of ganglion cells which only provides information regarding the summation of all synaptic inputs along the dendritic tree, it has been difficult to determine whether orientation tuning is due to a global summation of untuned inputs or if it is driven by individual, locally tuned inputs. To address this question in the DSGC, we first utilized the calcium permeability of glutamatergic NMDA receptors to analyse individual synaptic inputs from bipolar cells to DSGCs. High chloride internal solution was used, and cells were voltage-clamped at 0 mV to minimize the impact of clamp error on the calcium signals observed while maintaining a large driving force for calcium ions. Under these conditions, approximately half of the regions of interest (ROIs) observed exhibited orientation tuning (36 of 62) to approximately the same angle (Figure 4.4 C, D). This preferred angle of the calcium responses matches the preferred angle observed from spiking activity of each of the cells taken prior to imaging (data not shown). Additionally, application of an NMDA receptor antagonist (50 μM D-AP5) completely abolished the calcium signals, indicating that the calcium responses observed under these conditions were indeed due to NMDA receptor activation (Figure 4.4 B). These results indicate that orientation-selectivity in the DSGC may arise presynaptically, at the level of glutamate release from presynaptic excitatory cells.

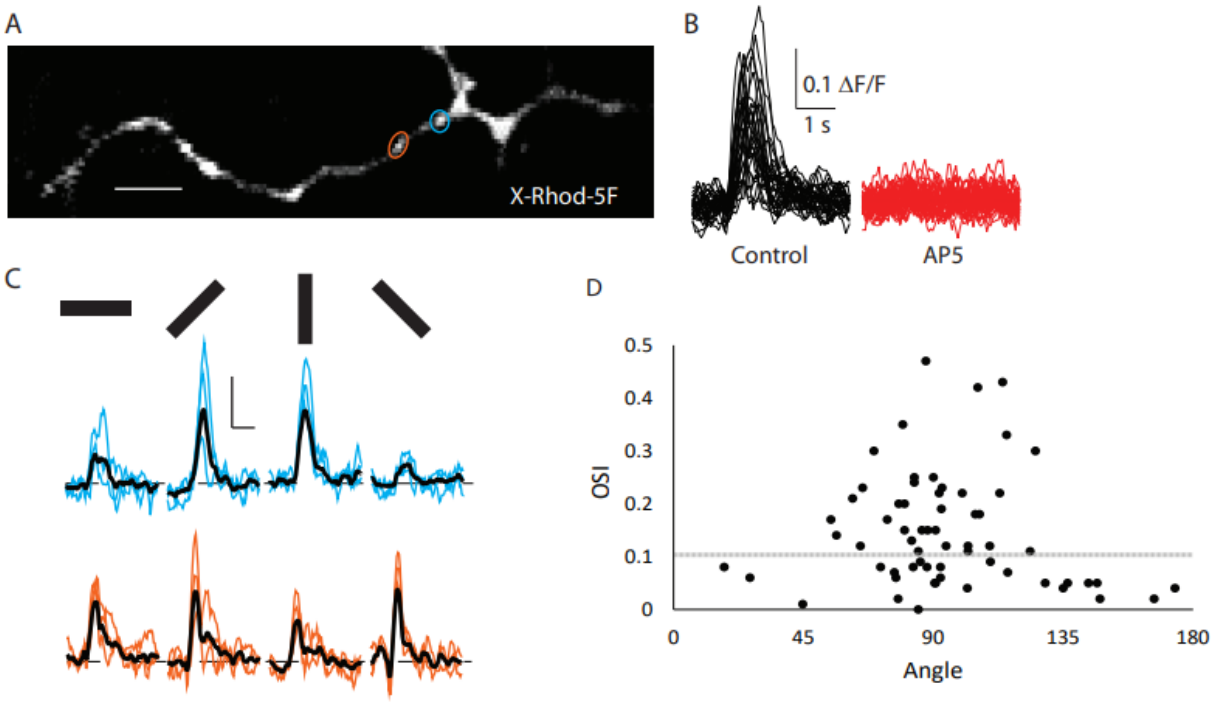

Figure 4.4 Glutamatergic inputs to DSGCs are tuned presynaptically

(**A**) Dendrite of a TRHR+ DSGC filled with the red calcium indicator X-Rhod-5F, colored circles indicate the ROIs analyzed in panel C. (**B**) Calcium responses from multiple ROIs in control and after application of AP5 indicated that the calcium transients are mediated by NMDA receptors. (**C**) Two example ROIs showing responses to static bar in 4 orientations show regions which are highly OS and neighbouring regions which are non-OS. (**D**) Relationship between preferred angle and OSI calculated from the peak DF/F values across the population (n= 5 cells, 62 ROIs), points below the grey dashed line are considered non-OS.

ON-OFF DSGCs receive glutamatergic inputs from multiple types of bipolar cells, as well as glutamatergic amacrine cells (Vaney, Sivyer and Rowland Taylor, 2012; Helmstaedter *et al.*, 2013; Matsumoto, Briggman and Yonehara, 2019). To identify the source of the orientation tuned glutamate release we utilized the previously described Kcng4-cre mouse line crossed to floxed GCaMP6f to study the responses of type 5a(i) bipolar cells which are known to make glutamatergic connections with DSGCs (Duan *et al.*, 2014). Since labelling in the Kcng4cre mouse line is not specific to only the type 5a bipolar cells, DSGCs were filled with

sulfurhodamine-101 to allow for colocalization of bipolar terminals with DSGC dendrites (Figure 4.5 A, B). When using a stationary bar stimulus, the measured calcium responses observed in the terminals of type 5a bipolar cells exhibit orientation selectivity, responding stronger to bars oriented vertically (preferred) than to bars oriented horizontally (null) (Figure 4.5 C, D). Interestingly, although the strength of the tuning varied across terminals, each terminal shared a similar preferred angle for bars oriented vertically, along the dorsal/ventral axis of the retina (Figure 4.5 E). It is important to note that across experimental days, the retina was mounted in the recording chamber in different configurations then responses were normalized to the nasal axis which was marked during retinal preparation (as described in Wei, Elstrott and Feller, 2010). This ensured that the orientation selectivity that was observed did not arise from a bias in the experimental setup. These results provide further evidence that orientation-selectivity observed in DSGCs originates at the level of bipolar cell terminals. Whether other bipolar cells are also orientation-selective or if it is unique to the type 5a remains to be determined.

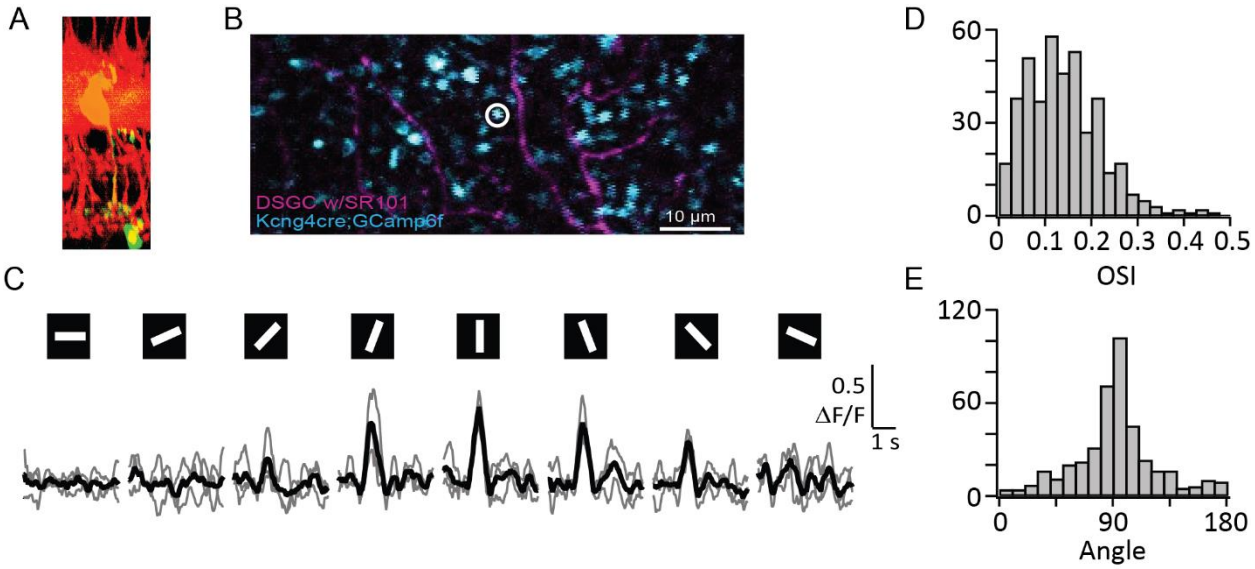

Figure 4.5 Type 5a bipolar cells are orientation-selective

(**A**) Example bipolar cell sharp electrode electroporated with Alexa-488 (green) in the Kcng4cre mouse line (red). (**B**) Example field of view of bipolar cell terminals in Kcng4cre;GCaMP6f mouse line with a DSGC filled with SR-101 to ensure imaging is being performed in the proper layer of the IPL. (**C**) Calcium responses measured from the example ROI indicated in B. Stimuli are 50 µm x 500 µm static bar flashes in 8 orientations, showing a strong preference for vertically oriented bars. (**D**) Distribution of OSI values across the population. (**E**) Distribution of angles across the population show a strong preference for bars oriented to 90 degrees (vertical along the dorsal/ventral axis of the retina, n=16 retina, 362 ROIs).

4.4.5 Mechanisms of bipolar cell OS

A common property that many retinal cell types exhibit, including bipolar cells, is a center-surround receptive field organization (Kuffler, 1953; Zhang and Wu, 2009; Franke *et al.*, 2017). This results in cells receiving predominantly excitatory inputs when only the center of the receptive field is stimulated and inhibitory during stimuli that extend beyond the excitatory center inputs. In bipolar cells, this inhibitory surround can originate both presynaptically, at the level of horizontal cells to photoreceptors as well as postsynaptically, with feedback inhibition

from wide-field amacrine cells to the bipolar cell terminals (Zhang and Wu, 2009). Previous findings have indicated that the surround inhibition mediated by wide-field amacrine cells relies on sodium spikes and is therefore TTX sensitive while horizontal cell inhibition is TTX insensitive (Hoggarth *et al.*, 2015). To test if the orientation selectivity observed here is due to asymmetries in the wide-field surround inhibition, we applied TTX (1 μM) while recording the calcium responses in the bipolar terminals. Although TTX caused an increase in the calcium responses, indicating a loss of inhibition, it only had a small effect on the orientation selectivity observed (Figure 4.6 A, B). Additionally, the application of TTX resulted in an approximately equal increase in both the preferred and null orientations, indicating a symmetric inhibitory input (Figure 4.6 C). These results allow us to conclude that although wide-field inhibition appears to be important in gain control, it is not required for generating orientation-selectivity in the type 5a bipolar cell terminals.

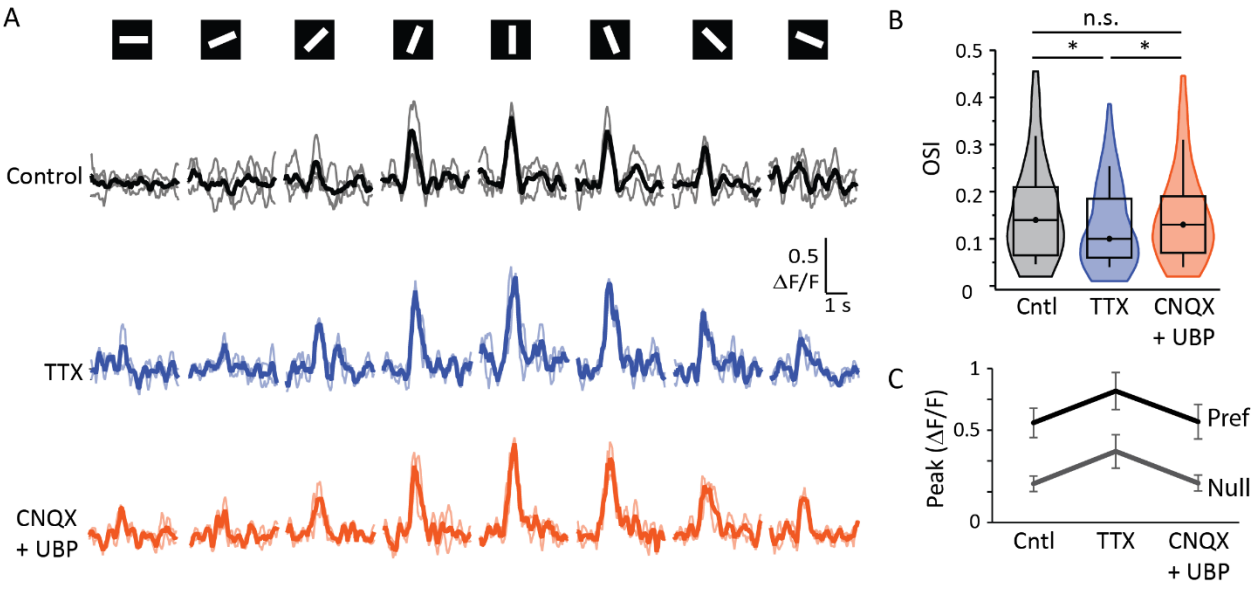

Figure 4.6 Surround inhibition is not required for orientation-selectivity in bipolar cells

(**A**) Calcium responses recorded from bipolar cell terminals in the Kcng4cre;GCaMP6f mouse line during static bar stimuli of 8 orientations in control (top), TTX (middle) and CNQX + UBP-310 (bottom). (**B**) Orientation-selectivity decreases in TTX ($p<0.005$) but increases back to

control levels with the addition of CNQX and UBP-310 (p=0.3). (**C**) Peak responses see similar changes for both the preferred and null orientated stimuli (n=5 retina, 84 ROIs).

To further test the mechanisms that may be driving the orientation-selectivity in bipolar cell terminals, after application of TTX, CNQX (20 μM) and UBP-310 (10 μM) were bath applied to disrupt the AMPA and kainate receptor mediated transmission, respectively. Application of CNQX and UBP-310 leaves the photoreceptor to ON bipolar cell pathway intact since it relies on metabotropic glutamate receptors (mGluR) while removing any downstream inputs from amacrine cells or horizontal cells which rely on AMPA or kainate receptors to be activated, therefore removing other sources of TTX insensitive surround inhibition. When CNQX and UBP-310 is first applied, the calcium response is lost in most cells, indicating that under both the control and TTX conditions observed here, activation of the bipolar cells is predominantly rod mediated, as CNQX blocks the rod pathway by disrupting the rod bipolar cell to AII amacrine cell transmission. However, upon increasing the light intensity to shift to cone mediated activity, the responses are recovered and remain OS (Figure 4.6 A, B, C). This indicates that the orientation selectivity observed in the type 5a bipolar cell terminals is likely driven via gap-junction coupling, as all other chemical transmission to the bipolar terminals should be disrupted in the excitatory blockers. Additionally, it shows that the type 5a bipolar cells are orientation-selective during both rod and cone mediated activity. Due to the saturation of the calcium signal, control and TTX conditions were not able to be obtained using the higher contrast that was necessary to evoke responses in the CNQX and UBP-310 condition.

It has previously been shown that the type 5a bipolar cells are heavily gap-junction coupled to amacrine cells as well as other types of bipolar cells (Tsukamoto and Omi, 2017). Although CNQX/UBP-310 removes the glutamatergic activation of amacrine cells, any electrical

coupling between cell types remains intact under these conditions, allowing us to hypothesize that the orientation selectivity observed in the bipolar cell terminals is mediated by gap-junction coupling. To directly test this, we crossed the Kcng4cre;GCaMP6f mouse line with the conditional connexin36 knockout (cx36 KO) mouse line (Yao *et al.*, 2018), allowing us to selectivity disrupt gap-junction coupling in the type 5a bipolar cells. Under these conditions, the 50 μm x 500 μm bar that was used previously to measure OS did not evoke a reliable calcium response with a large enough signal-to-noise ratio to allow for accurate analysis (data not shown). Because OS could not be directly measured using the Cx36 KO, we instead examined the spatial properties of the bipolar cells in control vs. Cx36 KO. Previous studies indicate that different bipolar cell types exhibit different receptive field properties and that these differences are predominantly driven by the surround inhibition (Zhang and Wu, 2009; Chen *et al.*, 2014; Franke *et al.*, 2017). Here, we wanted to examine whether electrical coupling also alters the receptive field properties of bipolar cells. This was done by examining the spatial integration during increasing bar stimuli in both the preferred and null orientations (Figure 4.7 A,B), as opposed to using spots of increasing diameter which does not address any asymmetries in the receptive field properties. In control animals, responses to increasing bars in the preferred orientation reached a peak amplitude around 100 μm – 200 μm (Figure 4.7 A, C), much larger than the reported dendritic fields of these cells (Behrens et al., 2016) but similar to previously reported values obtained from increasing spots (Chen *et al.*, 2014; but see Franke *et al.*, 2017). In comparison, increasing bars in the null orientation peaked around 50 μm – 100 μm (Figure 4.7 B, C). In the cx36 KO animals, this large spatial integration in the preferred orientation was not observed, and both the preferred and null oriented increasing bars exhibited a similar trend, where the response peaked at 50 μm then decreased as the bar size increased (Figure 4.7). These

results indicate that the asymmetric spatial integration that is required to generate orientation selectivity in the type 5a bipolar cells relies on gap-junction coupling mediated by the connexin36 protein.

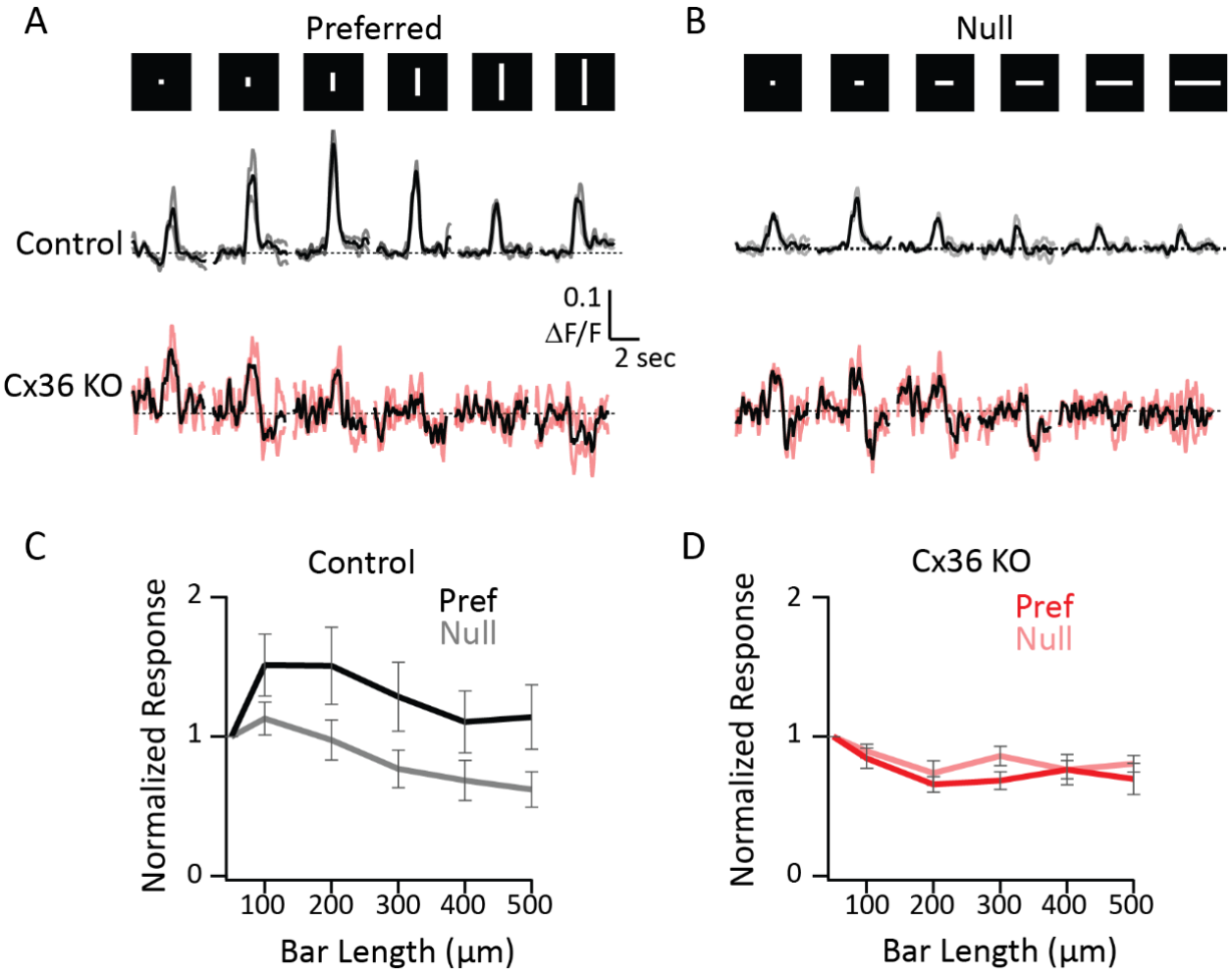

Figure 4.7 Gap-junctions drive asymmetric spatial integration

(**A**) Calcium responses recorded from bipolar cell terminals in the Kcng4cre;GCaMP6f mouse line with or without the Cx36 KO. Top shows the increasing bar stimuli in the preferred orientation (faint lines = individual trials, black lines = average). (**B**) Same as in A but in the null orientation. (**C**) Peak responses from control animals to increasing bar sizes in the preferred (black) and null (grey) orientations shows that the type 5a bipolar cells have an asymmetric receptive field in control. Responses are normalized to the 50 µm x 50 µm flash (n=6). (**D**) Same as C but for Cx36 KO animals, indicating that gap-junctions are required for generating the asymmetry seen in control (n=5).

4.5 Discussion

4.5.1 The role of orientation selectivity in DS cells

In the cortex, cells which are direction-selective are also reliably orientation-selective. Here, we show that this relationship is present in the visual system as early as the retina, raising the question of what significance does this orientation selectivity have on the direction encoding in the visual system? The DSGCs examined here are nasal (posterior) coding, meaning the predominant motion they are tasked with detecting is during self-motion, while the animal is moving forward through the environment (Rivlin-Etzion *et al.*, 2011). In nature, there is a bias towards vertically oriented edges such as trees or blades of grass that animals must quickly and accurately navigate through in order to survive (Coppola *et al.*, 1998). In the mouse dorsal lateral geniculate nucleus (dLGN) which receives direct input from the retina, and more specifically, from TRHR DSGCs, there is also a bias towards vertically tuned orientation selectivity (Rivlin-Etzion *et al.*, 2011; Zhao *et al.*, 2013). This relationship between forward motion and vertically oriented edges in the natural scene match the directional and orientational preferences exhibited by the nasal coding TRHR+ On-off DSGCs examined here. Because of this relationship, the orientation selectivity in these cells may act to enable them to more reliably detect the direction of motion by first transmitting the visual signal through a spatial orientation filter at the level of the bipolar cell output, removing some of the contaminating visual signals that would complicate the task of detecting the direction of motion of the more prominent vertically oriented edges.

4.5.2 Orientation-selectivity may be stimulus dependent

Direction-selective ganglion cells have been studied extensively over the past 50 years raising the question of why the orientation selectivity observed here has not been discovered sooner? One main reason is that typically, orientation selectivity across cell populations is studied using moving bars or drifting gratings, which, in the DSGC, appears to mask any OS tuning due to the strong direction selectivity (Baden *et al.*, 2016). Another possible explanation could be that the OS is stimulus dependent. Since the OS observed here appears to be mediated by gap-junction coupling, the degree of orientation-selectivity may depend on the level of light adaptation. In the retina, gap-junction coupling is strongly regulated by the release of dopamine from the dopaminergic amacrine cells. In scotopic conditions (low light levels), the level of dopamine in the retina is also low, resulting in a high level of electrical coupling, however, during photopic conditions (high light level), the amount of dopamine in the retina is increased, resulting in a dramatic decrease in the amount of electrical coupling between cells due to a dopamine dependent dephosphorylation of connexin (Baldridge, Vaney and Weiler, 1998; reviewed by Roy and Field, 2019). Since the experiments performed here were conducted under low background luminance and retina were dark-adapted prior to dissection, the level of gap-junction coupling may be maximal, causing stronger orientation selectivity than would be observed if the retina is light adapted. Additionally, the type 5a bipolar cell has been shown to be strongly coupled to the AII amacrine cell, which acts as the conduit between the rod pathway and the cone bipolar cells (Tsukamoto and Omi, 2017). Because of this strong coupling, the type 5a bipolar cell may be providing stronger excitatory input to the DSGC during rod driven responses than the other bipolar cell types which are not strongly coupled to the rod pathway, creating stronger orientation-selectivity under these conditions. In comparison, cone dominated responses

may be driven more by the other types of untuned bipolar cells, resulting in weaker OS at the level of the DSGCs. This effect can be seen by the high variability in the orientation-selectivity measured from the EPSCs recorded in the DSGC (Figure 4.3 F). This would implicate that the orientation-selectivity observed here may be having the largest impact under scotopic conditions, when the mice are thought to be most active.

4.5.3 Source of gap-junction coupling to type 5a bipolar cells

Preliminary data from electron-microscopy (EM) reconstructions of type 5a bipolar cell terminals indicates that these bipolar cells receive synaptic connections from wide-field amacrine cells which are biased towards the vertical orientation (in collaboration with Dr. David Berson). If these synaptic inputs were solely inhibitory, it would be expected that the bipolar cells would exhibit horizontal orientation selectivity as opposed to vertical orientation selectivity. Because of the vertical bias, these cells are an ideal candidate for the source of gap-junction coupling to the bipolar cells. To test this hypothesis, neurobiotin tracing could be performed by performing single cell electroporation of either type 5a bipolar cells or the wide-field amacrine cells and identifying the tracer coupled cells because neurobiotin is able to pass through the gap-junction pore. Alternately, one could provide current pulses to wide-field amacrine cells while imaging the calcium response in the type 5a bipolar cell terminals to determine whether the activation of wide-field amacrine cells evoke a response in bipolar cells.

4.6 Conclusions

Here we have shown that, addition to being strongly DS, the TRHR population of ON-OFF DSGCs also exhibit robust OS. This orientation tuning is independent from the DS tuning,

as abolishing SAC release does not impact the OS spiking or excitation recorded from the TRHR+ cells. Using 2-photon calcium imaging, pharmacology and genetic knockouts, we show that the orientation selectivity in DSGCs arises from at least one type of bipolar cells (type 5a) which exhibit asymmetric spatial integration mediated by the connexin36 containing gap-junctions.

These findings allow us to propose that during more complex, natural stimuli, ON-OFF DSGCs utilize a hierarchical scheme to process visual information by receiving signals that are pre-filtered for vertically oriented edges or objects from the glutamatergic bipolar cells prior to computing the direction of motion of those images. How this visual integration affects the ON-OFF DSGC output during complex stimuli remains to be examined.

Chapter 5: Discussion

5.1 Summary

This research examines the different mechanisms and circuitry involved in feature selectivity in the mouse retina. I start by examining the mechanisms involved in generating direction selectivity at the level of the SAC and the DSGC. Using a combination of genetic knockouts and optogenetic stimulation I investigate parallel mechanisms for generating DS in SAC dendrites. By rendering the GABAergic release from SAC dendrites non-DS, I also highlight the role of temporal asymmetries between inhibition and excitation as an alternate mechanism of DS in DSGCs.

In chapter 3, I turn my focus to the excitatory glutamatergic inputs to the DSGC. Building on previous work in our lab showing that NMDA and AMPA receptors exhibit different contrast sensitivities in DSGCS, I identify 'silent' NMDA-only synapses by analyzing the spontaneous activity in these cells and observing separate populations of NMDA and AMPA mediated events. Additionally, I find that the synaptic NMDA receptors are able to encode a range of contrasts without saturating, arguing against the findings that NMDA receptors reach saturation during univesicular glutamate release (Zhang and Diamond, 2009; Manookin *et al.*, 2010; Singh *et al.*, 2011).

Chapter 4 focuses on how presynaptic signal integration in bipolar cells modifies the output at the level of the DSGC. I show that at least one subtype of DSGC which encodes nasal motion also exhibits orientation selectivity. This orientation selectivity originates from asymmetric gap-junction coupling in the type 5a bipolar cells, indicating a hierarchical scheme to complex visual processing in the retina.

5.2 Natural Stimuli

Throughout this research, simple stimuli were utilized to allow me to analyze retinal computations across varying parameters. However, animals in the wild are very rarely tasked with encoding simple stimuli and instead need to be able to reliably encode different features of the visual environment during more complex visual inputs. One way that they may be able to reliably encode direction of motion during different more complex tasks is with the use of redundant mechanisms such as those described in chapter 2. The different mechanisms of encoding direction-selectivity at both the level of starburst amacrine cells as well as at the level of DSGCs may enable to DSGC to accurately encode direction across varying contrasts, speeds and background levels or noisy backgrounds (Chen *et al.*, 2016). Additionally, the use of orientation-selective filters such as that described in chapter 4 may simplify the task of encoding the direction of moving edges by filtering the visual signal at the level of the bipolar cells, similar to what is observed in other areas of the visual system (Hubel and Wiesel, 1959, 1962; Henry, Bishop and Dreher, 1974). The use of natural scene stimuli may resolve the question of why the retina implements multiple mechanisms, however, analysis of the results obtained using such stimuli becomes much more intricate. Identifying which feature or aspect of the stimuli evokes a particular response becomes more difficult as the stimuli becomes more complex.

5.3 Stimulus conditions and light adaptation

The retina is challenged with the task of detecting and encoding visual information over a wide range of background luminance and stimulus intensity. To do this accurately, it must alter the way it integrates the visual signal across different conditions (Baldridge, Vaney and Weiler, 1998; Rieke and Rudd, 2009). Across all layers of the retina and all cell types, gap junction

coupling plays a major role in how these signals are integrated (reviewed by Völgyi *et al.*, 2013). In this research, the stimulus parameters and retinal preparation were kept consistent across experimental days and conditions (ex. wild-type vs. knockout animals) to try to limit any variability due to changes in the degree of coupling throughout the retina. Experiments were always performed around the same time of day and the mouse was consistently dark adapted for 1 hour prior to retinal preparation to account for circadian rhythms and adaptation levels. This is an important control to consider when making comparisons across groups. However, because similar conditions were used across all experiments, we do not know whether the results shown here would be consistent if these experiments were replicated using higher background luminance or light-adapted retina as opposed to the dark-adapted retina used here. Changes in the strength of gap-junction coupling can results in increases or decreases in cells receptive field size, therefore changing a cells response properties (Dacey *et al.*, 2000). Additionally, different bipolar cell types may be modulated differently based on the degree of coupling and the different receptors expressed across types, changing the contribution of each cell type separately (Roy and Field, 2019). If this is the case, there may be differences in the weight of NMDA vs. AMPA receptor inputs in DSGCs across conditions. It may also alter the ratio of sustained and transient inputs to the starburst amacrine cell dendrites, therefore disrupting that mechanism of SAC DS, causing the SAC to rely more heavily on the SAC-SAC inhibition. The degree of orientation selectivity will also be heavily modulated by the amount of gap-junction coupling occurring in the retina, not only because the type 5a bipolar cells rely on gap-junction coupling to generate OS but also because the contribution of the type 5a compared to the other bipolar cell types providing inputs to the DSGC may be altered. This phenomenon may explain some of the

inconsistencies that have been reported across the retinal literature and is an important factor to consider during future experiments.

5.4 Techniques for studying retinal circuitry and cell signaling

Throughout this research, many different techniques were utilized to study different aspects of the DS circuitry. Each individual technique offers its own unique benefits as well as caveats which need to be understood to accurately interpret the results.

Single cell electrophysiology is a very useful technique to determine the different inputs that cells are receiving, the receptors that are expressed and the temporal and kinetic properties of different inputs. The responses that are observed during loose patch recordings or whole-cell patch clamp recordings are a result of the summation of all inputs along the dendritic tree and can be useful to determine the output of that cell or the relationship between excitation and inhibition on a global level. However, because of this summation, these types of recordings cannot provide information regarding individual synaptic inputs in terms of time and/or space along the dendritic tree (global vs. local information) during evoked responses.

In contrast to electrophysiological recordings, calcium imaging can provide more direct information regarding individual synaptic inputs and signal localization along the dendritic tree. It can also be performed in synaptic release sites to gain information about neurotransmitter release from particular cell types. However, the relationship between the calcium signal observed in synaptic release sites and neurotransmitter release are not fully understood. Due to the dependence on voltage-gated calcium channels for release, very small differences in calcium signals may result in differences in transmitter release (Katz and Miledi, 1969). Additionally, it

is unknown whether the calcium responses observed in these experiments are due to calcium influx from the receptors coupled to the release machinery or from other sources (other calcium channels or internal calcium stores)(Südhof, 2013). When looking for small differences in calcium signals, the affinity and kinetics of different calcium indicators also need to be taken into account. If the indicators or the PMTs are saturated or near saturation, small differences in the calcium responses will not be detected. In this research, 2-photon glutamate imaging was also utilized by viral transfection of iGluSnFR. This technique can provide valuable information regarding glutamate release and localization, however, similar information regarding the affinity and kinetics of the indicator need to be considered. In this research, we used the high affinity, iGluSnFR-A184S (Marvin *et al.*, 2018). This allowed us to see small quantal concentrations of glutamate, however, it saturates at much lower concentrations of glutamate than other lower affinity indicators and therefore cannot be used for measuring increases during multivesicular release. Additionally, whether iGluSnFR gets expressed in the synapse is not known and therefore it may only be responding to glutamate spillover. Due to the high affinity, iGluSnFR may also out compete the endogenous receptors in binding glutamate and may also impact glutamate diffusion and uptake (Armbruster, Dulla and Diamond, 2020).

An additional technique that is used in this research is optogenetic stimulation with channelrhodopsin2. Optogenetic stimulation of the starburst amacrine cell allowed us to disrupt the mechanism of SAC dendritic DS which relied on the kinetic differences of spatially separated bipolar cell inputs by directly stimulating the starburst under pharmacological conditions (Figure 2.2, Figure 2.3). Under these conditions, the ChR2 is expressed throughout the dendritic tree and in the soma, creating an artificial stimulus paradigm that does not accurately match what would be expected under natural stimulus conditions. Because of this, we may also be altering the

dendritic integration in the SAC as well as the isotonic isolation of the dendrites due to strong activation of ChR2 in the soma, both of which may also impact the dendritic DS (Tukker, Taylor and Smith, 2004; Hausselt *et al.*, 2007; Koren, Grove and Wei, 2017).

Because of these limitations, multiple different techniques were used in unison to obtain a more complete understanding of the mechanisms and circuitry involved in retinal DS.

5.5 Future directions

In chapter 2 I identified different mechanisms of DS at both the level of the SAC and the DSGC which appear to be redundant. However, the stimuli used throughout these experiments are simple spots of positive contrast moving uniformly across a dark background in 8 different directions. To test whether the different mechanisms identified here are truly redundant, one would need to test a battery of different stimulus parameters such as contrast, speed, frequency and background luminance/complexity. Using these different parameters may uncover differences in the contributions from each mechanism.

In chapter 3, spontaneous EPSCs and 2-photon imaging was used to show that the AMPA and NMDA mediated responses to ON-OFF DSGCs are arising from different synaptic sites, however, we did not identify whether these inputs are coming from separate populations of bipolar cells and if so, which types are making NMDA dominated connections vs. AMPA dominated connections. One way to investigate this would be to utilize optogenetic stimulation to selectively activate different bipolar cell types individually and measure whether the resulting EPSCs in the ON-OFF DSGC are mediated by AMPA or NMDA receptors.

Chapter 4 identifies a subtype of bipolar cell which is orientation-selective and can generate OS in at least one population of ON-OFF DSGC. To better understand the role that this orientation selectivity is having in DS computation, different combinations of stimuli will need to be used which may highlight the importance of OS filtering at the level of bipolar cells. Additionally, the Kcng4cre;Cx36KO mouse line could be used to determine if DS tuning is altered when bipolar cell OS is disrupted.

Bibliography

Amthor, F. R., Grzywacz, N. M. and Merwine, D. K. (1996) 'Extra-receptive-field motion facilitation in on-off directionally selective ganglion cells of the rabbit retina', *Visual Neuroscience*, 13, pp. 303–309. doi: 10.1017/S0952523800007549.

Andreae, L. C. and Burrone, J. (2015) 'Spontaneous Neurotransmitter Release Shapes Dendritic Arbors via Long-Range Activation of NMDA Receptors', *Cell Reports*. The Authors, 10(6), pp. 873–882. doi: 10.1016/j.celrep.2015.01.032.

Antinucci, P. *et al.* (2016) 'Neural Mechanisms Generating Orientation Selectivity in the Retina', *Current Biology*. The Author(s), 26(14), pp. 1802–1815. doi: 10.1016/j.cub.2016.05.035.

Antinucci, P. and Hindges, R. (2018) 'Orientation-Selective Retinal Circuits in Vertebrates', *Frontiers in Neural Circuits*, 12(February). doi: 10.3389/fncir.2018.00011.

Ariel, M. and Daw, N. W. (1982) *Pharmacological analysis of directionally sensitive rabbit retinal ganglion cells, J. Physiol*.

Armbruster, M., Dulla, C. G. and Diamond, J. S. (2020) 'Effects of fluorescent glutamate indicators on neurotransmitter diffusion and uptake', *eLife*, 9, pp. 1–27. doi: 10.7554/eLife.54441.

Baden, T. *et al.* (2016) 'The functional diversity of retinal ganglion cells in the mouse', *Nature*. Nature Publishing Group, 529(7586), pp. 345–350. doi: 10.1038/nature16468.

Baldridge, W. H., Vaney, D. I. and Weiler, R. (1998) 'The modulation of intercellular coupling in the retina', *Seminars in Cell and Developmental Biology*, 9(3), pp. 311–318. doi: 10.1006/scdb.1998.0235.

Barlow, H. B., Hill, R. M. and Levick, W. R. (1964) 'Retinal ganglion cells responding selectively to direction and speed of image motion in the rabbit', *J. Physiology*, 173, pp. 377–407. Available at: https://www.ncbi.nlm.nih.gov/pmc/articles/PMC1368915/pdf/jphysiol01195-0058.pdf.

Barlow, H. B. and Levick, W. R. (1965) 'The Mechanism of Directionally Selective Units', *J Physiol*, 178, pp. 477–504.

Baylor, D. A. *et al.* (1984) *The photocurrent, noise and spectral sensitivity of rods of the Monkey Macaca Fascicularis, J. Physiol*.

Bloomfield, S. A. (1991) 'Two types of orientation-sensitive responses of amacrine cells in the mammalian retina', *Nature*, 350, pp. 347–350.

Bloomfield, S. A. (1994) 'Orientation-sensitive amacrine and ganglion cells in the rabbit retina', *Journal of Neurophysiology*, 71(5), pp. 1672–1691. doi: 10.1152/jn.1994.71.5.1672.

Bloomfield, S. A. and Völgyi, B. (2009) 'The diverse functional roles and regulation of neuronal gap junctions in the retina', *Nature Reviews Neuroscience*, pp. 495–506. doi: 10.1038/nrn2636.

Briggman, K. L., Helmstaedter, M. and Denk, W. (2011) 'Wiring specificity in the direction-

selectivity circuit of the retina.', *Nature*. Nature Publishing Group, 471(7337), pp. 183–188. doi: 10.1038/nature09818.

Brombas, A., Croft, S. K. and Williams, S. R. (2017) 'Dendro-dendritic cholinergic excitation controls dendritic spike initiation in retinal ganglion cells', *Nature Communications*. Nature Publishing Group, 8, pp. 1–14. doi: 10.1038/ncomms15683.

Chen, M. *et al.* (2014) 'Receptive field properties of bipolar cell axon terminals in direction-selective sublaminas of the mouse retina', *Journal of Neurophysiology*. American Physiological Society, 112(8), pp. 1950–1962. doi: 10.1152/jn.00283.2014.

Chen, Q. *et al.* (2016) 'Stimulus-dependent recruitment of lateral inhibition underlies retinal direction selectivity', *eLife*, 5, pp. 1–19. doi: 10.7554/eLife.21053.

Chen, S. and Diamond, J. S. (2002) 'Synaptically Released Glutamate Activates Extrasynaptic NMDA Receptors on Cells in the Ganglion Cell Layer of Rat Retina', *Stimulus*, 22(6), pp. 2165–2173. doi: 22/6/2165 [pii].

Chiao, C. C. and Masland, R. H. (2002) 'Starburst cells nondirectionally facilitate the responses of direction-selective retinal ganglion cells', *Journal of Neuroscience*, 22(24), pp. 10509–10513. doi: 10.1523/jneurosci.22-24-10509.2002.

Clements, J. D. *et al.* (1992) 'The Time Course of Glutamate in the Synaptic Cleft', *Science*, 258(5087), pp. 1498–1501.

Coppola, D. M. *et al.* (1998) 'The distribution of oriented contours in the real world', *PNAS*, 95(7), pp. 4002–4006. doi: 10.1073/pnas.95.7.4002.

Cruz-Martín, A. *et al.* (2014) 'A dedicated circuit links direction-selective retinal ganglion cells to the primary visual cortex', *Nature*, 507(7492), pp. 358–361. doi: 10.1038/nature12989.

D'Angelo, E., Rossi, P. and Garthwaite, J. (1990) 'Dual-component NMDA receptor currents at a single central synapse'.

Dacey, D. *et al.* (2000) 'Center surround receptive field structure of cone bipolar cells in primate retina', *Vision research*, 40, pp. 1801–1811.

Demb, J. B. and Singer, J. H. (2012) 'Intrinsic properties and functional circuitry of the AII amacrine cell', *Visual neuroscience*, 29, pp. 51–60. doi: 10.1017/S0952523811000368.

Ding, H. *et al.* (2016) 'Species-specific wiring for direction selectivity in the mammalian retina.', *Nature*. Nature Publishing Group, 535(7610), pp. 105–10. doi: 10.1038/nature18609.

Duan, X. *et al.* (2014) 'Type II Cadherins Guide Assembly of a Direction-Selective Retinal Circuit', *Cell*. Elsevier Inc., 158(4), pp. 793–807. doi: 10.1016/j.cell.2014.06.047.

Dowling, J. E. (1987). *The retina: an approachable part of the brain.* Cambridge, Mass: Belknap Press of Harvard University Press.

Durand, G. M., Kovalchuk, Y. and Konnerth, A. (1996) 'Long-term potentiation and functional synapse induction in developing hippocampus', *Nature*, 381, pp. 71–75.

Dzubay, J. A. and Jahr, C. E. (1996) 'Kinetics of NMDA channel opening', *Journal of Neuroscience*, 16(13), pp. 4129–4134. doi: 10.1523/jneurosci.16-13-04129.1996.

Euler, T., Detwiler, P. B. and Denk, W. (2002) 'Directionally selective calcium signals in dendrites of starburst amacrine cells', *Nature*, 418, pp. 845–852.

Euler, T. and Masland, R. H. (2000) 'Light-evoked responses of bipolar cells in a mammalian retina', *Journal of Neurophysiology*, 83(4), pp. 1817–1829. doi: 10.1152/jn.2000.83.4.1817.

Farrow, K. *et al.* (2013) 'Ambient Illumination Toggles a Neuronal Circuit Switch in the Retina and Visual Perception at Cone Threshold', *Neuron*. Elsevier Inc., 78(2), pp. 325–338. doi: 10.1016/j.neuron.2013.02.014.

Franke, K. *et al.* (2017) 'Inhibition decorrelates visual feature representations in the inner retina', *Nature*. Nature Publishing Group, 542(7642), pp. 439–444. doi: 10.1038/nature21394.

Fransen, J. W. and Borghuis, B. G. (2017) 'Temporally Diverse Excitation Generates Direction-Selective Responses in ON- and OFF-Type Retinal Starburst Amacrine Cells', *Cell Reports*. ElsevierCompany., 18(6), pp. 1356–1365. doi: 10.1016/j.celrep.2017.01.026.

Frerking, M. and Wilson, M. (1996) 'Saturation of postsynaptic receptors at central synapses?', *Current Opinion in Neurobiology*, 6(3), pp. 395–403. doi: 10.1016/S0959-4388(96)80125-5.

Fried, S. I., Mu, T. A. and Werblin, F. S. (2005) 'at Multiple Levels by Laterally Offset Inhibition in the Rabbit Retina', 46, pp. 117–127. doi: 10.1016/j.neuron.2005.02.007.

Fried, S. I., Munch, T. A. and Werblin, F. S. (2002) 'Mechanisms and circuitry underlying directional selectivity in the retina', pp. 411–414.

Gavrikov, K. E. *et al.* (2006) 'Dendritic compartmentalization of chloride cotransporters underlies directional responses of starburst amacrine cells in retina', *PNAS*, 103(49), pp. 1–6.

Girshick, A. R., Landy, M. S. and Simoncelli, E. P. (2011) 'Cardinal rules: visual orientation perception reflects knowledge of environmental statistics', *Nature Neuroscience*, 14(7), pp. 926–932. doi: 10.1038/nn.2831.

Graydon, C. W. *et al.* (2014) 'Specialized postsynaptic morphology enhances neurotransmitter dilution and high-frequency signaling at an auditory synapse', *Journal of Neuroscience*, 34(24), pp. 8358–8372. doi: 10.1523/JNEUROSCI.4493-13.2014.

Grzywacz, N. M., Merwine, D. K. and Amthor, F. R. (1998) 'Complementary roles of two excitatory pathways in retinal directional selectivity', *Visual Neuroscience*, 15, pp. 1119–1127. doi: 10.1017/S0952523898156109.

Grzywacz, N. M., Tootle, J. S. and Amthor, F. R. (1997) 'Is the input to a GABAergic or cholinergic synapse the sole asymmetry in rabbit's retinal directional selectivity?', *Visual Neuroscience*, 14, pp. 39–54. doi: 10.1017/S0952523800008749.

Haas, K., Cline, H. and Malinow, R. (1998) 'No change in NMDA receptor-mediated response rise-time during development: Evidence against transmitter spillover', *Neuropharmacology*, 37(10–11), pp. 1393–1398. doi: 10.1016/S0028-3908(98)00137-3.

Hanse, E., Seth, H. and Riebe, I. (2013) 'AMPA-silent synapses in brain development and

pathology', *Nature Publishing Group*. Nature Publishing Group, 14(December). doi: 10.1038/nrn3642.

Hansen, K. B. *et al.* (2014) 'Distinct functional and pharmacological properties of triheteromeric GluN1/GluN2A/GluN2B NMDA receptors', *Neuron*, 81(5), pp. 1084–1096. doi: 10.1016/j.neuron.2014.01.035.

Hansen, K., Brauner-Osborne, H. and Egebjerg, J. (2008) 'Pharmacological Characterization of Ligands at Recombinant NMDA Receptor Subtypes by Electrophysiological Recordings and Intracellular Calcium Measurements', *Combinatorial Chemistry & High Throughput Screening*, 11(4), pp. 304–315. doi: 10.2174/138620708784246040.

Hausselt, S. E. *et al.* (2007) 'A dendrite-autonomous mechanism for direction selectivity in retinal starburst amacrine cells', *PLoS Biology*, 5(7), pp. 1474–1493. doi: 10.1371/journal.pbio.0050185.

He, S., Levick, W. R. and Vaney, D. I. (1998) 'Distinguishing direction selectivity from orientation selectivity in the rabbit retina.', *Visual neuroscience*. University of Victoria Libraries, 15(3), pp. 439–47. doi: 10.1017/S0952523898153038.

Heidelberger, R., Thoreson, W. B. and Witkovsky, P. (2005) 'Synaptic transmission at retinal ribbon synapses', *Progress in Retinal and Eye Research*, 24(6), pp. 682–720. doi: 10.1016/j.preteyeres.2005.04.002.

Helmstaedter, M. *et al.* (2013) 'Connectomic reconstruction of the inner plexiform layer in the mouse retina', *Nature*. Nature Publishing Group, 500(7461), pp. 168–174. doi: 10.1038/nature12346.

Henry, G. H., Bishop, P. O. and Dreher, B. (1974) 'Orientation, axis and direction as stimulus parameters for striate cells', *Vision Research*, 14(9), pp. 767–777. doi: 10.1016/0042-6989(74)90141-2.

Herrero, J. L. *et al.* (2013) 'Attention-induced variance and noise correlation reduction in macaque v1 is mediated by NMDA receptors', *Neuron*. Elsevier Inc., 78(4), pp. 729–739. doi: 10.1016/j.neuron.2013.03.029.

Hillier, D. *et al.* (2017) 'Causal evidence for retina-dependent and -independent visual motion computations in mouse cortex', *Nature Communications*, 20(7), pp. 960–672. doi: 10.1038/nn.4566.

Hoggarth, A. *et al.* (2015) 'Specific wiring of distinct amacrine cells in the directionally selective retinal circuit permits independent coding of direction and size', *Neuron*. Elsevier Inc., 86(1), pp. 276–291. doi: 10.1016/j.neuron.2015.02.035.

Hubel, D. H. and Wiesel, A. T. N. (1962) *Receptive fields, binocular interaction and functional architecture in the Cat's visual cortex, J. Phyiiol*.

Hubel, D. H. and Wiesel, T. N. (1959) 'Receptive Fields of Single Neurones in the Cat's Striate Cortex', *J. Physiology*, 148, pp. 574–591.

Isaac, J. T. R., Nicoll, R. A. and Malenka, R. C. (1995) 'Evidence for silent synapses: Implications for the expression of LTP', *Neuron*, 15(2), pp. 427–434. doi: 10.1016/0896-

6273(95)90046-2.

James, B. *et al.* (2019) 'An amplitude code transmits information at a visual synapse', *Nature Neuroscience*. Springer US, 22(7), pp. 1140–1147. doi: 10.1038/s41593-019-0403-6.

Jarsky, T. *et al.* (2011) 'A synaptic mechanism for retinal adaptation to luminance and contrast', *Journal of Neuroscience*, 31(30), pp. 11003–11015. doi: 10.1523/JNEUROSCI.2631-11.2011.

Johnston, J. *et al.* (2019) 'A Retinal Circuit Generating a Dynamic Predictive Code for Oriented Features', *Neuron*, 102(6), pp. 1211-1222.e3. doi: 10.1016/j.neuron.2019.04.002.

Katz, B. and Miledi, R. (1969) *Spontaneous and evoked activity of motor nerve endings in calcium ringer, J. Phy8iol*.

Kerchner, G. A. and Nicoll, R. A. (2008) 'Silent synapses and the emergence of a postsynaptic mechanism for LTP', *Nature Reviews Neuroscience*, 9(11), pp. 813–825. doi: 10.1038/nrn2501.

Kim, J. S. *et al.* (2014) 'Space – time wiring specificity supports direction selectivity in the retina', *Nature*. Nature Publishing Group, 509(7500), pp. 331–336. doi: 10.1038/nature13240.

Kittila, C. A. and Massey, S. C. (1997) 'Pharmacology of directionally selective ganglion cells in the rabbit retina', *Journal of Neurophysiology*, 77(2), pp. 675–689. doi: 10.1152/jn.1997.77.2.675.

Koch, C., Poggio, T. and Torre, V. (1982) 'RETINAL GANGLION CELLS: A FUNCTIONAL INTERPRETATION OF DENDRITIC MORPHOLOGY', *Phil. Trans. R. Soc. Lond. B*, 298, pp. 227–264. Available at: https://royalsocietypublishing.org/.

Koren, D., Grove, J. C. R. and Wei, W. (2017) 'Cross-compartmental Modulation of Dendritic Signals for Retinal Direction Selectivity', *Neuron*. Cell Press, 95(4), pp. 914-927.e4. doi: 10.1016/j.neuron.2017.07.020.

Kostadinov, D. and Sanes, J. R. (2015) 'Protocadherin-dependent dendritic self- avoidance regulates neural connectivity and circuit function', 6, pp. 1–23. doi: 10.7554/eLife.08964.

Kuffler, S. W. (1953) 'Discharge patterns and functional organization of mammalian retina', *Journal of neurophysiology*, 16(1), pp. 37–68. doi: 10.1152/jn.1953.16.1.37.

Kuo, R. I. and Wu, G. K. (2012) 'The Generation of Direction Selectivity in the Auditory System', *Neuron*. Elsevier Inc., 73(5), pp. 1016–1027. doi: 10.1016/j.neuron.2011.11.035.

Lee, S., Kim, K. and Zhou, Z. J. (2010) 'Role of ACh-GABA Cotransmission in Detecting Image Motion and Motion Direction', *Neuron*. Elsevier Inc., 68(6), pp. 1159–1172. doi: 10.1016/j.neuron.2010.11.031.

Lee, S. and Zhou, Z. J. (2006) 'The Synaptic Mechanism of Direction Selectivity in Distal Processes of Starburst Amacrine Cells', *Neuron*, 51, pp. 787–799. doi: 10.1016/j.neuron.2006.08.007.

Levick, W. R. (1967) 'Receptive fields and trigger features of ganglion cells in the visual streak of the Rabbit's retina', *J. Physiol*, 188, pp. 285–307.

Li, G. L., Cho, S. and von Gersdorff, H. (2014) 'Phase-locking precision is enhanced by

multiquantal release at an auditory hair cell ribbon synapse', *Neuron*. Elsevier Inc., 83(6), pp. 1404–1417. doi: 10.1016/j.neuron.2014.08.027.

Li, Y.-T. *et al.* (2015) 'Strengthening of Direction Selectivity by Broadly Tuned and Spatiotemporally Slightly Offset Inhibition in Mouse Visual Cortex', *cerebral cortex*, 25(9), pp. 2466–2477. doi: 10.1093/cercor/bhu049.

Lien, A. D. and Scanziani, M. (2018) 'Cortical direction selectivity emerges at convergence of thalamic synapses', *Nature*. doi: 10.1038/s41586-018-0148-5.

Manookin, M. B. *et al.* (2010) 'NMDA receptor contributions to visual contrast coding', *Neuron*, 67(2), pp. 280–293. doi: 10.1016/j.neuron.2010.06.020.

Marvin, J. S. *et al.* (2018) 'Stability, affinity, and chromatic variants of the glutamate sensor iGluSnFR', *Nature Methods*, 15. doi: 10.1038/s41592-018-0171-3.

Masland, R. H. (2001) 'The fundamental plan of the retina', *Nature Neuroscience*, 4(9), pp. 877–886. Available at: http://neurosci.nature.com.

Matsumoto, A., Briggman, K. L. and Yonehara, K. (2019) 'Spatiotemporally Asymmetric Excitation Supports Mammalian Retinal Motion Sensitivity', *Current Biology*. Elsevier Ltd., 29(19), pp. 3277-3288.e5. doi: 10.1016/j.cub.2019.08.048.

Mauss, A. S. *et al.* (2017) 'Visual Circuits for Direction Selectivity', *Annu. Rev. Neurosci.*, 40, pp. 211–232.

Mayer, M. L., Westbrook, G. L. and Guthrie, P. B. (1984) 'Voltage-dependent block by Mg2+ of NMDA responses in spinal cord neurones', *Nature*, 309, pp. 261–263.

McAllister, A. K. and Stevens, C. F. (2000) 'Nonsaturation of AMPA and NMDA receptors at hippocampal synapses', *Proceedings of the National Academy of Sciences of the United States of America*, 97(11), pp. 6173–6178. doi: 10.1073/pnas.100126497.

Mooney, R. and Konishi, M. (1991) *Two distinct inputs to an avian song nucleus activate different glutamate receptor subtypes on individual neurons (N-methyl-D-aspartate/excitatory postsynaptic potentials/birdsong), Proc. Natl. Acad. Sci. USA*.

Münch, T. A. and Werblin, F. S. (2006) 'Symmetric interactions within a homogeneous starburst cell network can lead to robust asymmetries in dendrites of starburst amacrine cells', *Journal of Neurophysiology*, 96(1), pp. 471–477. doi: 10.1152/jn.00628.2005.

Murphy-Baum, B. L. and Taylor, W. R. (2015) 'The Synaptic and Morphological Basis of Orientation Selectivity in a Polyaxonal Amacrine Cell of the Rabbit Retina', *Journal of Neuroscience*, 35(39), pp. 13336–13350. doi: 10.1523/JNEUROSCI.1712-15.2015.

Nath, A. and Schwartz, G. W. (2016) 'Cardinal Orientation Selectivity Is Represented by Two Distinct Ganglion Cell Types in Mouse Retina.', *The Journal of neuroscience : the official journal of the Society for Neuroscience*, 36(11), pp. 3208–21. doi: 10.1523/JNEUROSCI.4554-15.2016.

Nath, A. and Schwartz, G. W. (2017) 'Electrical synapses convey orientation selectivity in the mouse retina', *Nature communications*. Springer US, 8(1), p. 2025. doi: 10.1038/s41467-017-

01980-9.

O'Malley, D. M. and Masland, R. H. (1989) *Co-release of acetylcholine and y-aminobutyric acid by a retinal neuron (retina/amacrine cell/neurotransmitter/colocalization), PNAS*.

Oesch, N., Euler, T. and Taylor, W. R. (2005) 'Direction-selective dendritic action potentials in rabbit retina', *Neuron*, 47(5), pp. 739–750. doi: 10.1016/j.neuron.2005.06.036.

Oesch, N. W. and Diamond, J. S. (2011) 'Ribbon synapses compute temporal contrast and encode luminance in retinal rod bipolar cells', *Nature Neuroscience*. Nature Publishing Group, 14(12), pp. 1555–1561. doi: 10.1038/nn.2945.

Oyster, C. W. and Barlow, H. B. (1967) 'Direction-Selective Units in Rabbit Retina : Distribution of Preferred Directions Published by : American Association for the Advancement of Science Stable URL : https://www.jstor.org/stable/1720260 REFERENCES Linked references are available on JSTOR for ', 155(3764), pp. 841–842.

Pack, C. C. and Born, R. T. (2001) 'Temporal dynamics of a neural solution to the aperture problem in visual area MT of macaque brain', *Nature*, 409, pp. 1040–1042. Available at: www.nature.com.

Park, S. J. H. *et al.* (2014) 'Excitatory Synaptic Inputs to Mouse On-Off Direction- Selective Retinal Ganglion Cells Lack Direction Tuning', *J Neurosci*, 34(11), pp. 3976–3981. doi: 10.1523/JNEUROSCI.5017-13.2014.

Pei, Z. *et al.* (2015) 'Conditional Knock-Out of Vesicular GABA Transporter Gene from Starburst Amacrine Cells Reveals the Contributions of Multiple Synaptic Mechanisms Underlying Direction Selectivity in the Retina.', *J Neurosci*, 35(38), pp. 13219–32. doi: 10.1523/JNEUROSCI.0933-15.2015.

Petralia, R. S. *et al.* (1999) *Selective acquisition of AMPA receptors over postnatal development suggests a molecular basis for silent synapses*. Available at: http://neurosci.nature.com.

Poleg-Polsky, A. and Diamond, J. S. (2011) 'Imperfect Space Clamp Permits Electrotonic Interactions between Inhibitory and Excitatory Synaptic Conductances, Distorting Voltage Clamp Recordings', *PLoS ONE*, 6(4), p. 19463. doi: 10.1371/journal.pone.0019463.

Poleg-Polsky, A. and Diamond, J. S. (2016) 'Retinal circuitry balances contrast tuning of excitation and inhibition to enable reliable computation of direction selectivity', *Journal of Neuroscience*, 36(21), pp. 5861–5876. doi: 10.1523/JNEUROSCI.4013-15.2016.

Poleg-Polsky, A., Ding, H. and Diamond, J. S. (2018) 'Functional Compartmentalization within Starburst Amacrine Cell Dendrites in the Retina', *Cell Reports*. ElsevierCompany., 22(11), pp. 2809–2817. doi: 10.1016/j.celrep.2018.02.064.

Raviola, E. and Gilula, N. B. (1973) *Gap Junctions between Photoreceptor Cells in the Vertebrate Retina (membranes/electron microscopy/freeze-fracturing)*.

Renger, J. J., Egles, C. and Liu, G. (2001) 'A Developmental Switch in Neurotransmitter Flux Enhances Synaptic Efficacy by Affecting AMPA Receptor Activation Synapsin I Localization Precedes Functional Dye Uptake during Synaptic Maturation Cultured hippocampal neurons extend neurites and', *Neuron*, 29, pp. 469–484.

Rieke, F. and Rudd, M. E. (2009) 'The Challenges Natural Images Pose for Visual Adaptation', *Neuron*. Elsevier Inc., 64(5), pp. 605–616. doi: 10.1016/j.neuron.2009.11.028.

Rivadulla, C., Sharma, J. and Sur, M. (2001) 'Specific roles of NMDA and AMPA receptors in direction-selective and spatial phase-selective responses in visual cortex', *Journal of Neuroscience*, 21(5), pp. 1710–1719. doi: 10.1523/jneurosci.21-05-01710.2001.

Rivlin-Etzion, M. *et al.* (2011) 'Transgenic mice reveal unexpected diversity of On-Off direction selective retinal ganglion cell subtypes and brain structures involved in motion processing', *J Neurosci*, 31(24), pp. 8760–8769. doi: 10.1523/JNEUROSCI.0564-11.2011.Transgenic.

Rivlin-Etzion, M., Wei, W. and Feller, M. B. (2012) 'Visual Stimulation Reverses the Directional Preference of Direction-Selective Retinal Ganglion Cells', *Neuron*. Elsevier Inc., 76(3), pp. 518–525. doi: 10.1016/j.neuron.2012.08.041.

Roy, S. and Field, G. D. (2019) 'Dopaminergic modulation of retinal processing from starlight to sunlight', *Journal of Pharmacological Science*. Elsevier Ltd, 140(1), pp. 86–93. doi: 10.1016/j.jphs.2019.03.006.

Rudolph, S. *et al.* (2015) 'The ubiquitous nature of multivesicular release', *Trends in Neurosciences*. Elsevier Ltd, 38(7), pp. 428–438. doi: 10.1016/j.tins.2015.05.008.

Sagdullaev, B. T., McCall, M. A. and Lukasiewicz, P. D. (2006) 'Presynaptic Inhibition Modulates Spillover, Creating Distinct Dynamic Response Ranges of Sensory Output', *Neuron*, 50(6), pp. 923–935. doi: 10.1016/j.neuron.2006.05.015.

Saul, A. B., Carras, P. L. and Humphrey, A. L. (2005) 'Temporal properties of inputs to direction-selective neurons in monkey V1', *Journal of Neurophysiology*, 94(1), pp. 282–294. doi: 10.1152/jn.00868.2004.

Schachter, M. J. *et al.* (2010) 'Dendritic spikes amplify the synaptic signal to enhance detection of motion in a simulation of the direction-selective ganglion cell', *PLoS Computational Biology*, 6(8). doi: 10.1371/journal.pcbi.1000899.

Self, M. W. *et al.* (2012) 'Different glutamate receptors convey feedforward and recurrent processing in macaque V1', *PNAS*, 109(27), pp. 11031–11036. doi: 10.1073/pnas.1119527109.

Sethuramanujam, S. *et al.* (2016) 'A Central Role for Mixed Acetylcholine/GABA Transmission in Direction Coding in the Retina', *Neuron*. Elsevier Inc., 90(6), pp. 1243–1256. doi: 10.1016/j.neuron.2016.04.041.

Sethuramanujam, S. *et al.* (2017) '"Silent" NMDA Synapses Enhance Motion Sensitivity in a Mature Retinal Circuit', *Neuron*. Elsevier Inc., 96(5), pp. 1099-1111.e3. doi: 10.1016/j.neuron.2017.09.058.

Sethuramanujam, S., Awatramani, G. B. and Slaughter, M. M. (2018) 'Cholinergic excitation complements glutamate in coding visual information in retinal ganglion cells', *The Journal of Physiology*, 596, pp. 3709–3724. doi: 10.1113/JP275073.

Shekhar, K. *et al.* (2016) 'Comprehensive Classification of Retinal Bipolar Neurons by Single-Cell Transcriptomics', *Cell*. Elsevier Inc., 166(5), pp. 1308-1323.e30. doi: 10.1016/j.cell.2016.07.054.

Shima, K. and Tanji, J. (1998) 'Role for cingulate motor area cells in voluntary movement selection based on reward', *Science*, 282(5392), pp. 1335–1338. doi: 10.1126/science.282.5392.1335.

Silver, A., Traynelis, S. F. and Cull-Candy, S. (1992) 'Rapid-time-course miniature and evoke excitatory currents at cerebellar synapses in siut'.

Singer, J. H. (2007) 'Multivesicular release and saturation of glutamatergic signalling at retinal ribbon synapses', *Journal of Physiology*, pp. 23–29. doi: 10.1113/jphysiol.2006.125302.

Singh, P. *et al.* (2011) 'Computational investigation of the changing patterns of subtype specific NMDA receptor activation during physiological glutamatergic neurotransmission', *PLoS Computational Biology*, 7(6). doi: 10.1371/journal.pcbi.1002106.

Sivyer, B. *et al.* (2010) 'Synaptic inputs and timing underlying the velocity tuning of direction-selective ganglion cells in rabbit retina', *J Physiol*, 588, pp. 3243–3253. doi: 10.1113/jphysiol.2010.192716.

Sivyer, B. and Williams, S. R. (2013) 'Direction selectivity is computed by active dendritic integration in retinal ganglion cells', *Nature Publishing Group*, 16(8). doi: 10.1038/nn.3565.

Storchi, R. *et al.* (2019) 'Measuring vision using innate behaviours in mice with intact and impaired retina function', *Scientific Reports*. doi: 10.1038/s41598-019-46836-y.

Südhof, T. C. (2013) 'Neurotransmitter release: The last millisecond in the life of a synaptic vesicle', *Neuron*, 80(3), pp. 675–690. doi: 10.1016/j.neuron.2013.10.022.

Sun, W. *et al.* (2016) 'Thalamus provides layer 4 of primary visual cortex with orientation- and direction-tuned inputs', *Nature Neuroscience*, 19(2), pp. 308–315. doi: 10.1038/nn.4196.

Svoboda, K., Mainen, Z. F. and Malinow, R. (1999) 'Synaptic calcium transients in single spines indicate that NMDA receptors are not saturated', *Nature*, 399(6732), pp. 151–155. Available at: http://www.nature.com/doifinder/10.1038/20187%5Cnpapers2://publication/doi/10.1038/20187.

Tafazoli, S. *et al.* (2017) 'Emergence of transformation-tolerant representations of visual objects in rat lateral extrastriate cortex', *eLife*, 6. doi: 10.7554/eLife.22794.

Taylor, W. R. *et al.* (2000) 'Dendritic computation of direction selectivity by retinal ganglion cells', *Science*, 289(5488), pp. 2347–2350. doi: 10.1126/science.289.5488.2347.

Taylor, W. R. and Smith, R. G. (2012) 'The role of starburst amacrine cells in visual signal processing', *Visual Neuroscience*, 29, pp. 73–81. doi: 10.1017/S0952523811000393.

Taylor, W. R. and Vaney, D. I. (2002) 'Diverse Synaptic Mechanisms Generate Direction Selectivity in the Rabbit Retina', *J Neurosci*, 22(17), pp. 7712–7720.

Thiele, A. *et al.* (2004) 'Contribution of inhibitory mechanisms to direction selectivity and response normalization in macaque middle temporal area', *PNAS*, 101(26), pp. 9810–9815. Available at: www.pnas.orgcgidoi10.1073pnas.0307754101.

Torre, V. and Poggio, T. (1978) 'A synaptic mechanism possibly underlying directional selectivity to motion', *Proc. R. Soc. Lond.*, 202, pp. 409–416. Available at: https://royalsocietypublishing.org/.

Tovar, K. R., Sprouffske, K. and Westbrook, G. L. (2000) ‘Fast NMDA Receptor – Mediated Synaptic Currents in Neurons From Mice Lacking the 2 (NR2B) Subunit’, *J Physiol*, 2, pp. 0–4.

Tran, N. M. *et al.* (2019) ‘Single-Cell Profiles of Retinal Ganglion Cells Differing in Resilience to Injury Reveal Neuroprotective Genes’, *Neuron*. Elsevier Inc., 104(6), pp. 1039-1055.e12. doi: 10.1016/j.neuron.2019.11.006.

Trenholm, S. *et al.* (2013) ‘Lag normalization in an electrically coupled neural network’, *Nature Neuroscience*, 16(2), pp. 154–156. doi: 10.1038/nn.3308.

Trenholm, S. *et al.* (2014) ‘Nonlinear dendritic integration of electrical and chemical synaptic inputs drives fine-scale correlations’, *Nature Neuroscience*. Nature Publishing Group, 17(12), pp. 1759–1766. doi: 10.1038/nn.3851.

Tsukamoto, Y. and Omi, N. (2017) ‘Classification of mouse retinal bipolar cells: Type-specific connectivity with special reference to rod-driven AII amacrine pathways’, *Frontiers in Neuroanatomy*, 11(October), pp. 1–25. doi: 10.3389/fnana.2017.00092.

Tukker, J. J., Taylor, W. R. and Smith, R. G. (2004) ‘Direction selectivity in a model of the starburst amacrine cell’, *Visual Neuroscience*, 21(4), pp. 611–625. doi: 10.1017/S0952523804214109.

Umemiya, M., Senda, M. and Murphy, T. H. (1999) ‘Behaviour of NMDA and AMPA receptor-mediated miniature EPSCs at rat cortical neuron synapses identified by calcium imaging’, *Journal of Physiology*, 521.1, pp. 113–122.

Vaney, D. I., Sivyer, B. and Rowland Taylor, W. (2012) ‘Direction selectivity in the retina: symmetry and asymmetry in structure and function’, *Nature Publishing Group*. doi: 10.1038/nrn3165.

Venkataramani, S. and Taylor, W. R. (2010) ‘Orientation Selectivity in Rabbit Retinal Ganglion Cells Is Mediated by Presynaptic Inhibition’, *Journal of Neuroscience*, 30(46), pp. 15664–15676. doi: 10.1523/JNEUROSCI.2081-10.2010.

Venkataramani, S. and Taylor, W. R. (2016) ‘Synaptic Mechanisms Generating Orientation Selectivity in the ON Pathway of the Rabbit Retina’, *Journal of Neuroscience*, 36(11), pp. 3336–3349. doi: 10.1523/JNEUROSCI.1432-15.2016.

Vlasits, A. L. *et al.* (2014) ‘Visual Stimulation Switches the Polarity of Excitatory Input to Starburst Amacrine Cells’, *Neuron*, 83(5), pp. 1172–1184. doi: 10.1016/j.neuron.2014.07.037.

Vlasits, A. L. *et al.* (2016) ‘A Role for Synaptic Input Distribution in a Dendritic Computation of Motion Direction in the Retina’, *Neuron*. Cell Press, 89(6), pp. 1317–1330. doi: 10.1016/j.neuron.2016.02.020.

Völgyi, B. *et al.* (2013) ‘Gap junctional coupling in the vertebrate retina: Variations on one theme?’, *Progress in Retinal and Eye Research*. Elsevier Ltd, 34, pp. 1–18. doi: 10.1016/j.preteyeres.2012.12.002.

Wang, X. J. (2001) ‘Synaptic reverberation underlying mnemonic persistent activity’, *Trends in Neurosciences*, 24(8), pp. 455–463.

Wei, W., Elstrott, J. and Feller, M. B. (2010) 'Two-photon targeted recording of GFP-expressing neurons for light responses and live-cell imaging in the mouse retina', *Nature Protocols*, 5(7), pp. 1347–1352. doi: 10.1038/nprot.2010.106.

Wilent, B. and Contreras, D. (2005) 'Dynamics of excitation and inhibition underlying stimulus selectivity in rat somatosensory cortex', *Nature Neuroscience*, 8(10), pp. 1364–1370. doi: 10.1038/nn1545.

Wilson, D. E., Scholl, B. and Fitzpatrick, D. (2018) 'Differential tuning of excitation and inhibition shapes direction selectivity in ferret visual cortex', *Nature*. Springer US, 560(7716), pp. 97–101. doi: 10.1038/s41586-018-0354-1.

Yan, W. *et al.* (2020) 'Molecular identification of sixty-three amacrine cell types completes a mouse retinal cell atlas', *Journal of Neuroscience*, 40(27), pp. 5177–5195. doi: 10.1101/2020.03.10.985770.

Yang, G. and Masland, R. H. (1992) 'Direct Visualization of the Dendritic and Receptive Fields of Directionally Selective Retinal Ganglion Cells', *Science*, 258(5090), pp. 1949–1952.

Yao, X. *et al.* (2018) 'Gap Junctions Contribute to Differential Light Adaptation across Direction-Selective Retinal Ganglion Cells', *Neuron*. Elsevier Inc., 100(1), pp. 216-228.e6. doi: 10.1016/j.neuron.2018.08.021.

Ye, C. Q. *et al.* (2010) 'Synaptic mechanisms of direction selectivity in primary auditory cortex', *Journal of Neuroscience*, 30(5), pp. 1861–1868. doi: 10.1523/JNEUROSCI.3088-09.2010.

Yonehara, K. *et al.* (2011) 'Spatially asymmetric reorganization of inhibition establishes a motion-sensitive circuit', *Nature*, 469, pp. 407–410. doi: 10.1038/nature09711.

Yonehara, K. *et al.* (2013) 'The first stage of cardinal direction selectivity is localized to the dendrites of retinal ganglion cells', *Neuron*, 79(6), pp. 1078–1085. doi: 10.1016/j.neuron.2013.08.005.

Yoshida, K. *et al.* (2001) 'A key role of starburst amacrine cells in originating retinal directional selectivity and optokinetic eye movement', *Neuron*, 30(3), pp. 771–780. doi: 10.1016/S0896-6273(01)00316-6.

Zhang, A.-J. and Wu, S. M. (2009) 'Behavioral/Systems/Cognitive Receptive Fields of Retinal Bipolar Cells Are Mediated by Heterogeneous Synaptic Circuitry'. doi: 10.1523/JNEUROSCI.4984-08.2009.

Zhang, J. and Diamond, J. S. (2009) 'Subunit- and pathway-specific localization of NMDA receptors and scaffolding proteins at ganglion cell synapses in rat retina', *J Neurosci*, 100(2), pp. 130–134. doi: 10.1016/j.pestbp.2011.02.012.Investigations.

Zhang, L. I. *et al.* (2003) 'Topography and synaptic shaping of direction selectivity in primary auditory cortex', *Nature*, 424, pp. 201–205. doi: 10.1038/nature01743.

Zhao, X. *et al.* (2013) 'Orientation-selective responses in the mouse lateral geniculate nucleus', *Journal of Neuroscience*, 33(31), pp. 12751–12763. doi: 10.1523/JNEUROSCI.0095-13.2013.

Appendix

A. Figures

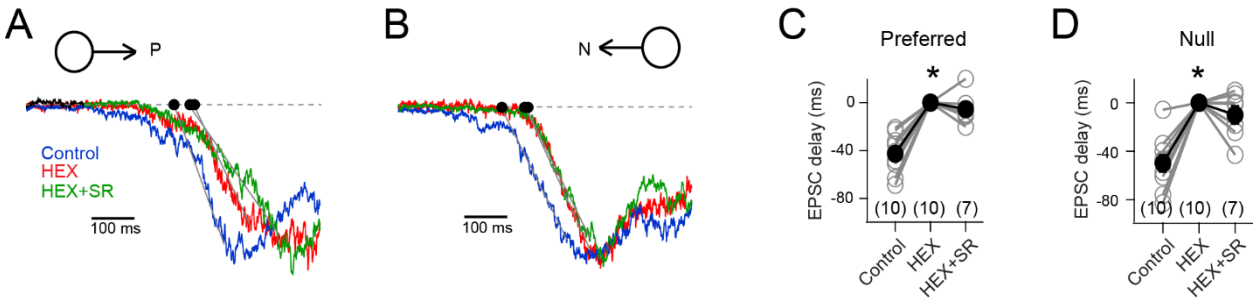

Figure 2.5– supplemental 1 The EPSC timing delay in HEX is independent of inhibition

(**A – B**) The EPSCs elicited in a DSGC to preferred (**A**) and null stimuli (**B**), in control, HEX (to block nicotinic acetylcholine receptors), and HEX + SR-95531 (to block $GABA_A$ receptors). Note that the responses have been normalized to show that the timing of the EPSCs is altered upon addition of HEX, but not upon further addition of SR. (stimulus velocity = 600 µm/s) (**C–D**) The onset of the preferred (**C**) and null EPSCs (**D**) in control (n = 10), HEX (n = 10), and HEX +SR (n = 7) shown relative to HEX. The EPSCs in HEX were significantly delayed to control (*p<0.001). But further addition of SR did not alter the timing. Pooled data are represented as mean ± SEM.

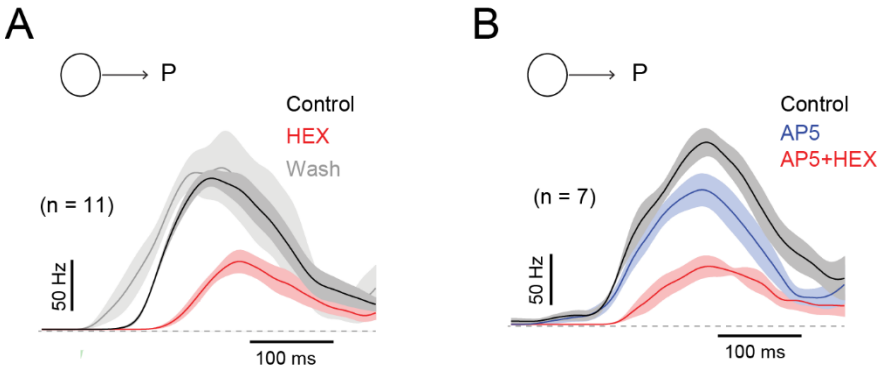

Figure 2.7– supplemental 1 The effects of blocking nACh receptors on the latency of the DSGC response is reversible, and contrasts with the effects of NMDA receptor antagonists

(**A**)The average ON spiking responses, convolved with a Gaussian kernel (σ = 25 ms), measured in control (black), in the presence of a nicotinic ACh receptor antagonist (50 µM hexamethonium; HEX, red) and in wash conditions (grey). HEX increased the spiking latency by 51 ± 7 ms. Traces depict the mean (solid line)± SEM (shaded region). (**B**) The average spiking responses measured in control (black), in the presence of a NMDA receptor antagonist (50 µM

D-AP5, blue) and in the added presence of HEX (red). AP5 did not alter the spike latency (2 ± 4 ms), while further addition of HEX increased the latency (45 ± 11 ms)

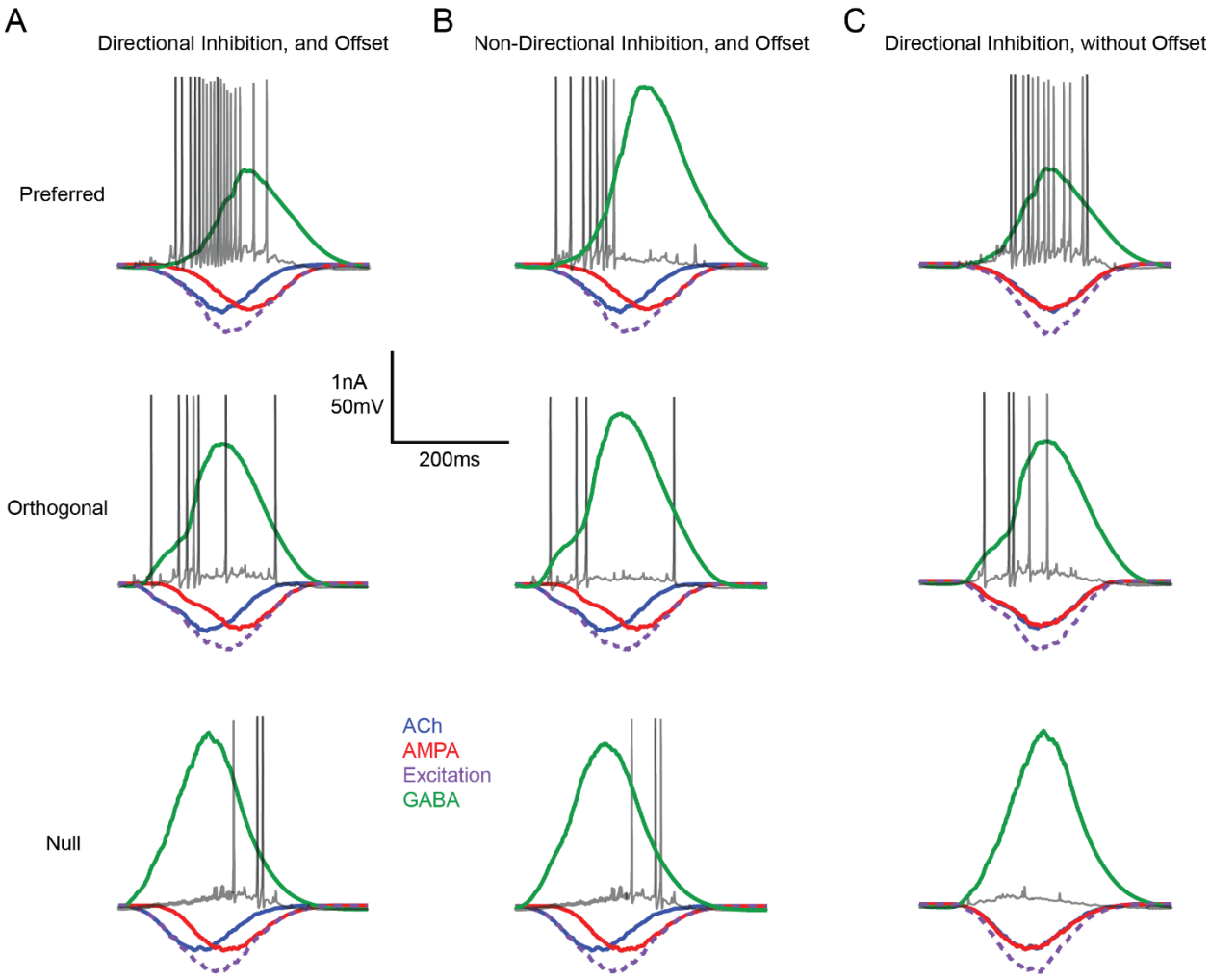

Figure 2.7– supplemental 2 Input/output measured in a model DSGC in which responses are driven by directional changes in inhibition and/or E/I temporal offsets

(**A**) Single representative spike trains in a model DSGC are overlaid over the underlying EPSCs and IPSCs (averaged over 20 trials) for preferred (*top*), orthogonal (*middle*) and null direction motion (*bottom*) under conditions in which both E/I ratios (directional inhibition) and E/I temporal offsets were present. Note that the spiking responses in the null direction were delayed compared to the preferred direction spiking, resulting in changes in direction selectivity over the time-course of the response. (**B**) As in (**A**) but only E/I temporal offsets were used to drive DS. The strength of inhibition is non-DS. (**C**) As in (**A**) but only directionally tuned inhibitory charge was used to drive DS. All E/I timing offsets were removed. This simulation illustrates the

workings of conventional models of DS. The spiking onset was delayed compared to (**A and B**), but DS did not evolve over time.